



National Library
of Canada

Acquisitions and
Bibliographic Services Branch

395 Wellington Street
Ottawa, Ontario
K1A 0N4

Bibliothèque nationale
du Canada

Direction des acquisitions et
des services bibliographiques

395, rue Wellington
Ottawa (Ontario)
K1A 0N4

Your file - Votre référence

Our file - Notre référence

NOTICE

The quality of this microform is heavily dependent upon the quality of the original thesis submitted for microfilming. Every effort has been made to ensure the highest quality of reproduction possible.

If pages are missing, contact the university which granted the degree.

Some pages may have indistinct print especially if the original pages were typed with a poor typewriter ribbon or if the university sent us an inferior photocopy.

Reproduction in full or in part of this microform is governed by the Canadian Copyright Act, R.S.C. 1970, c. C-30, and subsequent amendments.

AVIS

La qualité de cette microforme dépend grandement de la qualité de la thèse soumise au microfilmage. Nous avons tout fait pour assurer une qualité supérieure de reproduction.

S'il manque des pages, veuillez communiquer avec l'université qui a conféré le grade.

La qualité d'impression de certaines pages peut laisser à désirer, surtout si les pages originales ont été dactylographiées à l'aide d'un ruban usé ou si l'université nous a fait parvenir une photocopie de qualité inférieure.

La reproduction, même partielle, de cette microforme est soumise à la Loi canadienne sur le droit d'auteur, SRC 1970, c. C-30, et ses amendements subséquents.

Canada

SPHALERITE ACTIVATION IN THE PRESENCE OF IRON IONS

Qingsong Zhang

Department of Mining and Metallurgical Engineering

McGill University, Montreal

March, 1994

**A Thesis submitted to the
Faculty of Graduate Studies and Research
in partial fulfilment of the requirement of the degree of
Doctor of Philosophy**

© Qingsong Zhang, 1994



National Library
of Canada

Acquisitions and
Bibliographic Services Branch

395 Wellington Street
Ottawa, Ontario
K1A 0N4

Bibliothèque nationale
du Canada

Direction des acquisitions et
des services bibliographiques

395, rue Wellington
Ottawa (Ontario)
K1A 0N4

Your file *Votre référence*

Our file *Notre référence*

The author has granted an irrevocable non-exclusive licence allowing the National Library of Canada to reproduce, loan, distribute or sell copies of his/her thesis by any means and in any form or format, making this thesis available to interested persons.

The author retains ownership of the copyright in his/her thesis. Neither the thesis nor substantial extracts from it may be printed or otherwise reproduced without his/her permission.

L'auteur a accordé une licence irrévocable et non exclusive permettant à la Bibliothèque nationale du Canada de reproduire, prêter, distribuer ou vendre des copies de sa thèse de quelque manière et sous quelque forme que ce soit pour mettre des exemplaires de cette thèse à la disposition des personnes intéressées.

L'auteur conserve la propriété du droit d'auteur qui protège sa thèse. Ni la thèse ni des extraits substantiels de celle-ci ne doivent être imprimés ou autrement reproduits sans son autorisation.

ISBN 0-315-94730-6

Canada

To my wife Yuli Zhang
and my dear son Stephen Zhang

ABSTRACT

Flotation of sphalerite with xanthate in the presence of iron ions has been studied as a function of pH. Sphalerite floated readily at pH 8-11 in the presence of ferrous ions, but not in the presence of ferric ions. The Fe^{2+} ion concentration, pH and oxygen concentration were shown to be factors in controlling flotation. Electrokinetic measurements indicated that the surface charge increased in the presence of Fe^{2+} ions and oxygen, and decreased upon adding xanthate and in the presence of Fe^{2+} ions with the absence of oxygen.

As a prelude to surface analysis to try to identify the species responsible for the sphalerite flotation, bulk precipitates formed from iron salt and xanthate solutions under various conditions were obtained and analysed. Analysis techniques included ultraviolet spectroscopy, infrared spectroscopy, x-ray diffraction and Mössbauer spectroscopy.

It was tentatively concluded that the bulk precipitates contained three ferric components: two hydroxy xanthates, $\text{Fe}(\text{OH})_2\text{X}$ and $\text{Fe}(\text{OH})\text{X}_2$ and an iron oxide, FeO_x .

Iron xanthate precipitates prepared over the pH range 6-12 showed a flotation response and electrokinetic behaviour similar to those of Fe^{2+} /xanthate-treated sphalerite.

An *ex situ* X-ray photoelectron spectroscopic (XPS), *ex situ* infrared (DRIFTS) and *in situ* infrared (ATR) investigation of the interaction of sphalerite with ferrous, ferric and xanthate ions at pH 10 was undertaken. The formation of the hydrophobic surface species was found to involve initial adsorption of Fe^{2+} , followed by oxidation to Fe^{3+} and subsequent reaction with xanthate. There was no significant incorporation of Fe^{3+} .

A three-step reaction mechanism is proposed to account for Fe^{2+} ion activation of sphalerite: (i) adsorption of $\text{Fe}(\text{OH})^+$, (ii) oxidation to $\text{Fe}(\text{OH})^{2+}$ on the surface, (iii) reaction with xanthate to form $\text{Fe}(\text{OH})_2\text{X}$ or $\text{Fe}(\text{OH})\text{X}_2$.

RÉSUMÉ

On a étudié la flottation de la sphalérite avec du xanthate, en fonction du pH, en présence d'ions de fer. Entre un pH de 8 et 11, la sphalérite flotte facilement en présence d'ions ferreux, mais non en présence d'ions ferriques. On a démontré que les facteurs affectant la flottation sont : la concentration en ions Fe^{2+} , le pH et la concentration en oxygène. Des mesures électrocinétiques ont indiqué que la charge de surface s'accroît en présence d'ions Fe^{2+} et d'oxygène, et décroît lorsque l'on ajoute du xanthate et en présence d'ions Fe^{2+} en l'absence d'oxygène.

Précédent l'analyse des sulfures et afin d'identifier les espèces responsables de la flottation de la sphalérite, on a produit, sous différentes conditions, et analysé des précipités en vrac formés à partir de sels ferriques et de solutions de xanthates. On a utilisé les méthodes analytiques suivantes : la spectroscopie ultraviolette, la spectroscopie à infrarouge, la diffraction X et la spectroscopie Mössbauer.

On a conclu expérimentalement que les précipités en vrac contenaient trois composantes ferriques : deux xanthates hydroxyliques, $\text{Fe}(\text{OH})_2\text{X}$ et $\text{Fe}(\text{OH})\text{X}_2$ et un oxyde de fer, FeO_x .

Les précipités de xanthate de fer, préparés à un pH entre 6-12, ont démontré des réactions à la flottation et des comportements électrocinétiques similaires à ceux de la sphalérite traitée au Fe^{2+} /xanthate.

A pH 10, on a entrepris des recherches sur l'interaction de la sphalérite avec des ions ferreux, ferriques et de xanthates en utilisant la spectroscopie par photoélectron rayons-X ex situ (XPS), par infrarouge ex situ (DRIFTS) et par infrarouge in situ (ATR). La formation des espèces hydrophobiques à la surface provient d'une adsorption initiale de Fe^{2+} , suivie d'une oxydation en Fe^{3+} et subséquemment une réaction avec le xanthate. Il n'y a aucune incorporation significative de Fe^{3+} .

Pour expliquer l'activation de la sphalérite par des ions Fe^{2+} , un mécanisme impliquant une réaction en trois étapes a été proposée : (i) une adsorption de $\text{Fe}(\text{OH})^+$, (ii) une

oxydation à la surface en Fe(OH)^{2+} , (iii) une réaction avec du xanthate pour former du $\text{Fe(OH)}_2\text{X}$ ou du Fe(OH)X_2 .

ACKNOWLEDGEMENTS

I am indebted specially to two people: Prof. J. A. Finch for his advise, enthusiasm, keen interest and constant support throughout the research program, and Prof. Z. Xu for his friendship, his invaluable input to this work, and for the hours of fruitful discussions on surface chemistry.

I am also indebted to Dr. S. H. R. Brienne and Dr. S. R. Rao for their interest, encouragement, criticism and advice throughout this project.

I would like to thank Prof. D. Ryan, Physics Department of McGill University who performed Mössbauer measurements and interpreted the spectra, and Dr. S. Poulin, École polytechnique de Montréal for help in obtaining and interpreting the XPS spectra.

As well, I want to thank all members of the Department of Mining and Metallurgical Engineering, especially Ms. M. Riendeau for her invaluable help in the laboratory and Mr. Leroux for translation of abstract. I want to thank Prof. A. R. Laplante for his suggestions during this project. I am also indebted to all my colleagues in the mineral processing group.

TABLE OF CONTENTS

ABSTRACT	i
RESUME	ii
ACKNOWLEDGEMENTS	iv
TABLE OF CONTENTS	v
NOMENCLATURE	xi
LIST OF FIGURES	xv
LIST OF TABLES	xx
LIST OF APPENDICES	xxi

CHAPTER 1

INTRODUCTION 1

1.1 SPHALERITE CRYSTALLOGRAPHY 1

1.2 FLOTATION OF SPHALERITE 2

1.2.1 General Observations 2

1.2.2 With Activation 4

1.2.3 Without (Deliberate) Activation 5

1.3 STATEMENT OF THE PROBLEM AND OBJECTIVES 7

CHAPTER 2

SURFACE ANALYSIS TECHNIQUES AND

APPLICATIONS 8

2.1 INFRARED SPECTROSCOPY (IR) 8

2.1.1 Transmission IR Spectroscopy 8

2.1.2 Attenuated Total Reflection 10

2.1.3 Emission IR Spectroscopy	11
2.1.4 Fourier Transform Infrared (FTIR)	11
2.1.5 Diffuse Reflectance Infrared Fourier Transform Spectroscopy (DRIFTS)	12
2.2 PHOTO-ACOUSTIC SPECTROSCOPY (PAS)	14
2.3 MODERN VACUUM TECHNIQUES	16
2.2.1 Photoemission Spectroscopy	17
2.2.2 Auger Electron Spectroscopy (AES)	19
2.2.3 Secondary Ion Mass Spectrometry (SIMS)	20
2.2.4 Laser Induced Mass Spectrometry (LIMS)	22
2.2.5 Other (Vacuum) Techniques	23
2.4 RAMAN SPECTROSCOPY	24
2.5 SUMMARY	26

CHAPTER 3

EXPERIMENTAL MATERIALS AND

APPARATUS	29
3.1 MATERIALS	29
3.1.1 Sphalerite	29
3.1.2 Bulk Precipitates from Iron and Xanthate Solution	29
3.1.3 Reagents	30
3.2 FLOTATION AND SURFACE CHARGE APPARATUS	30
3.2.1 Microflotation	30
3.2.2 Mobile Mini Continuous Flotation System	31
3.2.3 Zeta Potential Measurement	35

3.3 BULK ANALYSIS APPARATUS	36
3.3.1 <i>UV-vis Spectrophotometry</i>	36
3.3.2 <i>Infrared Spectroscopy</i>	36
3.3.3 <i>X-Ray Diffraction</i>	36
3.3.4 <i>Mössbauer Spectroscopy</i>	37
3.4 SURFACE ANALYSIS APPARATUS	37
3.4.1 <i>XPS</i>	37
3.4.2 <i>DRIFTS</i>	37
3.4.3 <i>ATR</i>	38

CHAPTER 4

EXPERIMENTAL RESULTS	39
4.1 FLOTATION AND ZETA POTENTIAL	39
4.1.1 <i>Single Mineral (Micro) Flotation</i>	39
4.1.2 <i>Continuous (Minicell)</i>	41
4.1.3 <i>Zeta Potential Measurements</i>	44
4.1.4 <i>Adsorption of Ferrous Ions</i>	47
4.1.5 <i>Iron Xanthate Precipitates</i>	47
4.2 X-RAY PHOTOELECTRON SPECTROSCOPY	47
4.3 DRIFTS	55
4.4 ATR	57
4.5 ULTRA-VIOLET SPECTRA	59
4.6 INFRARED ABSORPTION SPECTRA	61
4.7 X-RAY DIFFRACTION	63
4.8 MÖSSBAUER MEASUREMENTS	64

CHAPTER 5**SURFACE IONIZATION AND****COMPLEXATION AT THE****SPHALERITE/WATER INTERFACE 66****5.1 INTRODUCTION 66****5.2 SURFACE IONIZATION EQUILIBRIA AND THE ELECTRICAL
DOUBLE LAYER 67****5.3 SITE-BINDING MODEL 68****5.4 THE CHARGE BALANCE 70***5.4.1 Surface Mass Balance 71**5.4.2 Double Layer Theories 71***5.5 NUMERICAL PROCEDURES 72****5.6 DISCUSSION 77****5.6 CONCLUDING REMARKS 80****CHAPTER 6****DEVELOPMENT OF MECHANISM OF IRON****ACTIVATION OF SPHALERITE 82****6.1 FLOTATION 82****6.2 SURFACE CHARGE 82****6.3 IRON XANTHATE PRECIPITATE 85***6.3.1 Infrared Studies 85**6.3.2 Other Studies (Mössbauer, UV and XRD) 86**6.3.3 Suggested Compounds 86*

6.3.4 <i>Hydrophobicity</i>	87
6.4 PROPOSED MECHANISM	87
6.5 THE MECHANISM AND SURFACE ANALYSIS	88
CHAPTER 7	
CONCLUSIONS AND SUGGESTIONS FOR FUTURE WORK	90
7.1 CONCLUSIONS	90
7.1.1 <i>Flotation</i>	90
7.1.2 <i>Bulk Flotation and Analysis</i>	90
7.1.3 <i>Surface Analysis</i>	91
7.1.4 <i>Proposed Mechanism of Sphalerite Flotation with Fe²⁺ Ions</i>	91
7.1.5 <i>Surface Complexation at Sphalerite/Water Interface</i>	91
7.2 CLAIMS FOR ORIGINAL RESEARCH	92
7.3 SUGGESTIONS FOR FUTURE WORK	92
REFERENCES	93
APPENDIX 1	
DETERMINATION OF ELECTROPHORETIC MOBILITIES USING MASS TRANSPORT METHOD: THE ZETA POTENTIAL ANALYZER	113
GENERAL DESCRIPTION	113
THEORY	114

APPENDIX 2**MATLAB™ PROGRAM ON SURFACE****IONIZATION AND COMPLEXATION AT****THE SPHALERITE/WATER INTERFACE .. 118****SINGLE SPHALERITE SYSTEM 118****MATLAB SCRIPT M-FILE 119***Zetacal1.M* 119*Zetafun1.M* 120*Zetafun2.M* 120*Constr.M* 121*Fminu.M* 132

NOMENCLATURE

\square	the terms in square brackets refer to concentrations, mol/l
AES	Auger electron spectroscopy
ATR	attenuated total reflectance
B	the conversion factor from mol/l to C/m ² of charge
c	the concentration of the supporting electrolyte, mol/l
c'	the concentration of sphalerite, g/dm ³
C_1	the capacitance of the inner region of the compact layer, F/m ²
C_2	the capacitance of the outer region of the compact layer, F/m ²
D	the dielectric constant of the liquid
DRIFTS	diffuse reflectance infrared Fourier transform spectroscopy
e	electron charge, C
E_B	the binding energy of the electron corresponding to the energy level from which the electron is excited
EDC	energy distribution curve
E_K	the kinetic energy of the emitted electron
EELS	electron energy loss spectroscopy
ESCA	electron spectroscopy for chemical analysis
EXAFS	extended x-ray absorption fine structure
f	the modulation frequency, (Hz)
F	Faraday constant, C/mol
FTIR	Fourier transform infrared
i.e.p.	the isoelectric point, $\sigma_d=0$

<i>I</i>	the current, A
IR	infrared spectroscopy
LIMS	laser induced ionization mass spectroscopy
NEXAFS	near extended x-ray absorption fine structure
N_s	the total number of surface sites available, sites/m ²
p.z.c.	the point of zero surface charge, $\sigma_0=0$
PAS	photo-acoustic spectroscopy
PES	photoelectron energy spectrum
<i>s</i>	the subscript <i>s</i> denotes the surface
<i>s</i>	the scattering coefficient
<i>S_a</i>	the surface area, m ² /g
SERS	surface enhanced Raman spectroscopy
SIMS	secondary ion mass spectroscopy
SZn, ZnS, ...,	surface species
<i>t</i>	the time, s
<i>T</i>	absolute temperature, K
UHV	ultra high vacuum
UPS	ultraviolet photoemission spectroscopy
VIR	visual infrared
XANES	x-ray absorption near edge structure
XPS	X-ray photoelectron spectroscopy
<i>z</i>	the charge of species

GREEK SYMBOLS

α	fractional concentration of species at the surface in CHAPTER 5
α	the thermal diffusivity in PAS
χ	the thermal conductivity
C	the specific heat of the sample material
ΔW	the net change of mass of the cell, g
ϕ	the volume fraction of the sample in zeta potential measurement
ϕ	the work function of the spectrometer in XPS
$h\nu$	the energy of the exciting X-ray
η	the liquid specific viscosity, P (g cm ⁻¹ s ⁻¹)
k	Boltzmann constant, J/K
κ	the optical absorption coefficient
λ	the specific conductance, Ω^{-1} cm ⁻¹
μ_s	the thermal diffusion length
ρ	the density of material
ρ_p	the density of the particles in the suspension, g cm ⁻³
ρ_l	the density of the liquid at a given temperature, g cm ⁻³
σ_0	the net charge densities at the surface, C/m ²
σ_β	the net charge densities in the plane of specifically adsorbed counter-ions, C/m ²
σ_d	the net charge densities in the diffuse layer, C/m ²
Ψ_0	the mean potentials in the plane of surface charge, volts

ψ_{β}	the mean potentials in the plane of specifically adsorbed counter-ions, volts
ψ_d	the mean potential in the plane of diffuse layer, volts
ζ	the electrokinetic (or zeta) potential near to the beginning of the diffuse double layer, volts

LIST OF FIGURES

Figure 1.1	Structure of sphalerite	1
Figure 2.1	Schematic picture of spectroscopic techniques	9
Figure 2.2	ATR infrared cell for adsorption studies of the mineral-aqueous solution interface	10
Figure 2.3	Schematic view of a photoacoustic cell. (Ph) primary photon beam; (W) window; (G) gas; (S) sample; (AT) acoustic transducer	14
Figure 3.1	Schematic illustration of the continuous mini flotation system	31
Figure 3.2	Measuring system of pulp potential, pH and dissolved oxygen	32
Figure 3.3	Minicell circuit for Zn flotation	33
Figure 3.4	Simplified flowsheet of Kidd Greek B and C divisions and minicell sample location	34
Figure 4.1	The relationship between recovery of sphalerite and pH with 1×10^{-4} M sodium isopropyl xanthate under various conditions	39
Figure 4.2	The relationship between recovery of sphalerite and the concentration of ferrous ions with 1×10^{-4} M sodium isopropyl xanthate	40
Figure 4.3	The relationship between recovery of sphalerite and pH with 1×10^{-4} M sodium isopropyl xanthate: effect of air and nitrogen (microflotation)	40
Figure 4.4	Cumulative Zn grade/recovery curves in Zn concentrate (Zn feed grade = 4-4.5%) (continuous minicell tests)	41
Figure 4.5	Cumulative Zn grade/recovery curves in Zn concentrate (Zn feed grade = 3-4%)	42
Figure 4.6	Zn recovery vs. the difference in recovery between Zn and Fe	42

Figure 4.7	Zn and Fe recoveries vs oxygen content	43
Figure 4.8	pH, DO and Ep in the first cell (test No. C3-1204)	44
Figure 4.9	The zeta potential of sphalerite as a function of pH in the presence of xanthate and ferrous ions (ionic strength controlled by 1×10^{-1} NaCl)	45
Figure 4.10	The zeta potential of sphalerite as a function of pH in the presence of xanthate and ferric ions (ionic strength controlled by 1×10^{-1} NaCl)	45
Figure 4.11	The relationship between zeta potential of sphalerite and the concentration of ferrous ions added at different pH (ionic strength controlled by 1×10^{-1} NaCl)	46
Figure 4.12	The relationship between zeta potential of sphalerite and pH in the presence of 10 ppm of ferrous ions (ionic strength is controlled by 1×10^{-1} M NaCl)	47
Figure 4.13	The change in ferrous ion (1 ppm initially), zinc ion and oxygen concentration and solution pH (initially pH 10), as a function of contact time with sphalerite (1 g in 50 mL)	48
Figure 4.14	The properties of iron xanthate precipitate prepared by mixing 1 M ferrous sulphate with 1 M sodium isopropyl xanthate at different pH (ionic strength controlled by 1×10^{-1} M NaCl)	49
Figure 4.15	XPS spectra of the Zn_{2p} region of sphalerite sample treated with: (a) distilled water, (b) 1×10^{-2} mol/L Fe^{3+} , (c) 1×10^{-2} mol/L Fe^{2+} , (d) 1×10^{-2} mol/L Fe^{2+} , followed by 1×10^{-3} M xanthate	50
Figure 4.16	XPS spectra of the Fe_{2p} region of sphalerite sample treated with: (a) distilled water, (b) 1×10^{-2} mol/L Fe^{3+} , (c) 1×10^{-2} mol/L Fe^{2+} , (d) 1×10^{-2} mol/L Fe^{2+} , followed by 1×10^{-3} M xanthate	50

- Figure 4.17** XPS spectra of the S_{2p} region of sphalerite sample treated with: (a) distilled water, (b) 1×10^{-2} mol/L Fe^{3+} , (c) 1×10^{-2} mol/L Fe^{2+} , (d) 1×10^{-2} mol/L Fe^{2+} , followed by 1×10^{-3} M xanthate 51
- Figure 4.18** XPS spectrum of the S_{2p} region of sphalerite that has been treated with 1×10^{-2} mol/L Fe^{2+} , followed by 1×10^{-3} M xanthate, showing the deconvolution of the band into components assignable to xanthate and sulfide (higher and lower binding energies, respectively) 54
- Figure 4.19** XPS spectra of the O_{1s} region of sphalerite sample treated with 1×10^{-2} mol/L Fe^{2+} , followed by 1×10^{-3} M xanthate. The component to higher (I) and lower (II) binding energies are assigned to oxygen present as hydroxide and oxide, respectively 55
- Figure 4.20** DRIFT spectra of sphalerite samples treated with: (a) 1×10^{-2} mol/L Fe^{2+} showing the presence of γ - $FeOOH$ and (b) sphalerite treated with 1×10^{-2} mol/L Fe^{3+} 56
- Figure 4.21** ATR spectra obtained from a sphalerite crystal treated with: (a) distilled water, (b) 1×10^{-3} mol/L xanthate, (c) washed from (b) and 1×10^{-2} mol/L Fe^{2+} added, (d) washed from (c) followed by addition of 1×10^{-3} M xanthate, (e) washing with distilled water from (d) showing the presence of intense bands due to a surface bound complex, (f) as for (e) but Fe^{3+} used in step (c) instead of Fe^{2+} showing no bands associated with a surface-bound complex. 57
- Figure 4.22** UV spectra of acetone solution derived from bulk precipitates prepared at three pHs 60
- Figure 4.23** UV spectra of acetone solutions of xanthate and dixanthogen in different acetone concentration 60
- Figure 4.24** Infrared spectrum of sodium isopropyl xanthate 61

Figure 4.25	Infrared spectrum of precipitate formed from ferrous sulphate and sodium isopropyl xanthate solution at pH 8	62
Figure 4.26	Infrared spectrum of precipitate formed from ferrous sulphate and sodium isopropyl xanthate solution at pH 10	62
Figure 4.27	Precipitate x-ray diffraction patterns	63
Figure 4.28	Fe-OH-X precipitate x-ray diffraction pattern	64
Figure 4.29	Mössbauer spectra of bulk precipitates from ferrous sulphate and xanthate solution at different pH	65
Figure 4.30	Summary of Mössbauer spectrum fits	65
Figure 5.1	Schematic representation of the electrical double layer around the sphalerite particle	68
Figure 5.2	Strategy of the program	73
Figure 5.3	The zeta potential of sphalerite as a function of pH at different NaCl concentrations	74
Figure 5.4	A fractional distribution diagram of the species on sphalerite surface as a function of pH	75
Figure 5.5a	Surface charge density and zeta potential of boehmite as a function of pH (Surf. area: 44 m ² /g) (The data were provided by authors (Woods, Fornasiero and Ralston, 1990))	76
Figure 5.5b	Surface charge density and zeta potential of boehmite as a function of pH (Surf. area: 0.044 m ² /g) (The data were provided by authors (Woods, Fornasiero and Ralston, 1990))	76
Figure 5.6	A fractional distribution diagram of the species on boehmite surface	78
Figure 6.1	Logarithmic concentration diagram for 1 × 10 ⁻⁵ M Fe ²⁺ from Acar and Somasundaran, 1992	83

- Figure 6.2** Logarithmic concentration diagram for 1×10^{-4} M Fe^{3+} . Equilibrium data from Butler, 1964 83
- Figure A1** Exploded view of mass-transport chamber 112

LIST OF TABLES

Table 1.1	Crystallographic data	2
Table 2.1	Comparison of various spectroscopic techniques in flotation studies	27
Table 2.2	Comparison of spectroscopic techniques available in mineral processing studies	27
Table 4.1	Band maxima (eV) and widths obtained from XPS data	49
Table 5.1	Best-fit parameters for the surface-charge and zeta-potential calculation of sphalerite using computational method with MATLAB software	74
Table 5.2a	Best-fit parameters for the surface-charge and zeta-potential calculation of boehmite using computational method with MATLAB software ($S_a = 44 \text{ m}^2/\text{g}$)	77
Table 5.2b	Best-fit parameters for the surface-charge and zeta-potential calculation of boehmite using computational method with MATLAB software ($S_a = 0.044 \text{ m}^2/\text{g}$)	77
Table A1	Physical constants of water as a function of temperature	116

LIST OF APPENDICES

Appendix 1	Determination of electrophoretic mobilities using mass transport method: The zeta potential analyzer	112
Appendix 2	MATLAB™ program on surface ionization and complexation at the sphalerite/water interface	117

CHAPTER 1

INTRODUCTION

1.1 SPHALERITE CRYSTALLOGRAPHY

Sphalerite ($\text{Zn},[\text{Fe}]\text{S}$) is the principal mineral of zinc, and is very widely distributed. In the sphalerite crystal, the S atoms are close-packed and the Zn atoms are in half the tetrahedral interstices. This arrangement is explained in terms of a donor-acceptor mechanism, Zn^{2+} losing two valence s -electrons at the expense of S^{2-} , retaining ten d -electrons and needing eight electrons in order to achieve a krypton-like configuration. The four pairs are formed from four neighboring S^{2-} anions in a tetrahedral arrangement (Kostov, 1982a). Each S is in turn tetrahedrally coordinated by Zn. The bonds have a large covalent character. In the cubic system, the Zn and S atoms are each in a face-centered cubic lattice, displaced from each other in the (111) direction. In the hexagonal type, the Zn atoms are in a lattice like that of the S atoms, but displaced along the c -axis. The S-S distance is larger than the ionic diameter of sulphur, 3.68 Å, so that direct S-S covalence may be neglected (Shuey, 1975). The surface concentration of Zn on a two zinc atoms per plane of the unit cell is 11.4 $\mu\text{moles}/\text{m}^2$ (Rönngren et al., 1991). The structure of sphalerite is shown in Fig. 1.1, and crystallographic data (Shuey, 1975 and Kostov, 1982b) are given in Table 1.1.

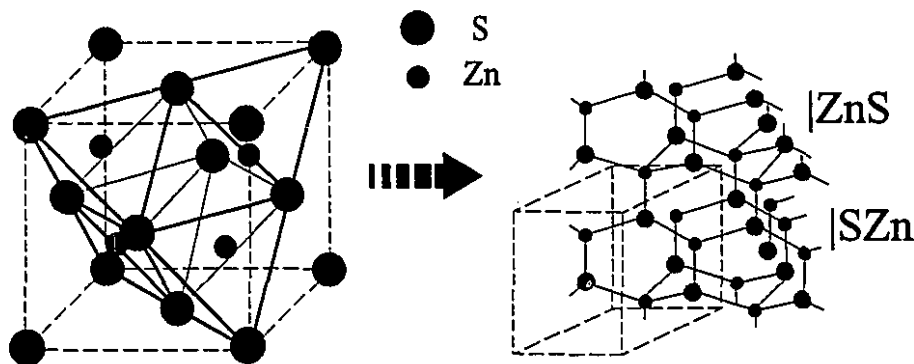


Figure 1.1. Structure of sphalerite

Table 1.1 Crystallographic data

System:	Cubic	Hexagonal
Space group:	216; T_d^2	186; C_{6v}^4
ZnS per cc:	2.52×10^{23}	
Zn-S:	2.34 Å	
S-S:	3.82 Å	

Sphalerite is resinous in appearance and varies in color from light tan to black, depending upon the content of substitutional iron. The mineral is referred to as marmatite when the ratio of Fe:Zn exceeds 1:8; above 5:6 the sphalerite structure no longer exists (Mason, 1968).

1.2 FLOTATION OF SPHALERITE

1.2.1 General Observations

The flotation characteristics of sphalerite have received considerable attention both in the absence and presence of activating metal ions (Gaudin, 1930; Ralston et al., 1930; Wark and Wark, 1936; Gaudin et al., 1959; Steininger, 1968; Girczys and Laskowski, 1972; Stewart and Finkelstein, 1973). However, a full understanding of the mechanisms involved in activation, xanthate adsorption and flotation is still lacking. This is especially true in the absence of deliberately added activating ions: For example, some investigators have observed flotation with xanthates whereas others have not (Wilkinson, 1935; Steininger, 1968; Girczys and Laskowski, 1972). These differences in flotation response may have been due to the differences in solution contaminants, iron content of the mineral or in the oxidation characteristics of the specimen involved.

Sphalerite commonly occurs in association with galena, chalcopyrite, pyrite and pyrrhotite. Consequently, the flotation of sphalerite is largely concerned with the problems encountered in separating it from these other sulphide minerals. A common approach is first to remove chalcopyrite and galena by flotation in a moderately alkaline pulp, with the simultaneous depression of sphalerite by one or other of sulphur dioxide, cyanide or zinc

sulphate. Sphalerite is subsequently activated with copper sulphate in a pulp made alkaline with lime and floated with a xanthate collector.

Alternatively, sphalerite can be activated by the addition of copper sulphate and collected in a bulk concentrate with the copper and lead sulphides. Sphalerite is then deactivated with cyanide and the components of the bulk concentrate can be separated according to the same principles as mentioned in above paragraph (Lozyk, 1978; Hall et al. 1990). In practice, the production of clean zinc sulphide concentrates at high recovery is a difficult problem, and is the subject of much research.

It is common practice to float zinc sulphides at a rougher pH 8.5 to 11.5 with cleaning at a pH above 10. However, some different routes for selective flotation of sphalerite have been considered. Labonté et al. (1989) illustrated the application of novel approaches based on an understanding of the system chemistry, including collectorless flotation of chalcopyrite, reverse flotation of pyrite from zinc concentrate, the use of N_2 and column flotation, all designed to increase recoveries and separation of sphalerite from complex ores. Some of these approaches have shown a clear potential in practice or plant trials (Kizilirmakli, 1989; Bogdanov et al., 1991; Xu et al., 1992).

In addition to alternative processes, new collectors with improved selectivity may eventually play an important role in the treatment of complex ores. In sulphide mineral flotation, two new collector families have been characterized by Klimpel and Fee (1993), one based on chelation chemistry, the other on sulphur association chemistry.

Chelate-forming compounds have long been known to selectively complex metal cations and are widely used in analytical chemistry. Marabini et al. (1993) synthesized a new class of collectors, Mercapto-Benzo-Oxazoles (MBO), which showed selective action on copper sulphides in the presence of Pb-Zn-Fe sulphides. The collectors have a mixed aliphatic-aromatic structure and contain functional groups which form chelates with copper. The results obtained showed that the synthesized collector was much better than potassium-amyloxanthate (KAX) as regards flotation rate and selectivity towards Pb and Zn sulphides. Moreover, it is possible to work at natural pH (6-7). However, the stability and industrial application of these new reagents have yet to be investigated thoroughly.

A potentially important research finding reported on sulphide minerals has been the tendency for certain minerals to exhibit self-induced floatability (Gardner and Woods, 1979; Fuerstenau and Sabacky, 1981; Yoon, 1981; Luttrell and Yoon, 1984; Walker et al., 1986). This phenomena is often referred to as collectorless flotation and is related to controlling the electrochemical potential during the flotation process. Many studies have corroborated the fact that sulphur has a significant effect on the increased hydrophobic nature of sulphides in the absence of normal collecting reagents; however, the presence of elemental sulphur on the mineral surface has not always been detected on the minerals recovered by collectorless flotation (Yoon, 1981). From this fact, it is then assumed that the phenomena is related to the development of hydrophobic species, such as metal deficient sulphide species and/or polysulphides as proposed by Hayes and Ralston (1988), on the mineral surface as oxidation proceeds from initial reducing conditions in grinding to the final oxidation state reached in flotation.

Self-induced (or collectorless) floatability of sphalerite was apparently first reported by Rey and Formanek (1960); other examples were reported by Boyce et al. (1970), and Stewart and Finkelstein, (1973). It is, however, more commonly encountered for galena, PbS (Boyce et al., 1970; Sen et al., 1975), and especially for chalcopyrite, CuFeS_2 (Stewart and Finkelstein, 1973; Lepetic, 1973; Finkelstein et al., 1975; Heyes and Trahar, 1977; Leroux et al., 1989). There are some references also to self-induced floatability of pyrite, FeS_2 (Stewart and Finkelstein, 1973; Finkelstein et al., 1975). There is at least one case where collectorless flotation was practiced on a plant scale, namely the flotation of ZnS and PbS at the Tsumeb mine in S.W. Africa (Boyce et al., 1970). However, the S-enrichment mechanism appears to have been excluded as the cause of self-induced floatability in that case (Finkelstein et al., 1975), which means one must look elsewhere for an explanation of this unusual behavior.

1.2.2 With Activation

The flotation of sphalerite in the presence of Cu^{2+} ions has been reviewed in detail by Gaudin (1957), Finkelstein and Allison (1976) and Fuerstenau (1982). In the case of ethyl xanthate the amount adsorbed on the surface of Cu-activated sphalerite was small

reaching only about 15% with respect to the statistical monolayer (Gaudin, 1957; Yonezawa, 1961; Pomianowski and Leja, 1964; Allison et al., 1972; Pomianowski et al., 1975). It was also found that the adsorption product formed could be easily washed off with water.

Yelloji and Natarajan (1989) studied the effect of galvanic interaction between grinding media and sphalerite on flotation. They found that contact of sphalerite with steel grinding medium lowered its floatability due to the iron contamination of the mineral surface brought about by electrochemical, i.e. galvanic, interaction. However, the presence of a sufficient concentration of an activator (like Cu^{2+}) during the galvanic contact helped in minimizing the deleterious effect of the galvanic interaction. The presence of a collector, either alone or before the addition of the activator, effectively prevented such a modification process.

1.2.3 Without (Deliberate) Activation

It was observed in the work of Yelloji and Natarajan (1989) that some of the sphalerite samples became floatable just after addition of a short-chain xanthate. Such behavior of sphalerite may be due to accidental activation e.g. by Cu^{2+} derived from soluble, oxidized copper minerals (Gaudin, 1957 and Bogdanov et al., 1965).

In 1990, Yelloji and Natarajan found that the flotation of sphalerite after contacting with galena for upto 4 hrs in the presence of oxygen was enhanced from its initial value of 53% (in the absence of contact) to about 77% for conditions where the sphalerite was floated in the presence of collector alone. The flotation recovery of sphalerite after 4 hr contact with both chalcopyrite and galena in the presence of oxygen was found to be increased to about 91% from the initial value of 53%, for the conditions where the sphalerite was floated in the presence of collector alone after contact with steel. Interestingly they did not give an explanation for the initial 53% recovery of sphalerite.

In practice, in addition to the Tsumeb mine in S.W. Africa cited before, the Zinkgruvan concentrator of the Vieille Montagne Company in Sweden is another example of sphalerite flotation without intentional activation (Mellberg, 1982). It was assumed that

sphalerite floated due to autogenous activation by Pb^{2+} ions, released in the primary grinding stage. However, it is difficult to explain the separation between galena and lead-activated sphalerite achieved in the separation circuit.

Flotation of sphalerite without deliberate Cu addition is usually attributed to accidental activation by Cu or Pb ions. In some instances, however, this explanation is not adequate.

Girczys and Laskowski (1972) observed good flotation of sphalerite which was in contact with ethyl or amyl xanthate in acidic solution. They explained this phenomenon by the presence of iron (1.7%) in the sample catalyzing the oxidation of the xanthate to dixanthogen, which was considered responsible for the sphalerite flotation; this explanation has not been confirmed.

Similar conclusions to those of Girczys and Laskowski were reached by Mukherjee and Sen (1976). They discovered that a series of sphalerites of varying iron content were floatable with potassium ethyl xanthate and diethyl xanthogen as collectors without using an activator in acid solution. The high iron samples were more floatable than low iron samples with ethyl xanthate; when using diethyl xanthogen as collector, reverse results were obtained (i.e. the low iron samples floated more readily).

Since Mukherjee and Sen did not present the experimental data, their interpretation was criticized. As can be concluded, even from the work of Mukherjee and Sen, the influence of iron in the sphalerite structure cannot be too critical to sphalerite flotation. The change in iron content from 0.13 to 3.9 wt.%, i.e. a thirty fold increase, caused a change in recovery from 45 to 55% only (Mukherjee and Sen, 1976). Finkelstein and Allison (1976) (reporting on work of Clifford (1971)) did not find differences in floatability of samples having 0.3 to 8.8% of iron. Also Fuerstenau et al. (1974) did not observe differences in flotation between sphalerite and marmatite (the high Fe end member).

Finkelstein and Allison (1976) suggested that the sphalerite floatability and xanthate adsorption reported in the studies of Girczys and Laskowski (1972) resulted from the occurrence of copper in the ore, which activated the sphalerite. Unfortunately, neither

Girczys and Laskowski (1972) nor Mukherjee and Sen (1976) reported on the copper content.

There is some circumstantial evidence that alkaline pH alone is capable of significant sphalerite flotation. McTavish (1980), for example, at Brunswick Mining found elevated pH caused Zn loss to the Cu/Pb bulk concentrate.

Leroux et al. (1987) found that sphalerite could be floated by xanthate from a Pb/Zn ore without Cu activation: They found a combination of xanthate, pH 9.5 to 11 and iron ions were required. A mechanism based on activation by $\text{Fe}(\text{OH})_2$, the Fe^{2+} ions being derived from superficial oxidation of the pyrite in the ore, was suggested. Possible flotation due to natural floatability or self-induced flotation was ruled out.

This Ph. D. research originated from the findings of Leroux et al.

1.3 STATEMENT OF THE PROBLEM AND OBJECTIVES

From this review of sphalerite flotation, it can be seen that sphalerite is one of the minerals which requires activation for effective adsorption of xanthate and flotation. The most commonly used activator is Cu^{2+} derived generally from CuSO_4 . Certain other heavy metal ions have also been used as activators (Sutherland and Wark, 1955; Gaudin, 1957; Finkelstein and Allison, 1976). In some cases, sphalerite is accidentally activated by metallic ions in the pulp: one such ion, which has received limited attention, appears to be Fe^{2+} (Leroux et al., 1987).

To better control the flotation of sphalerite, and to develop new strategies or new reagents for improving separation efficiency from other sulphide minerals, in particular galena, chalcopyrite and pyrite, it is necessary to understand the role of metal ions in activating sphalerite.

The objective of this research program, therefore, is to *determine the mechanism of sphalerite flotation in the presence of iron ions.*

To this end the following were employed: flotation tests (micro, batch and continuous), electrophoresis; and surface analysis using various spectroscopic techniques.

CHAPTER 2

SURFACE ANALYSIS TECHNIQUES AND APPLICATIONS

Surface properties play the essential role in many mineral processing systems such as flotation, selective flocculation, bioleaching, etc. In particular, an understanding of interaction mechanisms of different reagents (collectors, regulators, flocculants, etc.) with the mineral surface in an aqueous medium is of crucial importance in achieving systematic advances in the technology.

The general definition of a surface is that of a boundary layer of one phase at its interface with another. Surface analysis involves the use of vibrational, electron or ion spectroscopic and microscopic techniques for the study of material at the atomic/molecular level. Solid-vacuum interfaces provide ready access to a number of spectroscopic probes. On the other hand, interfacial phenomenon in a system involving two solid phases are particularly difficult because in most cases both phases are opaque to the available probes. The mineral-solution interface poses an intermediate level of difficulty. The relatively few techniques available for *in situ* analysis of mineral-water interfaces, often make it necessary to use a combination of methods.

2.1 INFRARED SPECTROSCOPY (IR)

Infrared spectroscopy is employed to study the structure of molecules. It permits identification of substances from their chemical and crystalline character (Farmer, 1974), and some aspects are well documented in books by Little (1966) and Hair (1967). Infrared spectroscopy can be performed in transmission, reflection and emission modes (Fig. 2.1).

2.1.1 *Transmission IR Spectroscopy*

In transmission mode, the part of the radiation that travels through the sample is detected. Absorption at the surface and in the bulk is thus ascertained. Therefore, to obtain

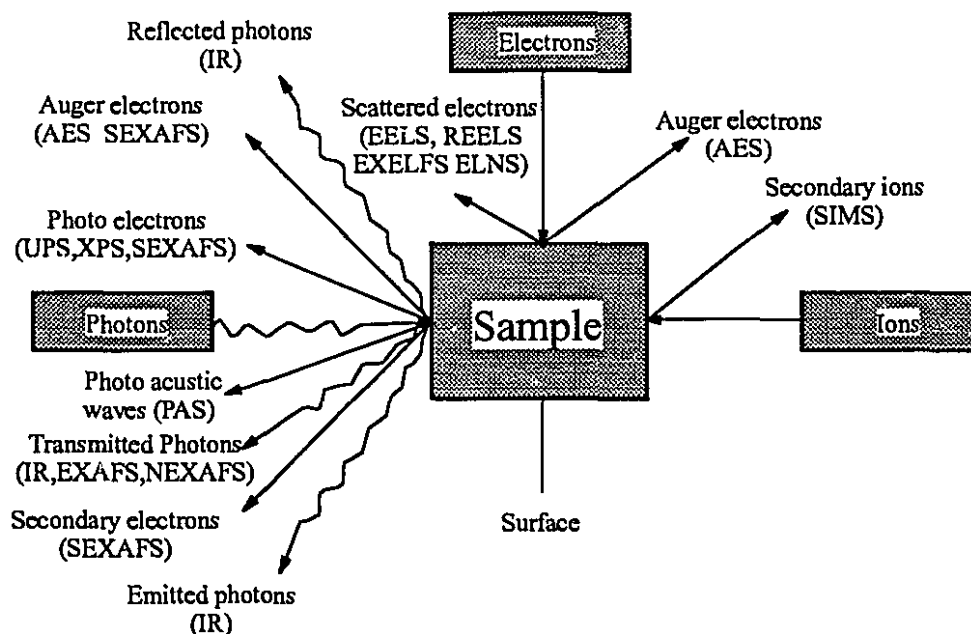
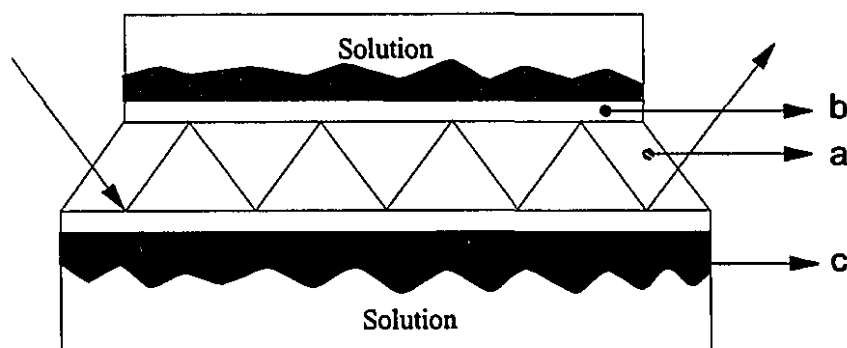


Figure 2.1 Schematic picture of spectroscopic techniques

information on the surface, the surface/volume ratio must be maximized. For this reason, the techniques most commonly adopted, namely KBr pellets and Nujol mull, utilize (dry) powdered solid samples. It is not possible to obtain *in situ* measurements since the absorption spectrum of the water obscures a good part of the analytical range of the experimental spectrum. Many studies on mineral surface/collector interaction have been performed *ex situ*, by comparing treated with untreated minerals (Marabini and Rinelli, 1982; Garbassi and Marabini, 1986). From major changes such as shifting, and the formation and/or disappearance of peaks in the experimental spectrum, IR transmission spectroscopy provides an indication of chemical bond formation between the mineral and the collector (Marabini and Cozza, 1988). One of the main drawbacks, in the case of chemisorption phenomena, is that the solid residue may contain not only the mineral and the surface-adsorbed species but also any agglomerates formed in solution and precipitated in bulk form. In order to avoid this limitation, Marabini and Cozza (1988) developed a double filtering method and used it to clarify the adsorption of potassium ethyl xanthate on cerussite by highlighting breakaway and corrosion phenomena that would not otherwise be revealed.

2.1.2 Attenuated Total Reflection

The Attenuated Total Reflectance (ATR) method is the one most commonly used for the surface study of mineral/aqueous-solution interactions because, being an *in situ* technique, it permits control of the solid-liquid interface to be maintained. To make the measurements, the sample is placed in contact with a crystal (generally Ge, AgCl, or ZnS) whose refractive index is higher than that of the sample. The radiation is incident on the crystal in such a manner that total reflection occurs at the crystal-sample interface (Fig. 2.2). When total reflection occurs, an evanescent wave, whose electric field falls off exponentially with the distance from the surface crystal, is present. Typically the depth of penetration, depending on the optical characteristics of the system, is some ten monolayers (Griffiths and Haseth, 1986; Harrick, 1967).



Key:
a = Germanium reflection element
b = Thin layer of evaporated mineral
c = Adsorbing reagent

Figure 2.2 ATR infrared cell for adsorption studies of the mineral-aqueous solution interface

Studies have been made to investigate the products obtained by adsorption of reagents on minerals. A comparison of qualitative and quantitative results obtained with electrochemical measurements has been reported (Mielczarski et al. 1979, 1983). Mielczarski et al. have characterized both chemical and physical adsorption in a study on the floatability of fluorite treated with sodium dodecyl sulphate.

2.1.3 Emission IR Spectroscopy

Emission IR spectroscopy can be used for surface studies because the emitting part of the solid consists mainly of the outer surface layers. It is easy, therefore, to obtain information on the surface elements even in regions where the bulk absorption bands are predominant. The characteristic sample penetration depth is two to four monolayers. This technique can be used to advantage when it is necessary to analyze samples at temperatures well above ambient conditions (typically 200-250 °C).

For infrared emission studies, the sample to be investigated is deposited on an inert support. If the latter is highly reflective, it is a poor emitter and does not contribute to the observed emission spectrum. The best conditions for this technique are at elevated temperatures, which not many mineral/reagent systems can handle. To the best of the author's knowledge, infrared emission spectra have rarely been reported in the literature on mineral-reagent systems. Primet et al. (1979) reported on an infrared emission spectroscopic study of V_2O_5 , suggesting that this technique is sufficiently sensitive to be considered for *ex situ* investigation of mineral-reagent interactions in flotation systems. A Fourier transform spectrometer was used in the study with multiple scans to enhance the relatively weak signal and ratio the emission spectrum against a black body spectrum.

2.1.4 Fourier Transform Infrared (FTIR)

The instruments generally used in the past were dispersion spectrometers that consisted of a polychromatic radiation source, a monochromator and a detector. However, more recently this type of apparatus has been superseded by interferometers which have greater potential and provide a considerable number of advantages. The most significant advantages of a Fourier Transform Infrared (FTIR) interferometer compared with a dispersion spectrometer are accuracy and precision in wavelength determination. Moreover the entire spectrum is acquired with one single measurement thus permitting a great saving in time, and resolution is constant throughout the spectrum. Last but not least, the sensitivity (i. sensitivity of detector, ii. better signal/noise ratio from the IR interferometers) of the FTIR interferometer is two orders of magnitude higher than that of the older apparatus.

This ensures more accurate determination of trace substances, which is vital in the study of surface interactions when the adsorbate has characteristic peaks in spectral regions where the influence of the bulk is marked.

For the characterization of adsorbates on mineral surfaces, various studies have been made using FTIR interferometers and conventional apparatus for *ex situ* and *in situ* measurements using the KBr-disc (Hu et al., 1986) and ATR techniques (Termes and Richardson, 1986) respectively.

In more recent years, IR and FTIR spectroscopy have found many applications relating to adsorption of collectors on mineral surfaces. De Donato et al. (1990), Cases et al. (1989; 1990a, b) and Kongolo et al. (1990) studied the influence of grinding, pH and oxidation on the adsorption of ethyl-xanthate and amyl-xanthate on galena and pyrite. *In situ* FTIR spectroscopy was used by Cross et al. (1991) to study the conformation of adsorbed species on fluorite and alumina and to determine the adsorption density of collectors on the mineral surface. Similar studies have been performed by Leppinen et al. (1989) on adsorption of ethyl-xanthate on chalcocite, chalcopyrite, pyrite and galena.

2.1.5 Diffuse Reflectance Infrared Fourier Transform Spectroscopy (DRIFTS)

Diffuse reflection results from the multiple scattering and partial absorption of the light flux impingement on (ideally) a matte-finish surface (Wendlandt and Hecht, 1966; and Kortüm, 1969). For a perfect diffuse reflector, the reflected radiation is unpolarized and its angular distribution is isotropic. In practice, since an ideal diffuse reflector does not exist, the reflected radiation also has a specular component which arises from mirror or regular reflection and is therefore polarized.

The dependence of diffuse reflection on the optical absorption coefficient and the scattering properties of the sample can be related to the relative reflectance $r_{\infty} = r_{sam}/r_{ref} = S/R$ by use of the Kubelka-Munk (K-M) equation

$$\kappa/s = (1 - r_{\infty})^2/2r_{\infty} \quad (2.1)$$

where κ is the optical absorption coefficient and s is the scattering coefficient. The K-M theory assumes an infinitely thick sample (a condition that is usually met for scattering

powders 1-3 mm thick), diffuse illumination, and the complete absence of specular reflection. The right side of eq. 2.1 is commonly referred to as the K-M function. A plot of this function vs. concentration is linear with a slope of s^{-1} for a limited range of concentrations. The K-M function is dominated by the absorption coefficient for strongly absorbing samples and by the scattering coefficient for weakly absorbing materials. The absorption and scattering coefficients also determine the effective depth of penetration of the incident light into the sample. For weakly absorbing materials, an increase in scattering significantly decreases the depth of penetration and results in a decrease in the fraction of light available for absorption. This causes an increase in the relative reflectance. For strongly absorbing samples, the depth of penetration is small (ca. $0.1 \mu\text{m}$) and is relatively unaffected by changes in scattering or absorption. When this is the case, the DR spectrum can be considered to be optically saturated.

Persson etc. (1991) analysed the chemical composition of galena, sphalerite and pyrite surfaces after dry and wet grinding, and after treatment with water and aqueous solutions by DRIFTS. They declared that lead alkylxanthate is formed as the only detectable alkylxanthate species on galena surface; chemisorbed complexes of ethylxanthate ions are formed on sphalerite surfaces in aqueous and acetone slurries; and dialkyl dixanthogen is formed as the only surface species in the reaction between oxidized pyrite and aqueous solution of potassium alkylxanthate. They also proposed that the oxidation products of the disulfide ion in pyrite, e.g. $\text{S}_2\text{O}_7^{2-}$ and $\text{S}_2\text{O}_8^{2-}$ are responsible for the oxidation of alkylxanthate ions to dialkyl dixanthogen.

Cases etc. (1993) used DRIFTS and XPS to study the reactions involved in the adsorption-abstraction of K-amyl xanthate on pyrite after fine grinding in a special stainless steel laboratory rod mill. After investigation of floated and non-floated products, they concluded that, for all samples prepared after grinding under basic conditions (pH between 9.0 and 12.0; regulators were NaOH and CaO), only diamyl dixanthogen was present on the pyrite surface after flotation. Hence dixanthogen was considered responsible for the hydrophobicity of the surface. It was demonstrated that in basic conditions, iron compounds and sulphony species are responsible for the process of oxidation of xanthate to dixanthogen.

2.2 PHOTO-ACOUSTIC SPECTROSCOPY (PAS)

A variety of difficulties encountered for mineral samples, such as highly opaque solutions, and optically diffusing samples make analysis difficult with the common optical spectroscopy techniques (UV, VIS, IR). This fact has led to the development of Photo-Acoustic Spectroscopy (PAS), which uses transformation of radiant energy into thermal energy to obtain the spectrum for the sample surface.

The solid sample to be investigated by PAS is enclosed in an acoustically isolated, sealed cell, which is filled with helium gas and fitted with a microphone and a window through which the sample is irradiated.

The photo-acoustic signal is generated when the sample absorbs modulated electromagnetic radiation of a specific wavelength. The energy thus absorbed by the sample is converted into heat by non-radiative de-excitation processes. Since the incident radiation is modulated, the thermal energy created in the

sample will be periodic, at the frequency of the modulation frequency, creating thermal waves that move towards the boundary of the sample. The periodic variation in the temperature at the surface of the sample generates an acoustic wave in the gas surrounding the sample. The acoustic wave propagates through the volume of the cell, and is detected by the microphone (Fig. 2.3).

In general, the PA signal is directly proportional to the power of the incident light flux, the energy of the incident photons, and, in favorable cases, the optical absorption coefficient. In addition to being related to the sample's optical properties, the PA signal is

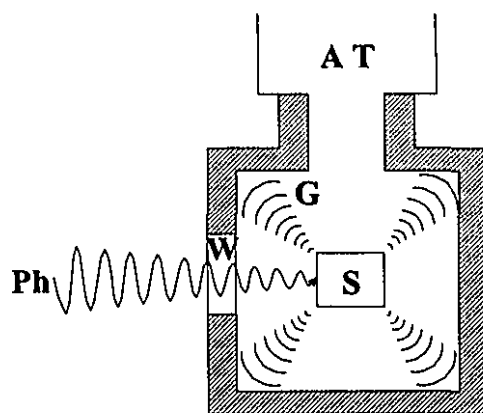


Figure 2.3 Schematic view of a photoacoustic cell. (Ph) primary photon beam; (W) window; (G) gas; (S) sample; (AT) acoustic transducer

also dependent on its thermal properties, specifically the thermal diffusivity, α , which is defined as

$$\alpha = \chi/\rho C \quad (2.2)$$

where χ is the thermal conductivity, ρ the density, and C the specific heat of the sample material. These properties are used, in addition to the modulation frequency, $f(\text{Hz})$, to define a thermal diffusion length, μ_s ,

$$\mu_s = (\alpha/\pi f)^{1/2} \quad (2.3)$$

which is the depth below the sample surface beyond which damping of the photon-generated thermal wave renders the heat produced ineffective for modulating the surface temperature. Thus, only light that is absorbed within the thermal diffusion length contributes to the PA signal. The thermal properties of the transfer gas and, for thermally thin samples, the thermal and optical properties of the substrate or backing material also affect the PA signal.

As the principal effect of the physical phenomenon involved is on the solid-gas contact zone where the thermal energy transfer occurs, the particular feature of the technique is that it mainly investigates the surface. Another aspect of the technique is that it offers the possibility of obtaining depth profiles of the solid by varying the modulation frequency of the incident radiation which is related to the depth of penetration of the incident radiation in the sample. By varying the modulation frequency from 100 Hz to 20 Hz, sampling depths in the range 0.1-100 μm can be investigated (Pao, 1977).

So far, most of the reported PAS studies on solids and related surface effects, use the frequencies in the ultraviolet, visible, and near-infrared domains. The absorption peaks of adsorbed species in this region of the electromagnetic spectrum are broad, structureless, and not very informative. In contrast, Low and Parodi (1980) found sharp, well-defined peaks in this region with PAS for certain adsorbates on silica with a surface area of 300 m^2/g . Less well-defined peaks were observed for adsorbents with smaller surface areas of 50 and 80 m^2/g . The infrared-PAS studies require an infrared laser of sufficient intensity over the whole of the range of infrared frequencies. However, this problem may be overcome by the use of Fourier-transform infrared PAS, which has been used on solids

(Rochley, 1980; Vidrine, 1980) and shows considerable promise for surface studies (Rochley and Delvin, 1980).

Childers etc. (1986) made a direct comparison of the capabilities of photoacoustic (PA) and diffuse reflectance (DR) spectroscopies in the ultraviolet, visible, and near-infrared spectral regions by collecting both types of spectra under nearly identical conditions. In terms of signal-to-noise ratio and spectral definition, the two techniques are virtually indistinguishable for weakly absorbing, finely divided powders. DRS is slightly more sensitive but has a lower saturation limit than does PAS and is more severely affected by changes in particle size. For particles larger than 100 μm , DR spectra are distorted and spectral definition is degraded. In terms of sample preparation, especially when only qualitative results are desired, PAS is clearly superior. For quantitative results both techniques require careful control of particle size, packing density, and total absorption.

So far few PAS studies have been reported on adsorbed species related to flotation. To what extent the generally low surface areas of minerals will be a limiting factor remains to be seen. The relative ease in preparation of the samples should nevertheless encourage some investigation in this direction.

2.3 MODERN VACUUM TECHNIQUES

Over the past few years, many different techniques arising out of the use of different excitations and emission analyses have accumulated. In most such techniques, the solid is placed in an ultra high vacuum (UHV), $<10^{-6}$ torr, and bombarded by photons, electrons, neutrons or ions and the emitted photons, electrons, neutrons or ions are analyzed (Fig. 2.1). In the low photon energy region ($h\nu < 50$ eV) the technique is called Ultraviolet Photoemission (or Photoelectron) Spectroscopy, UPS; in the high energy region ($h\nu > 1$ keV), it is called X-ray Photoelectron Spectroscopy, XPS (also known as Electron Spectroscopy for Chemical Analysis, ESCA). Other common techniques, considered most useful in characterizing the mineral surface, are Auger Electron Spectroscopy, AES, and Secondary Ion Mass Spectroscopy, SIMS. These techniques are often complementary.

The significance of these techniques is that they provide information on surface composition and chemical state (e.g. oxidation state, bonding type) for individual particles and complex mineral mixtures as a function of depth through the surface layers. The principal difficulty in their application is that they are *ex situ* techniques that operate in high vacuum creating some uncertainty in the relationship between the measured compositions or chemical states and those prevailing in the original pulp in the flotation circuit.

2.2.1 Photoemission Spectroscopy

In a typical photoemission apparatus, the energy of the photon source is fixed and the energy distribution of the photoemitted electrons is measured. This method of data acquisition goes by the name of Energy Distribution Curve, EDC (also called Photoelectron Energy Spectrum, PES).

The valence region, mainly investigated using an ultraviolet photon source in the UPS technique gives information on the structure of the valence band. In the XPS technique, the X-ray is used to excite electron emission from core and valence energy levels of the atoms in a solid surface. The kinetic energies of the emitted electrons are analysed in the spectrometer. The basic equation is:

$$h\nu = E_B + E_K + \phi \quad (2.4)$$

where $h\nu$ is the energy of the exciting X-ray,

E_B is the binding energy of the electron corresponding to the energy level from which the electron is excited,

E_K is the kinetic energy of the emitted electron, and

ϕ is the work function of the spectrometer.

This equation allows the E_B of the particular energy level of a given atom to be calculated, which helps in determining the electronic structure of the solid. Although core electrons are not involved in chemical bonding, the core energy levels of atoms are sensitive to structure and bonding. The value of the core level binding energy is determined by the type of atoms present in the solid and the chemical shifts give information on the chemical bonds of the elements, e.g. difference in the oxidation state, difference in

molecular environment, and difference in lattice site. Moreover, quantitative information on the atomic ratio between an element and its environment is given by measurement of the peak area. However, only emitted electrons close to the surface can escape from the solid, those electrons dislodged deeper in the solid are retarded by the material and are unable to escape. Therefore, XPS is a surface sensitive technique, capable of revealing the elemental and chemical composition of the surface and near surface down to a maximum depth of about 50 to 100 Å.

XPS has been used to characterize surfaces of sulphide minerals, particularly the effect of their exposure to air (oxygen) and water. Since this technique requires an ultra-high vacuum, only an *ex situ* investigation is possible. Nevertheless, some useful insight into the surface chemical reactions and products during flotation can be obtained. Unfortunately, direct answers are often obscured by extraneous effects arising from the method used or by the complexity of the chemical systems studied.

Clifford et al. (1975), using XPS, investigated ten natural sulphide minerals. Surface analyses of these minerals were carried out after they had been given the following treatment: (a) comminution in an atmosphere of air and nitrogen; (b) the adsorption of xanthate and dithiophosphate collectors; and (c) the adsorption of modifiers such as $\text{Na}_2\text{Cr}_2\text{O}_7$, SO_2 , starch, sodium cyanide, and CuSO_4 .

Predali et al. (1979) have used XPS to study the pyrite depression mechanism during flotation of a copper-zinc-lead-pyrite ore. They showed that depression occurs through the formation of an iron-oxy-hydroxide or hydroxide on the mineral surface with depressants like CaO. No significant formation of sulphur or oxidized sulphur on the pyrite surface was observed. Surface copper and zinc were also detected on the pyrite surface but these did not seem to be a factor in flotation. Similar characterization studies have been performed by Cecile et al. (1980) on the depression of galena with chromate ions after flotation with xanthate.

Brion (1980) used XPS to characterize the surface of pyrite, chalcopyrite, sphalerite and galena on exposure to air and to water. On their exposure to air, the rate of surface sulphation decreased in the order: $\text{FeS}_2 > \text{CuFeS}_2 > \text{PbS} > \text{ZnS}$. On their exposure

to water, however, FeS_2 , PbS and ZnS did not exhibit any surface degradation, and only CuFeS_2 showed the formation of iron oxy-hydroxide or hydroxide within the first layers.

Ranta et al. (1981) have reported on XPS studies of xanthate adsorption on sulphides. Special care was taken to improve the resolution of XPS spectra by using a monochromatic X-ray source. Further, more care was taken than in the previous studies to prepare the samples and to work at a lower vacuum. These precautions gave a better indication of the potential of XPS in studying xanthate adsorption on sulphide minerals.

Smart (1991) has used XPS and other surface-sensitive techniques to study the surface layers on metal sulphides as single minerals, mixed minerals, synthetic ores and real ores from eight Australian concentrator operations. He found substantial hydroxide content on the sulphide surfaces in three different chemical and physical forms, namely thin (~5-80 nm) layers; oxidised fine particles (0.1-5 μm); and colloidal iron hydroxide spheroids formed by precipitation from solution. He also developed a sampling methodology to introduce slurry to the spectrometer to minimize air exposure of the mineral surfaces.

Xanthate adsorption on various mineral surfaces, galena (Pillai et al., 1983; Page and Hazell, 1989; Buckley and Woods, 1990; Buckley and Woods, 1991), pyrite (Pillai et al., 1985), metals (Johansson et al., 1986; Laajalehto et al., 1988; Mielczarski et al., 1989) and sulphides (Mielczarski and Suoninen, 1984; Johansson et al., 1986) has been studied. The adsorption mechanism for xanthate on metals (Laajalehto et al., 1988) and on sulphides (Mielczarski and Suoninen, 1984), is found to consist of relatively rapid formation of a well-oriented monolayer on the surface substrate. The same mechanism has been found by Mielczarski and Minni (1984) for the adsorption of diethyldithiophosphate on sulphide minerals.

These examples illustrate the potential use of XPS to gain insight into mineral surface chemistry.

2.2.2 Auger Electron Spectroscopy (AES)

The Auger process involves the non-radiative de-excitation of a core hole (created by an XPS event): the hole is filled by an electron from an upper energy level, releasing an

amount of energy which can be used to photoeject another electron, the so-called Auger electron (Briggs and Riviere, 1983). The Auger electron is then ejected with kinetic energy that is dependent only on the atomic energy level involved in the process and not on the characteristics of the excitation source.

As mentioned above, this technique requires high energy electrons to irradiate the sample. Auger electron spectroscopy is concerned with analysis of the energies of the secondary electrons, superimposed on other inelastically scattered electrons. Like in XPS, the emitted Auger electron can only escape from the upper surface layers, to a maximum depth of 30 Å, making it a surface-sensitive technique. The energy of the Auger electron is characteristic of the atom from which it originates. Thus, AES enables a chemical analysis of surface elements, although identification of different atomic environments, i.e., a chemical shift effect, is not so pronounced as in XPS. In contrast, lateral resolution with AES is much better than for XPS, and scanning AES has become a valuable tool in surface characterization. X-rays are also capable of producing Auger electrons and are, therefore, observed in XPS spectra. Generally Auger is more surface sensitive than XPS. The electron beam used in AES is more destructive than the X-ray used in XPS, and more likely to induce surface change (Hall et al., 1985).

It is easier to detect different surface-chemical species of the same element by XPS than AES. It is therefore expected that XPS will be more useful in the study of adsorbed species on mineral surfaces in flotation systems. The use of AES has its place, however. For example, Chadwick and Hashemi (1979), investigated surface films formed by 2-mercaptobenzthiazole, MBT, (a corrosion inhibitor and flotation collector) on copper by XPS and X-ray induced AES. The latter technique was more useful in establishing the formation of a compound on the surface than XPS.

2.2.3 *Secondary Ion Mass Spectrometry (SIMS)*

In this technique the solid surface is bombarded with energetic heavy ions (typically low keV), noble gas ions, Cs⁺ or O⁺. These ions, which have a mean free path about 150 Å, produce a collision cascade of lattice atoms with a final emission of particles from

the solid surface. The ion fraction of the emitted particle is detected and analyzed by a mass spectrometer (Fig. 2.1).

This technique permits the detection of all the elements present in the sample, including H and Li, with sensitivity of the order of ppm-ppb. It also permits isotope selectivity, mapping of the surface of the sample with a resolution of 1 μm , and a depth profile detection of the elements. A SIMS instrument can be used in either static or dynamic modes, depending on the current density of the primary ions. In the static mode, the primary ion current density is $\sim 1 \text{ nA/cm}^2$ which ensures a sputtering rate of some nm per hour. Static SIMS analyses only the outermost surface layer and is employed when it is wished to modify the sample as little as possible. With dynamic SIMS a primary ion current density of some $\mu\text{A/cm}^2$ permits depth profiles of a few μm per hour.

Explicitly, static SIMS has the potential capability of providing the following:

- Detection of all elements including hydrogen.
- Extremely high sensitivity for all elements and compounds. Detection limits: $<10^{-6}$ monolayers, a thousand times more sensitive than XPS and AES.
- Isotope sensitivity.
- Very good lateral resolution.

The disadvantages are:

- Large differences in sensitivities for different surface structures.
- Problems in quantitative interpretation of molecular fragments.
- Ion-induced surface reactions.

The more complex the reagent adsorbed on the (mineral) surface, the more difficult will be the spectral interpretation, including by static SIMS. Studying mineral surfaces, prior to reagent addition, will therefore, presumably be necessary. SIMS provides a surface technique complementary to XPS or AES, identifying species that cannot be distinguished by the latter methods. It is an extremely sensitive technique and developments should be followed by those interested in mineral surface chemistry.

2.2.4 *Laser Induced Mass Spectrometry (LIMS)*

LIMS has been used to study the surface composition of mineral particles in relation to understanding fundamental principles of flotation and phenomena observed in base metal sulphide flotation circuits. The presence or absence and the relative concentration of inorganic surface elements on mineral particulates 20 - 100 μm in size, can be determined by probing several spots (5 - 10 μm in diameter) per particle. The analytical depth resolution is estimated to be only a few atomic layers.

Laser probe microanalysis has certain advantages: first, a small beam size, permitting the analysis of individual mineral grains as small as 5 - 10 μm across; second, a neutral primary beam, which means that the analysis of insulating particles does not present a problem; third, flexibility in terms of available laser wavelengths, permitting the analysis of adsorbed organic as well as increased sensitivity for a particular trace element (e.g. Au adsorbed on activated carbon); and, fourth, the power of the primary laser is adjustable, giving control over sampling depth. Perhaps the most significant advantage of the technique, however, is the rapidity of analysis (less than 1 min.), which means that the surface compositions of a large number of grains can be characterized in a reasonable short time - typically, 40 grains can be analysed in an hour which, in return, ensures that the data have the necessary statistical credibility.

Chryssoulis et al. (1992) studied the loss of selectivity in the differential flotation of a base-metal ore and the different floatabilities of coarse- and fine-grained pentlandite from a Cu-Ni ore with this laser-probe microanalysis technique. They found that the sphalerite grains recovered to the Cu-Pb concentrate had more Pb on their surface than grains in the Zn circuit. They also found that the surface concentration of Fe on sphalerite was higher in the grinding circuit and that sphalerite from the Zn rougher concentrate carried more surface Fe than sphalerite from the tails. They combined time-of-flight secondary ion mass spectrometry (TOF-SIMS) to map the distribution of elements on the surface of mineral particulates.

2.2.5 Other (Vacuum) Techniques

EELS:

High-resolution electron energy loss spectroscopy (EELS) has been successfully used to characterize adsorbed species on metal surfaces used as catalysts (Ibach et al., 1977; Chesters and Sheppard., 1981). The EEL spectrum yields information on the vibrational mode of the adsorbate and is complementary to the infrared spectrum, like a polarized IR reflectance spectrum.

The advantage of the EEL spectrum over the infrared spectrum is the high sensitivity and the wide spectral range, 200 to 3600 cm^{-1} that can be scanned within 20 min. Further, vibrational spectra of the adsorbate, down to about 200 cm^{-1} are observed without any difficulty with interfering bands of the substrate. The disadvantage of EELS over infrared transmission spectra is its relatively poor resolution. The electron beam reflection requires a high-vacuum system and is generally a more complicated and expensive apparatus.

To what extent EELS could be applied to adsorbed species on mineral surfaces remains to be seen. It should complement infrared studies. The ability with EELS to overcome the broad, interfering adsorption bands of the adsorbate (mineral), (also, as mentioned, overcome with infrared emission spectroscopy), seems an inviting prospect. Whether sufficient resolution of EEL spectra will be obtained when the electron beam is reflected from a mineral surface, remains an open question, however. Indeed, with broader vibrational bands in EELS, analysis of complicated spectra will be difficult. EELS is conducted in a high vacuum and is thus an *ex situ* technique.

EELS spectroscopy has been used in mineralogy for chemical and valence studies (Rask et al., 1987; Hawthorne, 1988; Wang and Cowley, 1988). In various minerals, different Mn (Rask et al., 1987; Wang and Cowley, 1988), Ti and Fe (Otten et al., 1985) oxidation states have been observed. Chemical shift as a function of the oxidation state has been determined for Ti (2 eV), Mn (3 eV) and Fe (2 eV) (Otten et al., 1985).

Mössbauer Spectroscopy:

Mössbauer spectroscopy is mainly used to study recoilless nuclear resonant absorption or fluorescence. The Mössbauer effect is of fundamental importance in that it provides a means of measuring some of the comparatively weak interactions between the nucleus and surrounding electrons. Although the effect is only observed in the solid state, it is precisely in this area that some of the most exciting advances in materials science are being made. Because it is specific to a particular atomic nucleus, the technique has been applied to determine the electronic structure of impurity atoms in alloys, the after-effects of nuclear decay, and the nature of the active sites in iron-bearing proteins.

One of the examples applying this technique to mineral processing is the investigation of the precipitates formed when solutions of iron ions are mixed with ethyl xanthate solutions by Sheikh and Leja (1977). They suggested the formation of ferric hydroxyl xanthate from a combination of Mössbauer and IR spectroscopy.

2.4 RAMAN SPECTROSCOPY

In contrast to infrared spectroscopy, which provides a powerful tool to investigate the molecular structure characterized by "polar" bonds and vibrations that change the molecular dipole, Raman spectroscopy is generally more sensitive to non-polar bonds and changes in the bond polarisability.

Takenaka (1979) reviewed the application of Raman spectroscopy to surface chemistry. Paul and Hendra (1976) gave a detailed discussion on the principles and experimental techniques. One of the most important aspects in the elucidation of the surface chemistry of flotation, is its applicability to aqueous solutions, since water is a weak Raman scatterer. In this regard the work reported by Yamamoto (1980) using Raman spectroscopy to study the reaction of xanthate and sulphide ions in aqueous media is illustrative.

Few Raman spectroscopy studies related to mineral-reagent adsorption have been conducted. Raman spectroscopy uses an intense laser beam of a well defined wavelength

to induce the Raman scattering effect. A problem in obtaining Raman spectra is encountered when traces of impurities, or the sample itself, emit fluorescent background radiation upon which the Raman spectrum is superimposed. Treatment of the mineral to eliminate or reduce the inherent fluorescence (Sheppard et al., 1971) may make it unsuitable for flotation research. In addition, scattered Raman radiation is very weak, so that large surface areas, $\sim 300 \text{ m}^2/\text{g}$, (Morrow, 1977) are required for detecting adsorbed species. The generally small specific surface areas of minerals, mitigates against the use of Raman spectroscopy in mineral systems, unless its sensitivity can be increased. This is possible in certain types of Raman spectroscopy.

The possible use of the resonant Raman effect for studying flotation systems should be considered. Raman intensities can be increased by a factor of 10^5 . For this to be achieved, it is necessary for the laser wavelength to lie within an electronic absorption band of the molecule to be investigated. Nakanaga and Takenaka (1977) and Takenaka and Nakanaga (1976) used this technique to measure the Raman spectra of a monolayer of surfactant at the interface between an aqueous solution and carbon tetrachloride. The use of a colored surface-active dye, or the formation of a colored complex between the surface-active agent and a dye, is essential under certain conditions if the resonant Raman condition is to be satisfied. In such studies, the orientation of the molecule of the surface-active agent at the interface may be ascertained from the Raman spectra. If suitable dyes could be found that did not affect flotation of the mineral, obtaining resonance Raman spectra of such systems could be an interesting possibility: the small surface areas of minerals would then no longer be an obstacle.

Surface-enhanced Raman spectroscopy (SERS) has been used to study adsorbates on certain metal electrodes, colloids and metallic silver films (Otto, 1980). The intensity of the scattered Raman spectrum is enhanced by a factor of 10^5 . The physical origin of the enhancement effect, which is observed for metal-adsorbate combinations, and other molecules close to the adsorbate surface, is a matter of vigorous debate at present. Whether this effect could be used to study mineral-reagent interaction is not clear.

The Raman molecular microprobe (Dhamelincourt et al., 1979; Etz, 1979; Rosasco, 1980), which has been useful in analyzing fine dust particles could also be useful in analyzing mineral particles in flotation systems. (The Raman microprobe is also known as MOLE, which is the acronym for Molecular Optics Laser Examiner.) This technique combines a conventional optical microscope with a Raman spectrometer. The source of irradiation is a laser, which is focused on a small particle, which can be up to a few microns in diameter. The Raman scattered radiation from the sample is then focused via lenses onto the entrance slit of a monochromator and then to a photomultiplier tube (PMT) that records the spectrum. Unlike scanning electron-microscopy or electron-microprobe analysis, which supplies elemental analysis of points in a sample, the Raman microprobe, via the Raman spectra, furnishes information about the molecules at the points analyzed. It is therefore possible to proceed with the mapping of *molecular* species in larger samples. One good application of the technique is the detection and localization of liquid inclusions in certain minerals. Some idea of the anticipated problems in detecting organics on a mineral surface by Raman microprobe analysis can be obtained by consulting the report by Blaha et al. (1978) who used the Raman microprobe to study carbonaceous material associated with air-borne dust particles. It was found that under the high laser irradiance, organics tended to decompose or polymerize. It remains to be seen whether the experimental technique can be improved to overcome these difficulties in order to study the presence of collectors and other reagents adsorbed on mineral surfaces.

2.5 SUMMARY

Giesekke (1983) tabulated some spectroscopic techniques from a practical point of view including cost on a scale of 1 to 5, indicating very difficult, poor, fair, good and very good, respectively. This table is shown in Table 2.1. The column listing the minimum surface area needed for studying the adsorbed species was taken from instances in the literature where such successful experiments were reported on adsorbed species on mineral or similar surfaces. This is also taken as an indication of the sensitivity of the particular technique. It is tempting to add the scores and compare the techniques, but this may be

misleading. A realistic evaluation of the techniques would be to compare scores of similar techniques, or to see how all the techniques score on one aspect of evaluation.

Marabini et al. (1993) made another comparison of spectroscopic techniques used in mineral processing studies in the terms of function and information obtained. This table is reproduced in Table 2.2.

Table 2.1 Comparison of various spectroscopic techniques in flotation studies (Giesekke, 1983)

	Infrared					Raman		ESR	Vacuum		
	Transmission	ATR	Reflection	Emission	FT-PAS	Scatter	Microprobe		XPS	AES	SIMS
Ease of sample preparation	4	1	2	2	5	4	3	5	3	3	3
Chemical information of adsorbed species	3	3	3	3	3	3	2	4	4	2	1
Low cost of apparatus	5	4	4	2	2	2	1	3	2	2	1
Ability to perform in situ studies	3	5	4	4	5	4	4	4	2	2	2
Minimum surface area: sensitivity (m ² /g)	1	1	1	1	80	300	?	10	0.1	0.1	>>0.1

Table 2.2 Comparison of spectroscopic techniques available in mineral processing studies (Marabini et al., 1993)

	In situ (S) or ex situ (Es)	Destructive (D) or not destructive (ND)	Sampling depth (monolayers)	Spatial resolution	Quantitative information on atomic ratio	Chemical information	Depth profile	Structural information
Air techniques								
IRS	Es	ND	-	1 cm ²	yes	yes	no	yes
Transmission								
Emission	Es	ND	2-4	1 cm ²	yes	yes	no	yes
ATR	S	ND	20	1 cm ²	yes	yes	no	yes
PAS	Es	ND	102	1 cm ²	yes	yes	yes	yes
Vacuum techniques								
UPS, XPS	Es	ND	206	100 μm	yes	yes	yes	no
Auger AES	Es	ND	2-6	0.2 μm	yes	yes	yes	no
SIMS:								
Static	Es	D	2	1 mm	yes	no	no	no
Dynamic	Es	D	40	1 μm	yes	no	yes	no
REELS	Es	ND	2	0.2 mm	yes	yes	no	yes
SEXAFS	Es	ND	2-6	100 μm	no	no	no	yes

The obvious advantage of using more than one spectroscopic measurement to study surfaces has hardly been exploited. Different studies complement each other as seen in the Cu-MBT studies (XPS and AES) discussed in the text. As another example, Gardella and Hercules (1981) used SIMS, XPS and ion scattering spectroscopy to study surfaces of acrylic fibers. The work presented in this thesis is another example of using combinations of spectroscopic techniques.

This chapter has outlined the most common spectroscopic techniques used in the study of mineral surfaces and reagent interaction involved in mineral processing. There are some other spectroscopic techniques which are widely used in other areas of surface chemistry. Two which may have application in flotation research are Extended X-ray Absorption Fine Structure (EXAFS) and Near Extended X-ray Absorption Fine Structure (NEXAFS) (also known as XANES, X-ray Absorption Near Edge Structure). These techniques have been applied in mineralogy by Brown et al. (quoted in Hawthorne, 1988) and Calas et al. (1984). Topological studies by EXAFS on Mn and Fe have been performed by Morrison et al. (1981), Waychunas et al. (1986) and Manceau and Combes (1988). Waychunas et al. (1986) obtained the X-ray K-edge absorption spectra of Fe minerals using synchrotron radiation.

CHAPTER 3

EXPERIMENTAL MATERIALS AND APPARATUS

3.1 MATERIALS

3.1.1 *Sphalerite*

A sample of copper-lead-zinc ore from Brunswick Mining and Smelting, New Brunswick, Canada, was ground and the -100+200 Tyler mesh fraction (74-150 μm) was isolated and subjected to repeated processing on a shaking table and Mozley separator. The resulting sphalerite sample was acid-cleaned with 5% HCl at room temperature three times to leach out alkaline gangue (calcite, dolomite) present, then was washed first with acetone (to remove any sulphur formed during the acid treatment) followed by deoxygenated-deionized water. It was dried in a vacuum oven at a temperature of ~ 70 $^{\circ}\text{C}$ and stored under nitrogen in a desiccator. Chemical analysis of the sample showed 63.8% Zn, 2.8% Fe, 0.38% Pb and $< 0.1\%$ Cu.

The cleaned sample was ground in an agate mortar: for microflotation tests, the size range -74+37 μm was selected; for zeta-potential and spectroscopy measurements, the size range was -37 μm .

3.1.2 *Bulk Precipitates from Iron and Xanthate Solution*

A number of 'iron xanthate' precipitates were prepared in open atmosphere by mixing 1 M solutions of sodium isopropyl xanthate and ferrous sulphate over the pH range 2.5-13 using the procedure of Sheikh and Leja (1977). The precipitates were washed with distilled water at 80 $^{\circ}\text{C}$ to remove any ions adsorbed at the precipitate surface.

Precipitates were also prepared in the absence of xanthate from both ferric sulphate and ferrous sulphate solutions by raising the pH to 10: In the case of ferrous, oxygen was used to oxidize the product.

Microflotation was performed after decanting fluid to remove suspended particles; zeta potential and *ex situ* spectroscopy (XRD, IR, UV and Mössbauer) measurements were conducted on samples prepared by filtering and drying at room temperature.

3.1.3 Reagents

Sodium isopropyl xanthate from Cyanamid was purified by dissolving in acetone and recrystallizing from petroleum ether following the standard method (Rao, 1971). Dixanthogen was prepared from purified xanthate by oxidation with a stoichiometric amount of aqueous iodine (with potassium iodide) followed by extraction into ether and removal of the solvent. Its UV spectrum showed the characteristic peak of dixanthogen (Leja, 1982). Methyl isobutyl carbinol (MIBC, laboratory grade) was used as frother; HCl and NaOH (both Fisher reagent grade) were the pH regulators.

Ferrous sulphate was used as the source for Fe^{2+} , and ferric sulphate for Fe^{3+} . The salts were Fisher reagent grade products.

3.2 FLOTATION AND SURFACE CHARGE APPARATUS

3.2.1 Microflotation

Tests were conducted with 1 g samples of sphalerite or iron xanthate precipitate in a modified Hallimond tube (Fuerstenau, 1957). 30 ml deoxygenated-deionized water (to minimize side reactions) was used and flotation conducted for 2 minutes with 74 ml/min. air. In the case of sphalerite, 1 minute of conditioning was allowed after adding any reagents.

The effect of the supporting NaCl electrolyte, as used in the zeta potential measurements, was tested by conducting flotation in the presence of NaCl in the concentration range 10^{-5} M to 1 M.

reagents continuously and each flowrate can be individually adjusted. There are two outputs from the conditioning tank, which can provide two different conditioning times for a given flowrate. Gas via a flowmeter and nozzle can be injected into the conditioning tank.

The ratio of flotation cell surface area to volume is similar to that of an industrial cell. The discharge pipe from the cell is used to regulate the pulp level in the cell. There is a mechanism for launder water addition. Gas to the cell is injected through a flowmeter and the impeller shaft. Baffles are installed at the bottom of the cell.

A control box to operate the mixers, launder water addition, reagent pump and the minicell impeller speed was constructed and attached on the back of the minicell.

Electrodes for pH, dissolved oxygen concentration (DO) and pulp potential (Ep) were installed on the side of the cell (these electrodes can also be inserted into the conditioning tank). The signals went through transmitters and were amplified and sent to the computer. The measuring system is composed of 6 transmitters (Fig. 3.2). Each transmitter is for one electrode and has temperature compensation. The signal from the electrode was

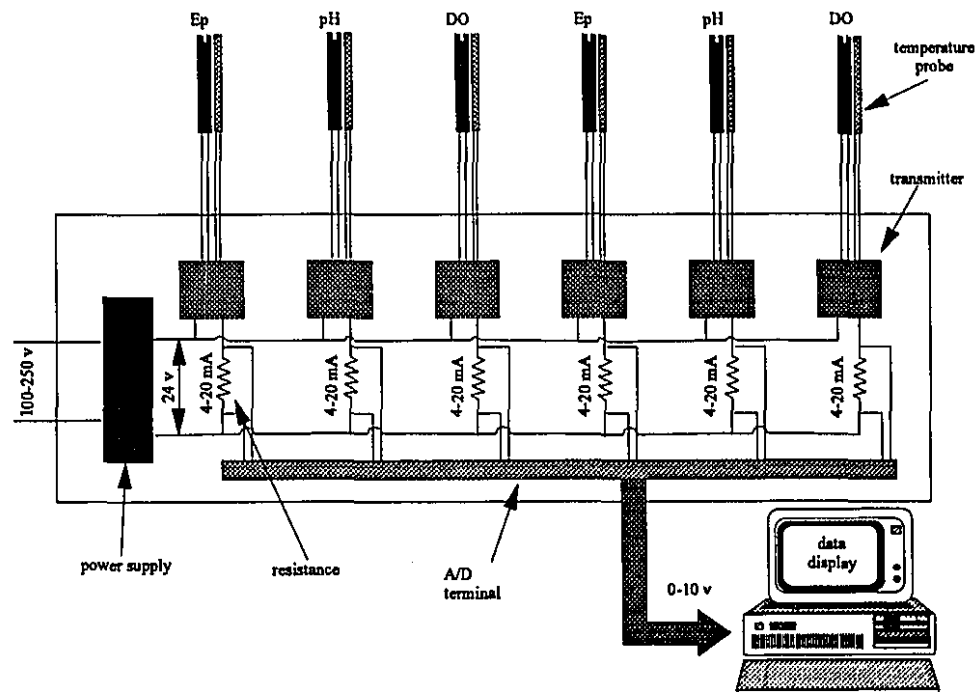


Figure 3.2 Measuring system of pulp potential, pH and dissolved oxygen

from -400 to 400 mV converted to 4 to 20 mA by the transmitter. The mA signal was converted to volts by a precise resistance of 440 ohm. This signal was then sent to the A/D board and computer. A Quick BASIC program was used to operate the measuring system for pH, DO and Ep.

The minicell circuit for Zn flotation is shown in Fig. 3.3 (two cells in series). Feed slurry from the plant circuit (Fig. 3.4) was pumped to the conditioning tank where reagents were added. Slurry was fed to the first flotation cell by gravity, with the tail from the first cell then pumped to the second flotation cell: pH, DO and Ep in the two flotation cells were measured during flotation. Once the operation reached steady state (usually judged by stability of signals), five samples were collected as indicated in Fig. 3.3 (one feed, two concentrates and two tails).

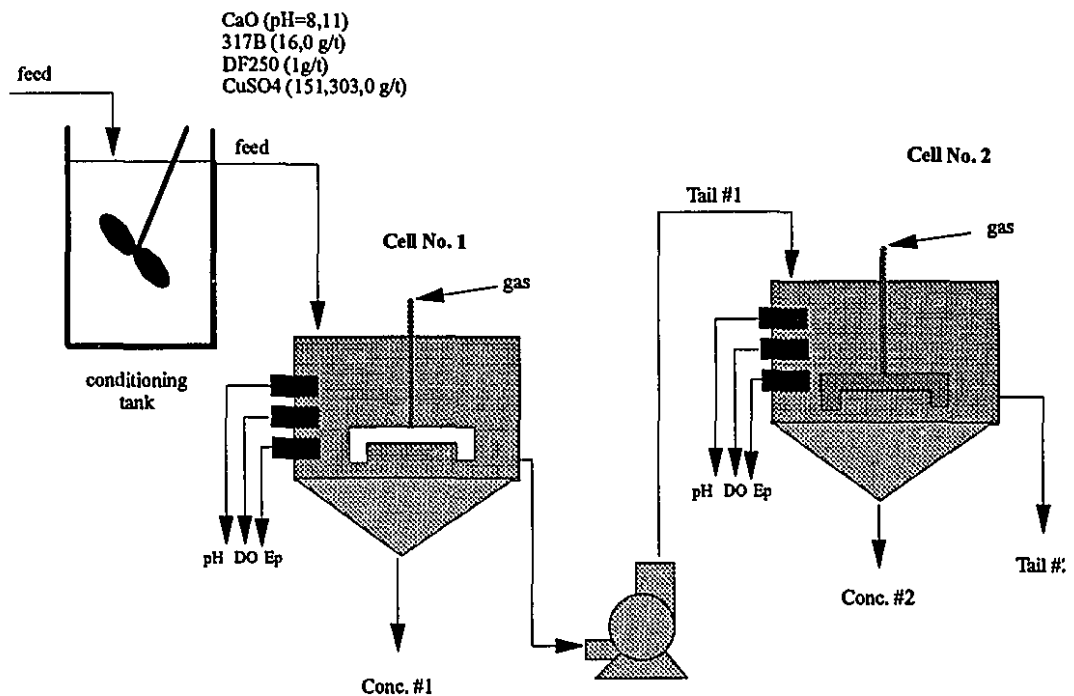


Figure 3.3 Minicell circuit for Zn flotation

The feed flowrate was varied from 1.0 to 3.5 L/min, to give different flotation times for constructing cumulative grade/recovery curves.

A simplified flowsheet of Kidd Creek B and C divisions is shown in Fig. 3.4. No Zn circuit reagents had been added to the pulp at the point of sampling. The feed to the Zn circuit contains about 2.5-5% Zn and 10-15% Fe (major sulphide minerals are sphalerite and pyrite). Collector, frother, lime and SO_2 had been added into the Cu circuit for Cu flotation.

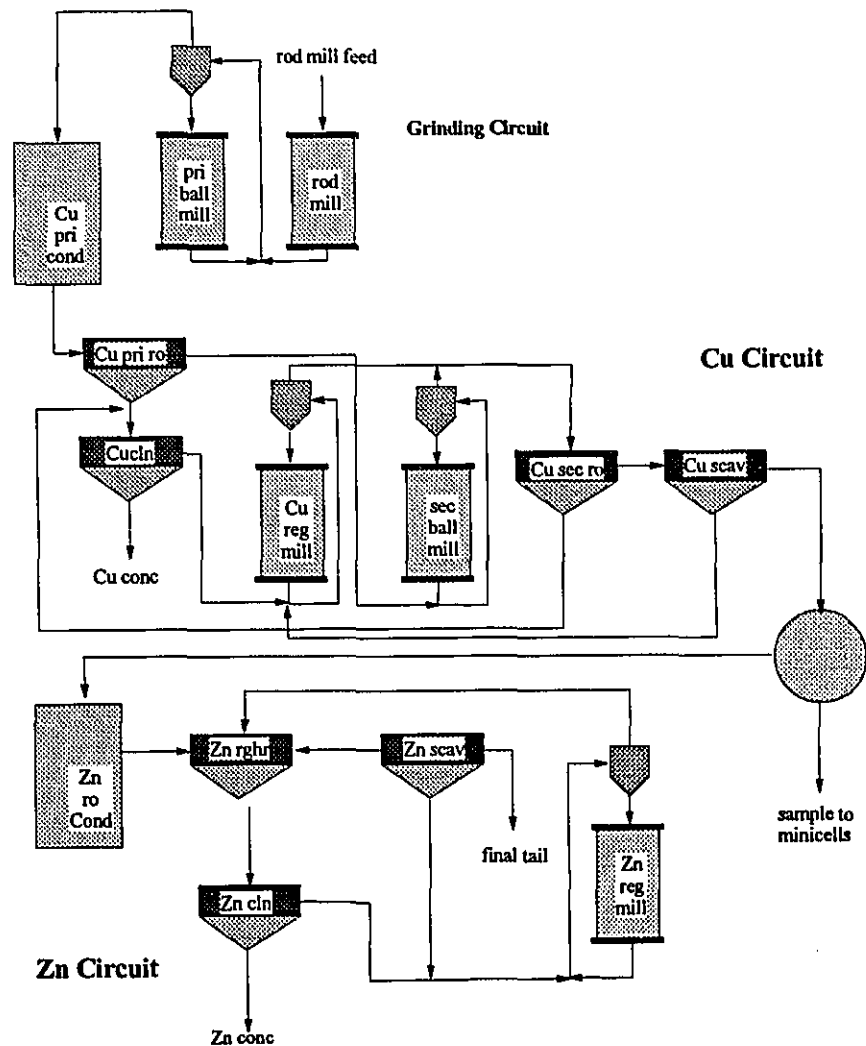


Figure 3.4 Simplified flowsheet of Kidd Creek B and C divisions and minicell sample location

3.2.3 Zeta Potential Measurement

The measurements were made with a zeta potential analyzer manufactured by the Micromeritics Instrument Corporation, U. S. A.. The instrument determines the conductivity of the suspension and net change of mass of the cell due to the mobility of particles in an electric field. To try to minimize contamination, both electrodes were coated with gold. For this test, 1 g of mineral or precipitate of 'iron xanthate' was conditioned with deionized water in a 200 ml beaker for 2 minutes. The ionic strength was controlled by NaCl addition. The effect of NaCl concentration was determined over the range 10^{-5} M to 10^{-1} M. The zeta potential value decreased with increasing electrolyte concentration until 10^{-2} M. There was no further obvious change at higher concentration. Measurements were conducted using a concentration of 10^{-1} M NaCl.

The conductivity of the slurry was measured and specific conductance was calculated by knowing the cell constant for the system (1.01 cm^{-1}). The suspension was then transferred to the analyzer cell and reservoir. The mass of the cell was measured. After an electric field was applied for 5 minutes, the mass of the cell was measured again and the net change in mass due to migration of the particles was determined. The zeta potential of the mineral is calculated (assuming that particles are in dilute suspension and liquid specific viscosity and dielectric constant do not change with the supporting electrolyte) from the following:

$$\zeta = 3768 \frac{\Delta W \cdot \lambda \cdot \eta}{t \cdot I \cdot \Phi \cdot (\rho_p - \rho_l) \cdot D} \quad (3.1)$$

Detailed description and calculations are given in Appendix I. Each experiment was repeated at least four times and the average and standard deviation calculated.

3.3 BULK ANALYSIS APPARATUS

3.3.1 *UV-vis Spectrophotometry*

The mineral samples were exposed to a certain concentration of xanthate (usually 10^{-3} M) solution for a limited time. The slurries were then filtered and residues were washed with deionized water. After that the mineral samples were mixed in acetone to dissolve the organic species on the mineral surface, and the solutions were put in 10 mm quartz UV cells and analyzed on a Milton Roy spectronic 1201, single beam, UV-vis spectrophotometer. This UV-vis spectrophotometer was driven by an IBM computer with Spec-Scan™ software.

3.3.2 *Infrared Spectroscopy*

The IR spectra (4000 to 200 cm^{-1}) were obtained with a Perkin-Elmer 1330 infrared spectrophotometer. Samples were dispersed with KBr in the ratio of 1:600 to make the pellet.

3.3.3 *X-Ray Diffraction*

The instrument used was a Model Max 3100 (American Instruments Inc.) X-ray generator, equipped with a PW 1710 diffractometer control system, PW 1386/55 automatic divergence slit (specimen length: 12.5 mm), PW 1752/00 monochromator, PW 1711/10 proportional detector and MICRO/PDP-11 computer system. The generator settings were 40 kV and 20 mA with the Cu-K α wavelength of 1.54060 Å. The peak angle range was 5-100 degree while the range in D spacing was 1-18 Å. The crystal peak width range was set between 0.00 and 2.00 degree. To simplify comparisons, only the spectrum between 5-60 degree was used because there were few peaks after 60 degree. The sample powder fraction used in the measurements was minus 37 μm .

3.3.4 Mössbauer Spectroscopy

Room temperature Mössbauer spectra were obtained on a conventional constant acceleration spectrometer (manufactured by Wissel) with a 25 mCi ^{57}Co *Rh* source also at room temperature. The spectrometer was calibrated using α -Fe foil at room temperature; isomer shifts are given relative to the centroid of this spectrum. All spectra were fitted using a standard nonlinear least-squares routine with variable line width, isomer shift and quadrupole splitting.

3.4 SURFACE ANALYSIS APPARATUS

3.4.1 XPS

X-ray photoelectron spectroscopy (XPS) spectra were obtained on an ESCALAB Mark-II instrument equipped with a non-monochromated Mg K_{α} anode ($h\nu = 1253.6$ eV) at a take off angle of 90° . The instrument was calibrated against the C_{1s} band (284.5 eV) and exhibited an energy resolution of 0.7 eV. Samples investigated by XPS were prepared by pressing the solid powders onto an adhesive-backed copper foil. The samples were maintained at the instrumental background pressure of 10^{-9} torr for about one hour before spectra were obtained. Spectra presented in this thesis were corrected for background charging by determining the C_{1s} core level of saturated hydrocarbons at 284.5 eV (Wagner et al., 1979) both at the outset and the end of a series of narrow scans for each sample. No significant charging was found to occur. No smoothing procedure was used to modify the measured spectra. Band fitting and spectral deconvolution were performed using the program Surf-softTM. A non-linear background was subtracted and the line shapes of the individual peaks were fitted by a gaussian line function using a non-linear least square fitting method.

3.4.2 DRIFTS

Mineral samples investigated by DRIFTS (Nicolet Advanced Diffuse Reflectance Accessory) employed a Bruker IFS 88 FTIR spectrometer equipped with a narrow band

MCT detector. A sample of finely crushed KBr was used as the background. DRIFTS spectra were obtained from the dried mineral powders and were usually the result of coaddition of 1000 scans at a nominal resolution of 3.0 cm^{-1} .

3.4.3 ATR

ATR spectra were obtained using a sphalerite (ZnS) ATR element with a Specac (PN 11160) accessory modified with a Teflon seal so that solutions could be introduced and removed without demounting the cell from the spectrometer. The total volume of solution contained in the fluid circuit was 10 mL. The crystal was cleaned before use by rinsing with ethanol and distilled water, followed by irradiation with a low pressure Hg lamp to remove any organic contaminants. Finally, the crystal was washed with deionized water at pH 2 and followed by a thorough wash with distilled water before assembly of the cell. The crystal was hydrophilic after this treatment and spectra obtained after this treatment showed no evidence of organic contaminants. ATR spectra were obtained as the coaddition of 500 scans using a Bruker IFS 48 spectrometer equipped with a DTGS detector at a nominal resolution of 3.0 cm^{-1} . No attempt was made to vary the polarization of the infrared radiation. ATR spectra presented here, were normalized against the bending energy of a water molecule, but not baseline corrected, nor smoothed, nor subjected to spectral subtraction.

CHAPTER 4

EXPERIMENTAL RESULTS

4.1 FLOTATION AND ZETA POTENTIAL

4.1.1 Single Mineral (Micro) Flotation

The results under different conditions are shown in Figs. 4.1-4.3. It can be seen that sphalerite did not float when alone or just in the presence of xanthate (Fig. 4.1). Ferrous ions, however, in the presence of xanthate, promoted flotation in the range pH 8-11 although ferric ions had no effect (Fig. 4.1). The concentration of ferrous ions affected the flotation results (Fig. 4.2); when the concentration of ferrous ions was over ~ 2 ppm, the activation effect decreased. The presence of oxygen is also shown to be a factor (Fig. 4.3).

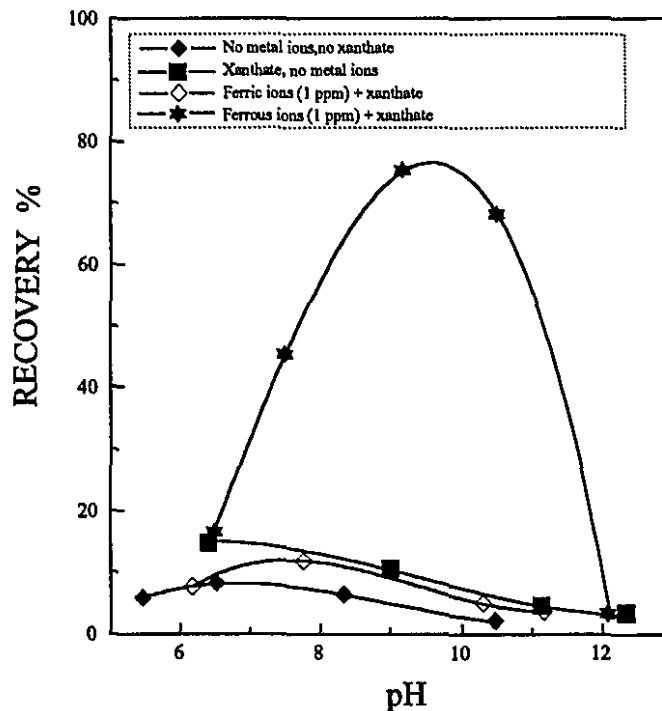


Figure 4.1 The relationship between recovery of sphalerite and pH with 1×10^{-4} M sodium isopropyl xanthate under various conditions

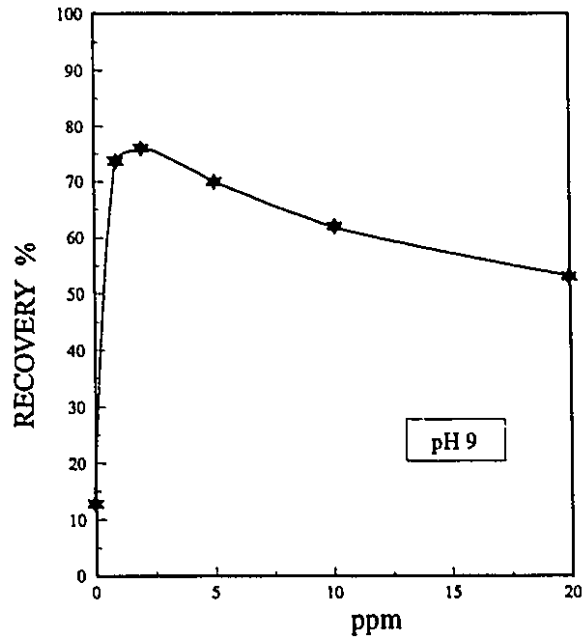


Figure 4.2 The relationship between recovery of sphalerite and the concentration of ferrous ions with 1×10^{-4} M sodium isopropyl xanthate

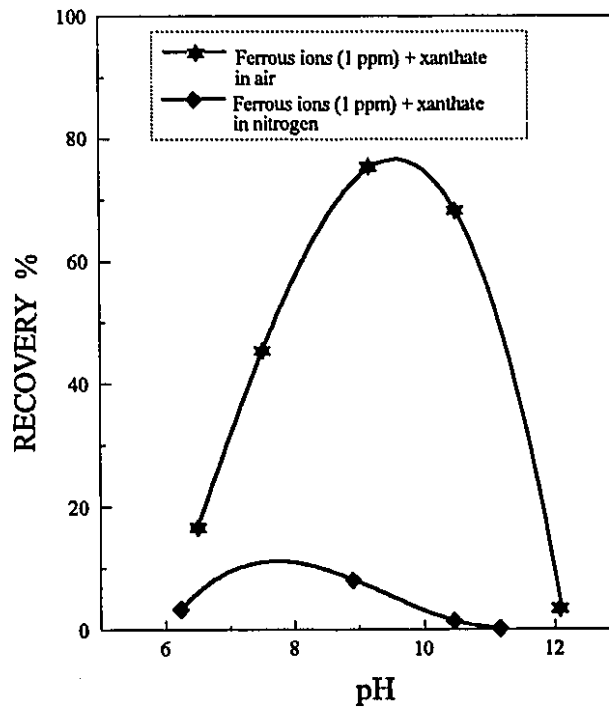


Figure 4.3 The relationship between recovery of sphalerite and pH with 1×10^{-4} M sodium isopropyl xanthate: effect of air and nitrogen

4.1.2 Continuous (Minicell)

At Kidd Creek, Cu circuit tails are typically at pH 8 while the Zn circuit is at pH 11. Figure 4.4 shows that raising the pH over this range enhances sphalerite flotation - Zn recoveries increased by about 30% at similar grades. In these tests, no collector (317B i.e. sodium isobutyl xanthate) was added (residual collector from the Cu circuit is presumably present, however).

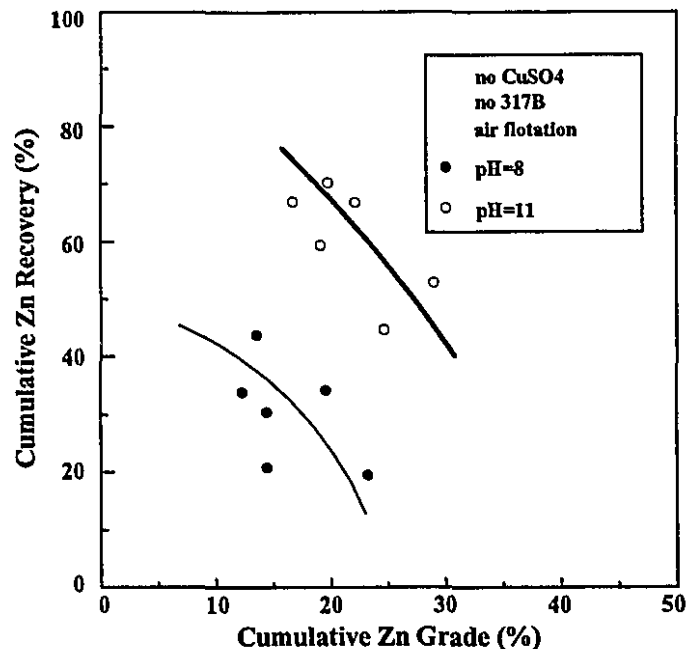


Figure 4.4 Cumulative Zn grade/recovery curves in Zn concentrate (Zn feed grade= 4-4.5%) (continuous minicell tests)

Flotation of sphalerite at pH 11 is further confirmed in Fig. 4.5 where Zn recovery is 40-60 % without CuSO_4 addition. Performance, however, was clearly superior with CuSO_4 . The flotation gas here was 50% O_2 ; gas composition was varied to test a proposed mechanism of sphalerite flotation at alkaline pH, which is discussed later.

Reviewing all the data (Xu et al., 1991), a consistent finding was that raising pH did induce sphalerite flotation but with CuSO_4 , the performance was superior. The CuSO_4 notably gave improved Zn/Fe separation. This is illustrated in Fig. 4.6: over a similar Zn

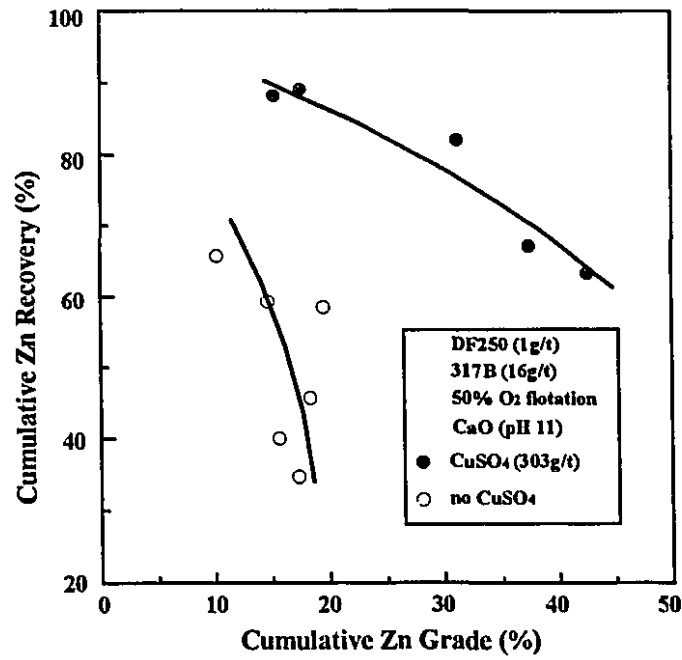


Figure 4.5 Cumulative Zn grade/recovery curves in Zn concentrate (Zn feed grade=3-4%)

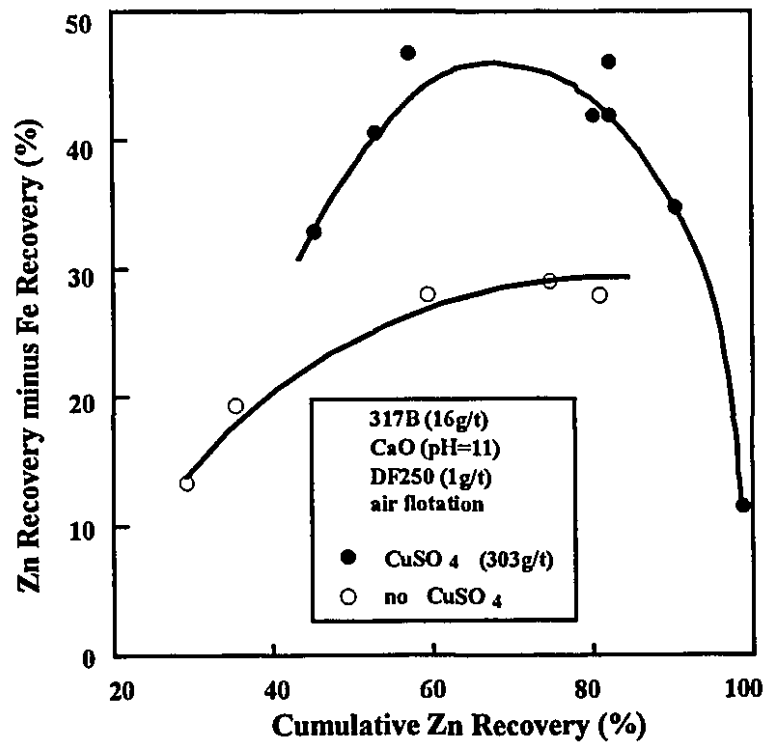


Figure 4.6 Zn recovery vs. the difference in recovery between Zn and Fe

recovery range, the difference in Zn and Fe recovery is greater in the presence of CuSO_4 . The flotation response of sphalerite to alkaline pH alone detected here is generally masked by the addition of CuSO_4 .

In the single sphalerite mineral flotation tests, changing the oxygen content of the flotation air was found to be important (Fig. 4.3). In-plant tests were conducted to explore this. Figure 4.7 shows that Zn (and Fe) recovery increase slowly with oxygen content in the gas, which offers some agreement with the single sphalerite mineral results.

The response in DO, pH and pulp potential (E_p) during the flotation is shown in Fig. 4.8 for one test: the pH remained constant; E_p was roughly constant above 20% O_2 ; but, the DO changed significantly (exceeding the scale above 50% O_2). This large increase in DO might have been expected to give more than the observed modest effect on Zn recovery. It is possible that the higher gas/pulp ratio in in-plant tests results in less sensitivity to the oxygen level compared to the single mineral tests.

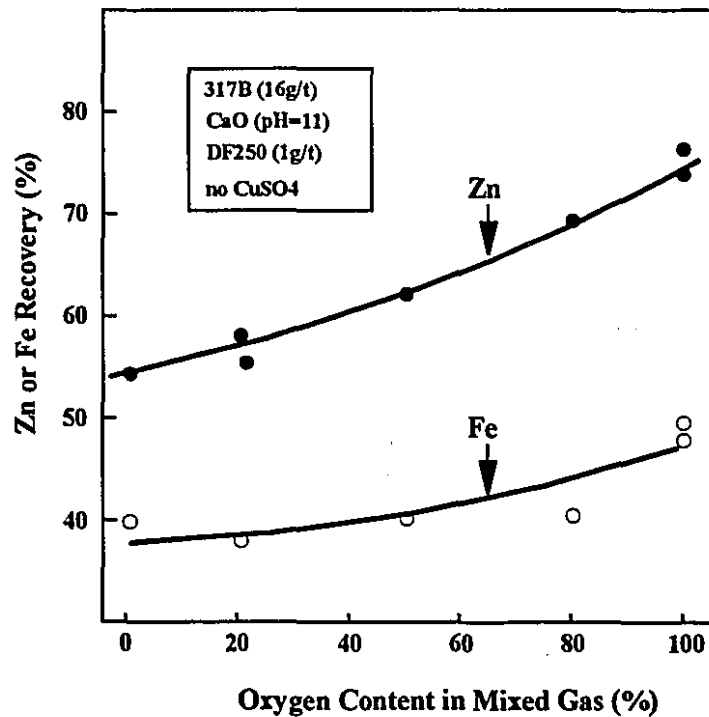


Figure 4.7 Zn and Fe recoveries vs oxygen content

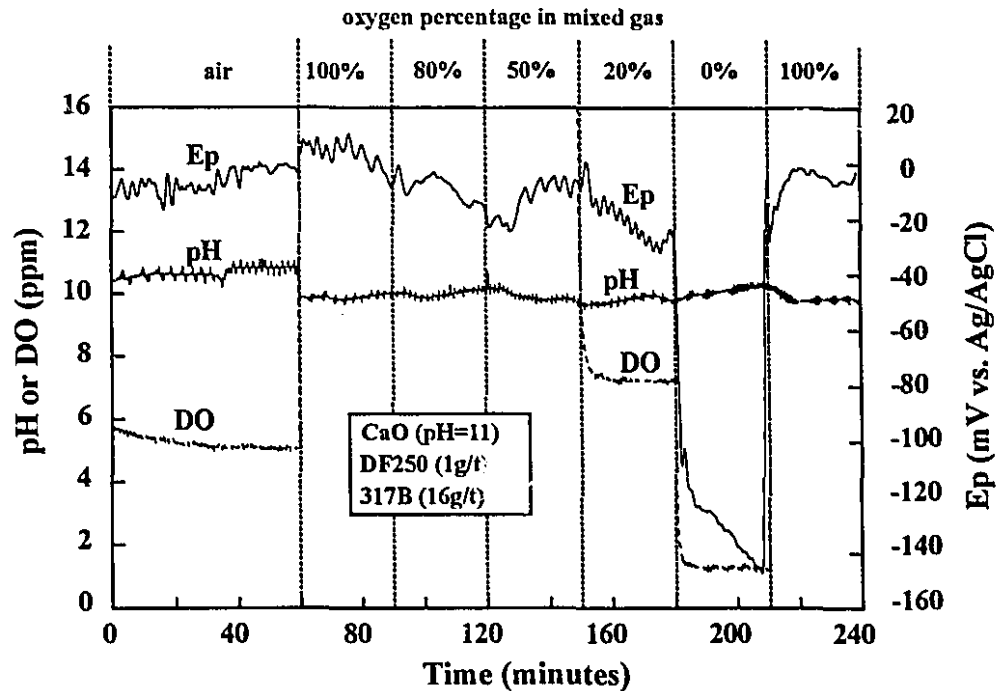


Figure 4.8 pH, DO and Ep in the first cell (test No.C3-1204)

4.1.3 Zeta Potential Measurements

The zeta potential of sphalerite was predominantly negative over the entire pH range with an isoelectric point (iep) of $\sim 2.5^{\dagger}$ (Fig. 4.9). With increasing pH, the zeta potential became progressively more negative, reaching -40 mV at pH 12.

When xanthate was added in the absence of Fe^{2+} ions, there was no significant change in the value of the zeta potential (Fig. 4.9). When the mineral was treated with Fe^{2+} ions, the zeta potential became less negative than that of sphalerite alone over the pH range 8-10.5. When xanthate was added to this Fe^{2+} -treated sphalerite, the zeta potential became more negative over the same pH range. The last two observations are compatible with a model of Fe^{2+} adsorption followed by xanthate (X^-) adsorption.

\dagger Note: The *point of zero charge* (pzc) is defined as the negative logarithm (base 10) of the concentration of potential-determining ions at which the surface charge density equals zero.
The *iso electric point* (iep) is defined as the negative logarithm (base 10) of the concentration of potential-determining ions at which the electrokinetic potential becomes zero.

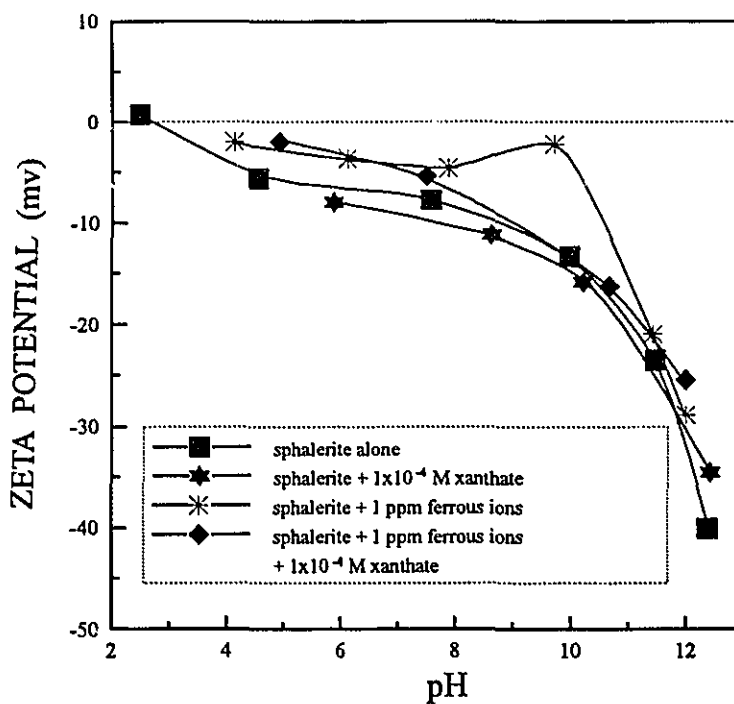


Figure 4.9 The zeta potential of sphalerite as a function of pH in the presence of xanthate and ferrous ions (ionic strength controlled by 1×10^{-1} NaCl)

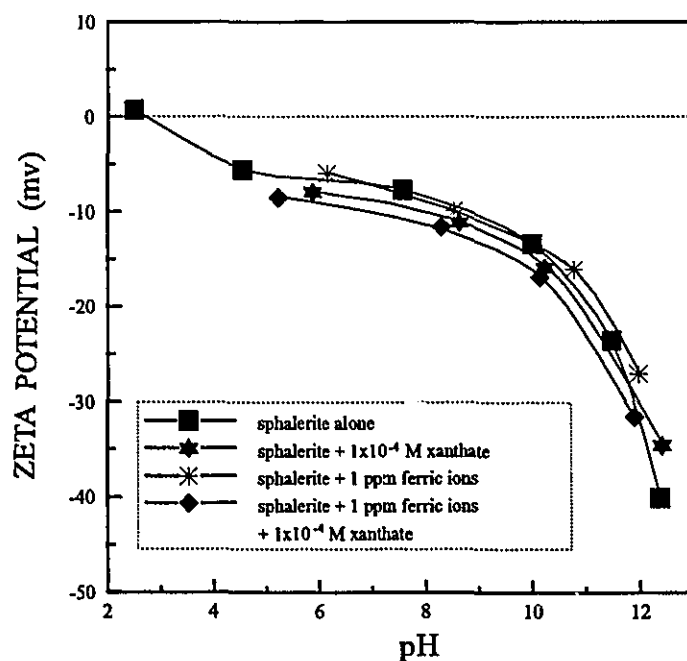


Figure 4.10 The zeta potential of sphalerite as a function of pH in the presence of xanthate and ferric ions (ionic strength controlled by 1×10^{-1} NaCl)

In contrast to Fe^{2+} ions, treatment with Fe^{3+} ions did not significantly alter the zeta potential (Fig. 4.10).

Figure 4.11 shows the effect of concentration of Fe^{2+} ions on the zeta potential. The zeta potential passed through a maximum at about 2-4 ppm Fe^{2+} : at pH 6.38, the zeta potential was essentially zero in this range of ferrous ion concentration.

Figure 4.12 shows the effect of oxygen on the zeta potential of sphalerite in the presence of 10 ppm Fe^{2+} (10 ppm was selected to determine if the decrease in zeta potential relative to that at 2 ppm was related to dissolved oxygen content). Conditioning with N_2 lowered the zeta potential (although it was still significantly greater than that for sphalerite alone) while conditioning with O_2 raised it, even reversing the charge at pH < 9.

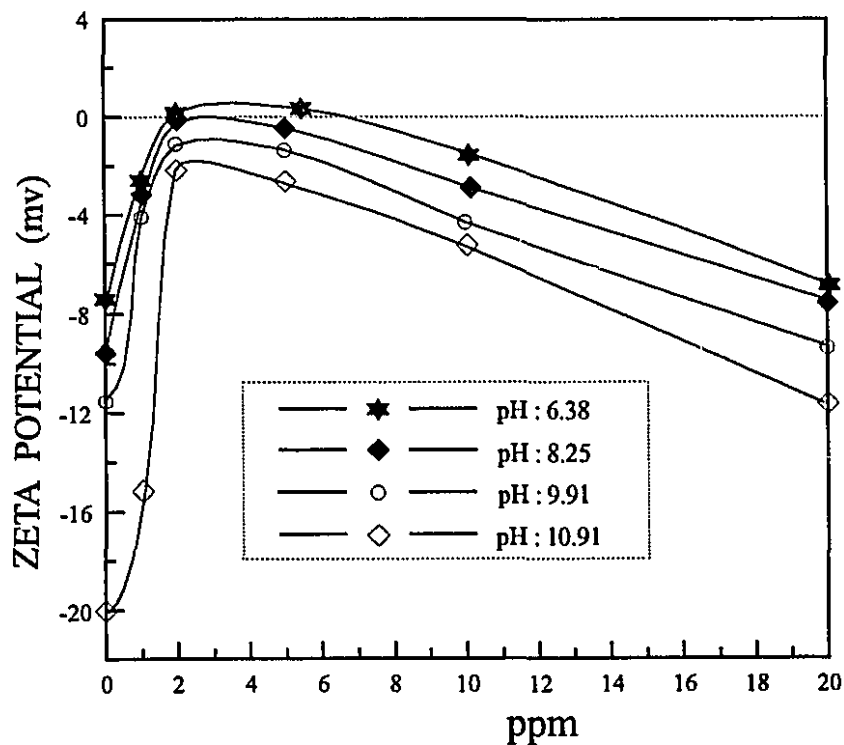


Figure 4.11 The relationship between zeta potential of sphalerite and the concentration of ferrous ions added at different pH (ionic strength controlled by 1×10^{-1} NaCl)

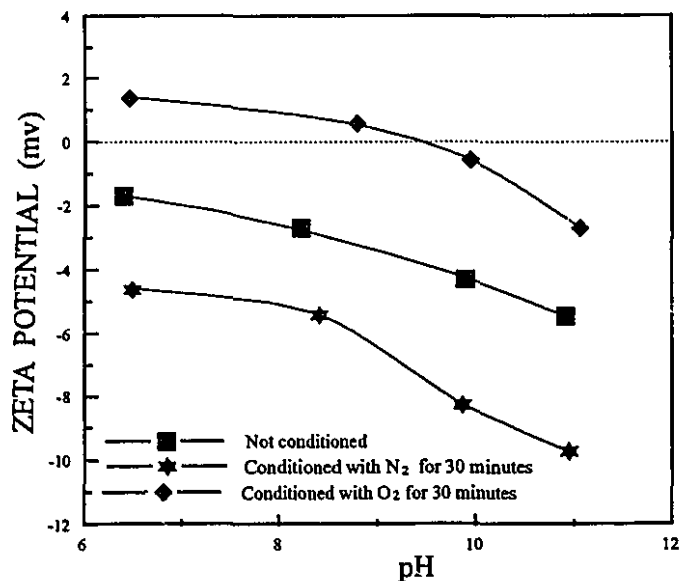


Figure 4.12 The relationship between zeta potential of sphalerite and pH in the presence of 10 ppm of ferrous ions (ionic strength is controlled by 1×10^{-1} M NaCl)

4.1.4 Adsorption of Ferrous Ions

To investigate further the role of ferrous ions and oxygen, the concentration of ferrous ions, zinc ions and oxygen was measured in solution as a function of time of contact with sphalerite (Fig. 4.13). The results show the concentration of Fe^{2+} and oxygen decreased, but there was no significant variation in pH or the concentration of Zn^{2+} (which remained less than 0.1 ppm).

4.1.5 Iron Xanthate Precipitates

The microflotation and zeta potential results are given in Figure 4.14: they show a similar behavior to that of sphalerite in the presence of Fe^{2+} ions and xanthate.

4.2 X-RAY PHOTOELECTRON SPECTROSCOPY

The XPS spectra were obtained on a sphalerite sample that had been: a) treated with distilled water, b) treated by Fe^{3+} , c) treated by Fe^{2+} , d) washed, and then contacted

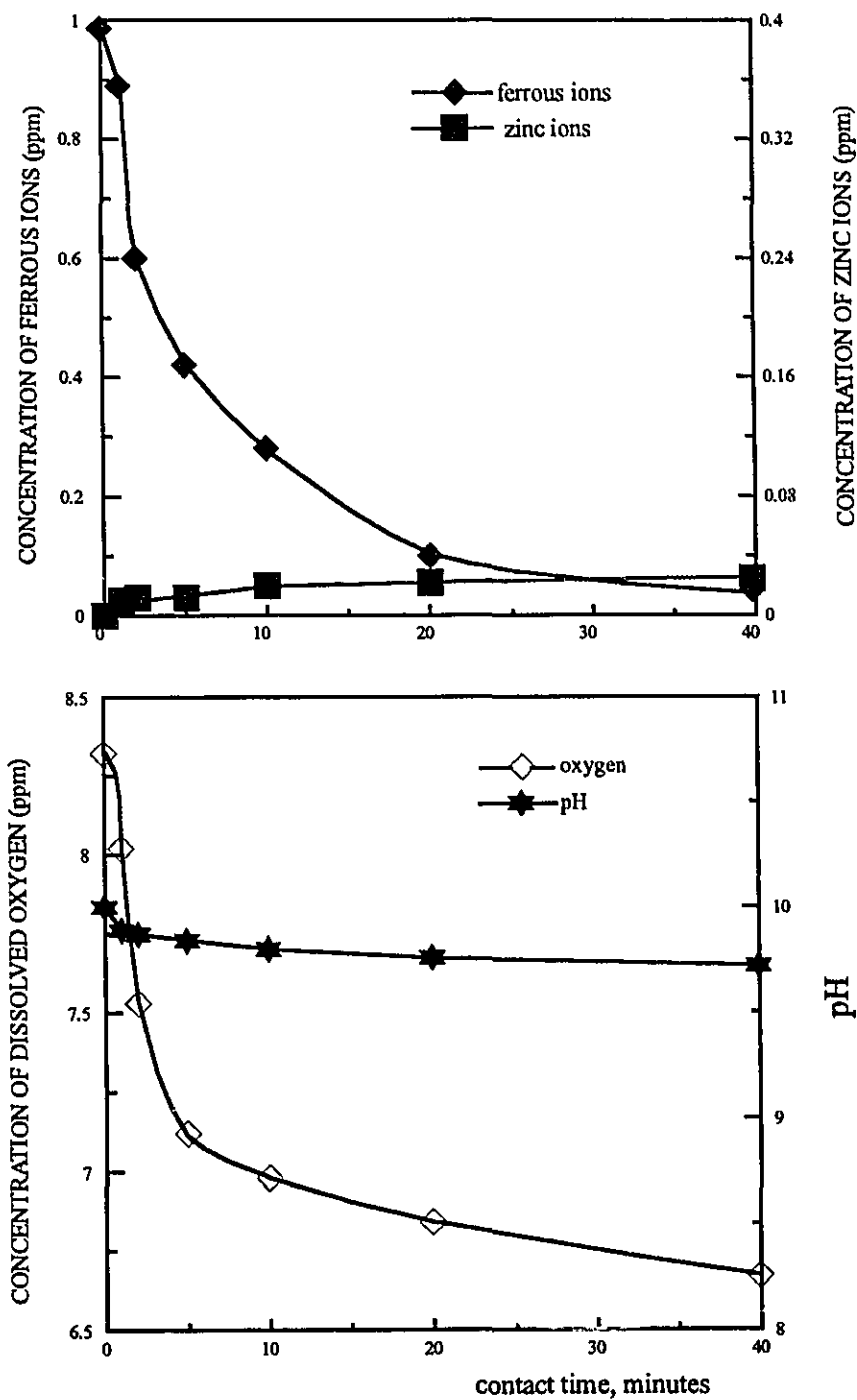


Figure 4.13 The change in ferrous ion (1 ppm initially), zinc ion and oxygen concentration and solution pH (initially pH 10), as a function of contact time with sphalerite (1 g in 50 ml)

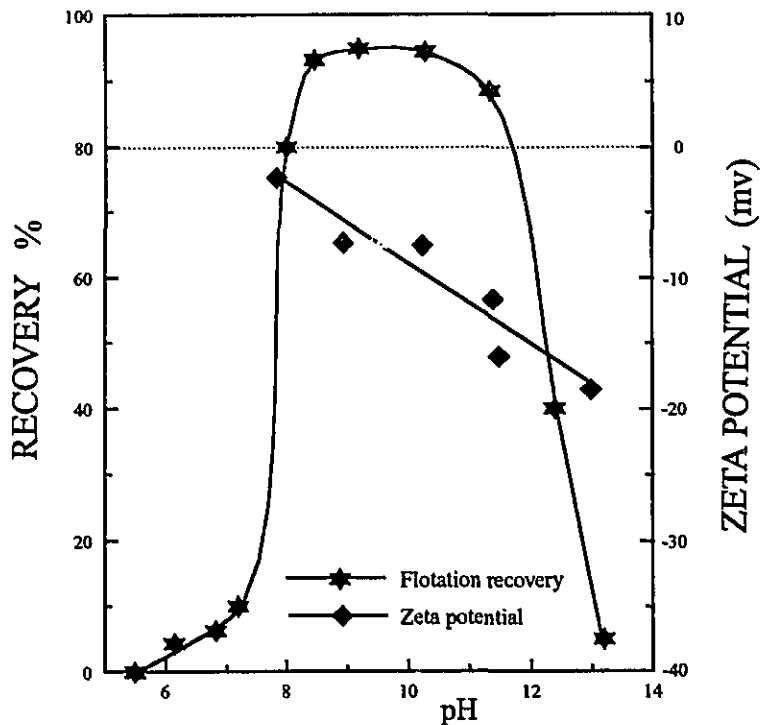


Figure 4.14 The properties of iron xanthate precipitate prepared by mixing 1 M ferrous sulphate with 1 M sodium isopropyl xanthate at different pH (ionic strength controlled by 1×10^{-1} M NaCl)

with sodium isopropyl xanthate (1×10^{-3} mol/L) before washing and filtration. Narrow-range scans of the elements Zn (2p), Fe (2p) and S (2p) are presented in Figs. 4.15, 4.16 and 4.17, respectively. The positions of bands in the XPS spectra are tabulated in Table 4.1.

Table 4.1 Band maxima (eV) and widths obtained from XPS data

System	Binding Energy (eV)			
	S (2p)	O (1s)	Zn (2p _{3/2})	Fe (2p _{3/2})
ZnS + H ₂ O	162.6	532.4	1021.9	not detected
ZnS + Fe ²⁺	161.9	530.1	1021.9	711.1
	169.9	531.6	-	-
ZnS + Fe ²⁺ + X ⁻	161.7	529.1	1021.9	711.1
	162.5	530.3	-	-
	-	531.6	-	-
ZnS + Fe ³⁺	162.6	532.4	1021.9	not detected

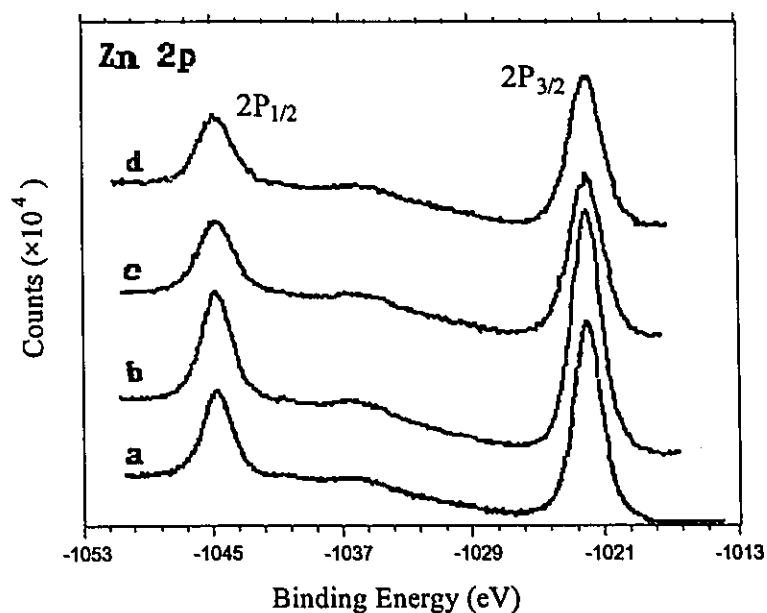


Figure 4.15 XPS spectra of the Zn_{2p} region of sphalerite samples treated with: (a) distilled water, (b) 1×10^{-2} mol/L Fe^{3+} , (c) 1×10^{-2} mol/L Fe^{2+} , (d) 1×10^{-2} mol/L Fe^{2+} , followed by 1×10^{-3} M xanthate.

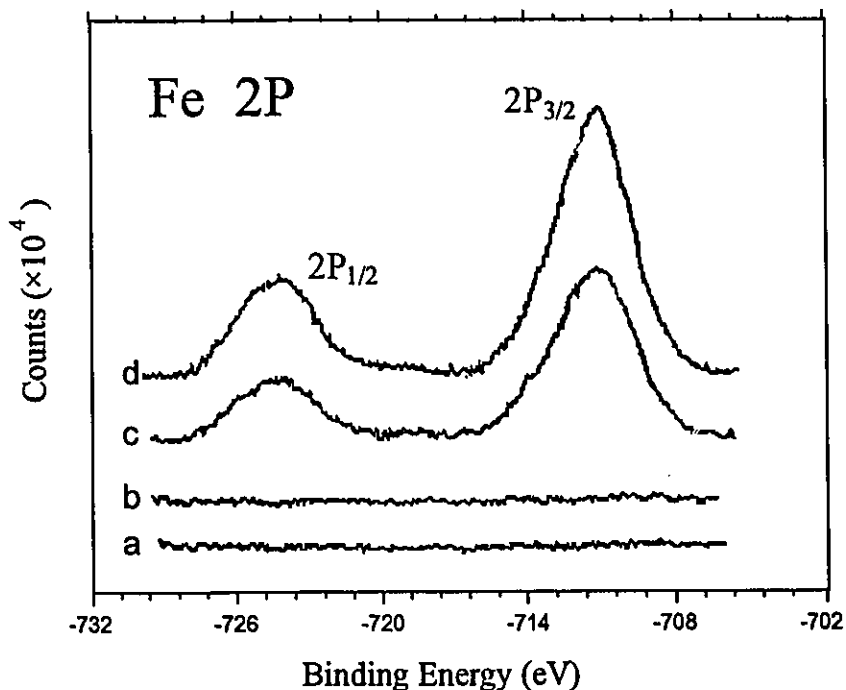


Figure 4.16 XPS spectra of the Fe_{2p} region of sphalerite samples treated with: (a) distilled water, (b) 1×10^{-2} mol/L Fe^{3+} , (c) 1×10^{-2} mol/L Fe^{2+} , (d) 1×10^{-2} mol/L Fe^{2+} , followed by 1×10^{-3} M xanthate.

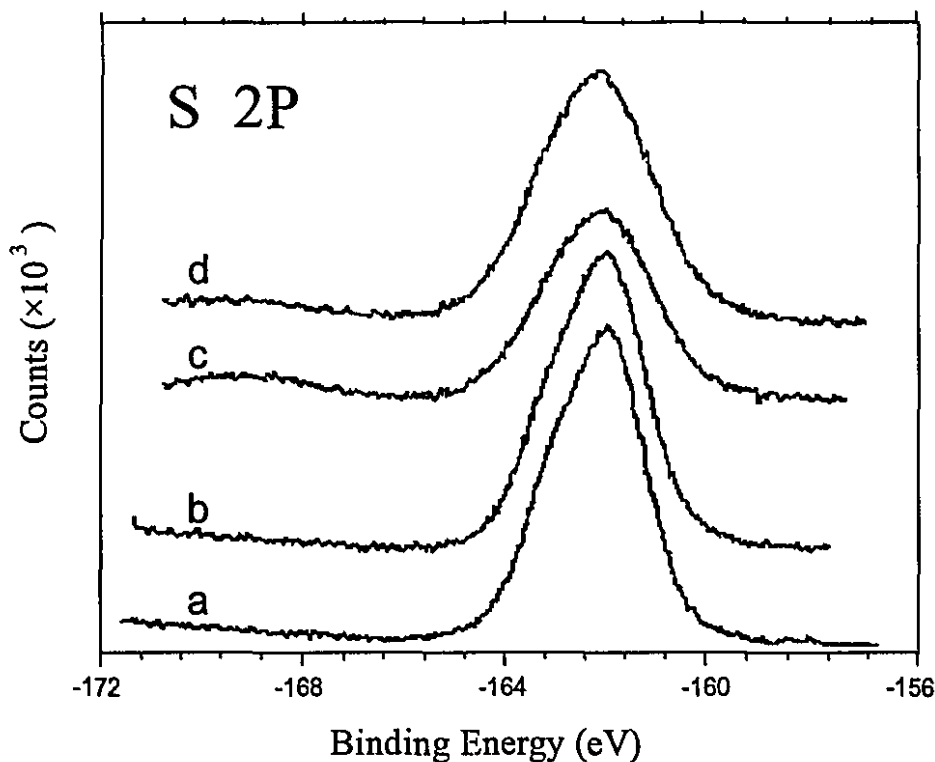


Figure 4.17 XPS spectra of S_{2p} region of sphalerite samples treated with: (a) distilled water, (b) 1×10^{-2} mol/L Fe^{3+} , (c) 1×10^{-2} mol/L Fe^{2+} , (d) 1×10^{-2} mol/L Fe^{2+} , followed by 1×10^{-3} M xanthate.

It is evident that the spectral features attributable to zinc ($2p_{3/2}$ at 1021.9 eV, Fig. 4.15) do not vary to any great extent with changes in method of treatment (Fig. 4.15 (a) - (d)). It should also be noted that the binding energy found in this work agrees well with published values (1021.6 eV) (Mukherjee and Sen, 1976; Rao, 1971), and the binding energy difference (23.1 eV) between the spin-doublet splitting ($2p_{3/2}$ and $2p_{1/2}$ states) is also similar to that determined previously (23.5 eV) for ZnS (Limouzin-Maire, 1981). The presence of a band that is insensitive to the method of treatment at this position in the spectrum is reasonable since little variation is expected in the state of oxidation of the Zn atom with the treatments described in this work.

Figure 4.16 shows the narrow scan over the binding energy range corresponding to Fe ($2p_{3/2}$) (McIntyre and Zetaruk, 1977; Limouzin-Maire, 1981). There is no detectable iron for the sphalerite sample without treatment with Fe ions, in spite of the iron being

present as an impurity (2.8%) in the sample used in this investigation. This indicates that no appreciable surface iron species are present in the original sphalerite. The absence of spectral features in the Fe $2p_{3/2}$ region of sphalerite that has been treated with Fe^{3+} (Fig. 4.16 (b)) suggests that ferric ions are not adsorbed into the sphalerite surface. This observation is consistent with the previous flotation results, in which it was found that the presence of solution-phase Fe^{3+} did not activate the sphalerite. In contrast, a distinct spectral feature at binding energy of 711.1 eV appeared for the sphalerite samples that had been treated with Fe^{2+} (Fig. 4.16 (c)). The presence of this spectral feature clearly suggests an uptake of Fe^{2+} by sphalerite at the pH value used in this experiment (pH=10). This is consistent with previous investigations: namely, that activation occurred only with Fe^{2+} ions and there was a decrease in the solution-phase concentration of Fe^{2+} when this solution was in contact with powdered sphalerite.

A more detailed analysis of the binding energy (Fe $2p_{3/2}$ 711.1 eV) and the spin-doublet splitting (Fe $2p_{3/2}$ and Fe $2p_{1/2}$) of 13.1 eV of iron adsorbed onto the sphalerite surface, indicates that the form of iron on the surface is ferric, i.e. it is in the 3+ oxidation state (McIntyre and Zetaruk, 1977; Limouzin-Maire, 1981). This finding suggests that the Fe^{2+} is oxidised once adsorbed into the surface, resulting in the formation of Fe^{3+} . The presence of Fe^{3+} at the surface of the mineral could have resulted from exposure of the mineral to the atmosphere prior to spectral acquisition; however, the presence of Fe^{3+} is compatible with the observed need for an oxidizing condition for flotation (Fig. 4.3). From iron binding energy and the spin-doublet splitting observed, it is suggested that the surface species is iron oxide(ϵ). Further evidence for this is discussed below.

The sulphur region in the XPS spectrum (Fig. 4.17) shows a distinct peak assignable to the S_{2p} band at a binding energy of ca. 162 eV (Mielczarski, 1986). This peak is asymmetric due to the presence of a splitting of 1.18 eV, which is just below the instrumental resolution of the XPS spectrometer used in the present investigation. This band is assignable to the sulphur present as the sulphide ion in the sphalerite lattice by comparison with the XPS spectra of clean sphalerite that has not been treated. The position and band-shape of this peak does not change either for sphalerite that has been freshly ground or for sphalerite treated with deionized water. This suggests that no large degree of surface

oxidation is induced by the treatments undertaken in this investigation. A weak, broad peak at higher binding energy, ca. 169 eV (Fig. 4.17 (c)), is observed when sphalerite is treated with a solution containing Fe^{2+} , with SO_4^{2-} as the counterion. The low intensity of this peak indicates that the atomic percentage of the species causing this spectral feature is small. This peak is assigned to sulphur present as sulphate (169.4 eV, Limouzin-Maire, 1981). The uptake of sulphate by sphalerite may be due to the requirements of charge neutralization (i.e. to balance the Fe^{2+} that is adsorbed). The sulphur present as sulphate was not observed in sphalerite samples treated with Fe^{3+} , suggesting that the sulphate was on the surface through true adsorption rather than arising from sulphate initially present on the surface. This was confirmed by noting that no XPS bands due to sulphate were observed in spectra obtained with untreated sphalerite.

The sulphate inferred from the XPS spectrum of sphalerite that had been treated with Fe^{2+} is not as evident after being brought into contact with xanthate solution as it was prior to treatment (Fig. 4.17 (d)). This observation suggests that the xanthate replaces the sulphate on the surface. It is expected that the xanthate ion exchange is favorable as the iron xanthate complex has a much lower solubility product ($\text{pK}_{\text{sp}} \sim 35$, Critchley and Hunter, 1986) than the iron sulphate species ($\text{pK}_{\text{sp}} \sim 24$, Critchley and Hunter, 1986) (Zhang et al., 1992). The FWHM (full width at half maximum) for the sulphur peak at 163.2 eV (ca. 4 eV) is increased on incorporation of the xanthate (Fig. 4.17), again suggesting that another sulphur environment is present.

The feature in the XPS spectrum assigned to the $\text{S}_{2\text{p}}$ peak in the presence of xanthate can be fitted by two components (Fig. 4.18), one of which is assignable to the sulphur present in the sulphide mineral (161.7 eV), and the other at higher binding energy is assignable to the sulphur in xanthate (162.9 eV). These peaks are consistent with the results from previous studies in which the binding energies were given as 162.0 and 162.6 eV, respectively (Mielczarski, 1986b). Peaks may also be fitted by three components; however, this necessitates a peak at a lower binding energy than the sulphur present as sulphide in sphalerite. This is not favored as it requires a sulphur environment that is more reduced than sulphide. The presence of one additional peak at higher binding energy relative to the mineral sulphide band implies that the xanthate may be co-ordinated in a

symmetrical fashion. It can therefore be inferred that other, asymmetric orientations of the xanthate relative to the central metal, as for example in the case of adsorption products of xanthate on galena (Laajalehto et al., 1993), are not observed here. The orientation of the xanthate is further considered below.

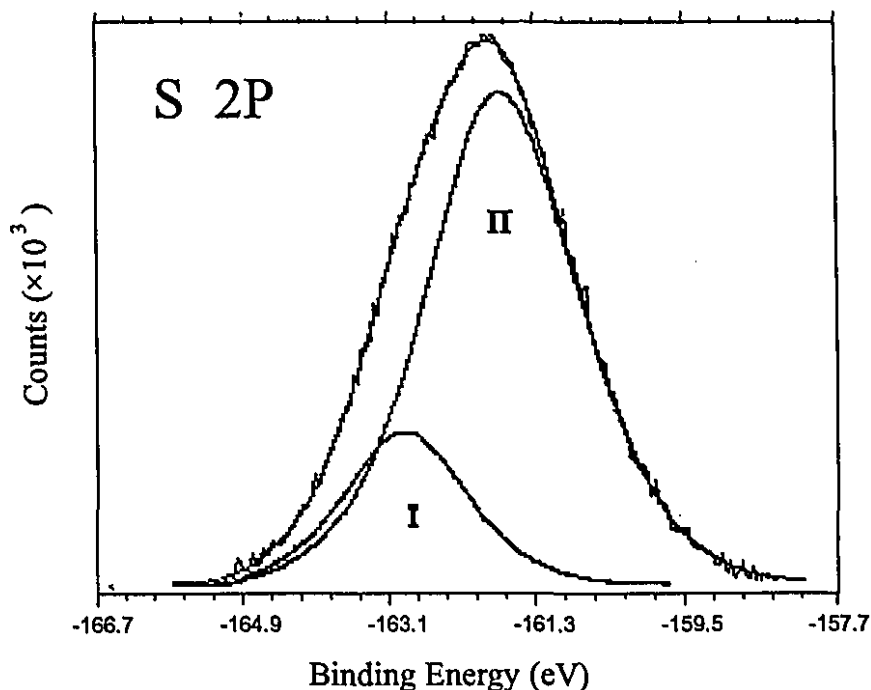


Figure 4.18 XPS spectrum of the S_{2p} region of sphalerite that has been treated with 1×10^{-2} mol/L Fe^{2+} , followed by 1×10^{-3} M xanthate, showing the deconvolution of the band into components assignable to xanthate and sulfide (higher and lower binding) energies, respectively).

The XPS spectrum obtained in the O_{1s} region for sphalerite that has been treated with Fe^{2+} is presented in Fig. 4.19. Two components, with band maxima at 530.1 and 531.6 eV, can be fitted to the experimental peak. These two peaks may be assigned to oxygen present as an oxide and a hydroxide, respectively, by comparison with the XPS spectrum of α -FeOOH in which spectral features are at 530.3 and 531.4 eV (McIntyre and Zetaruk, 1977). The nature of the surface oxide will be discussed in further detail below.

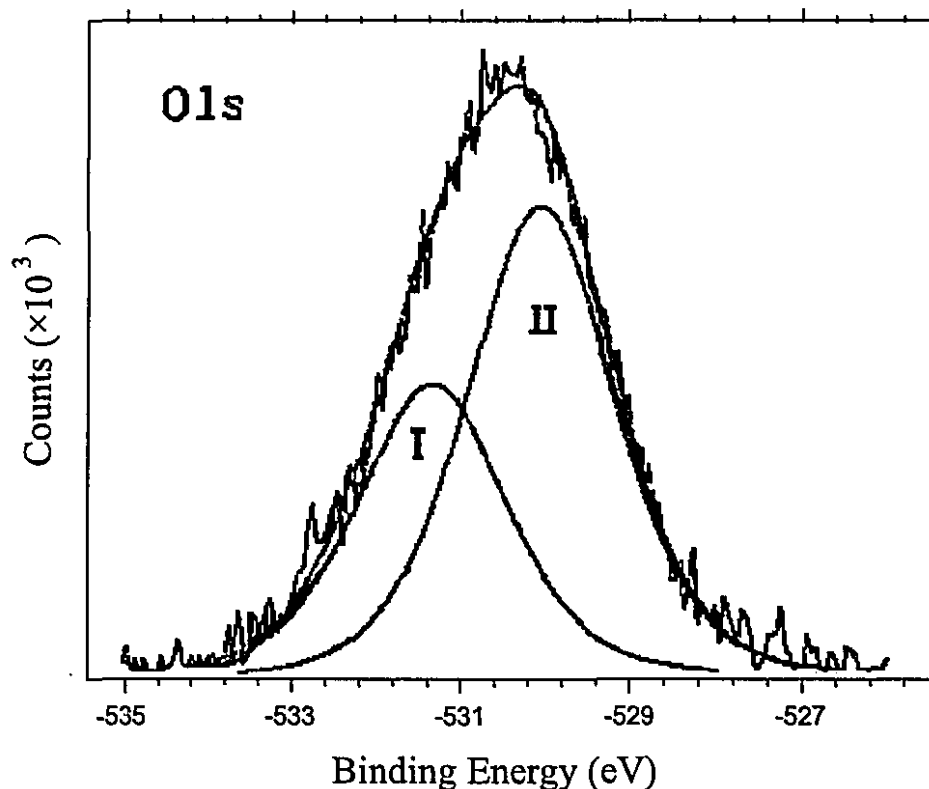


Figure 4.19 XPS spectra of the O_{1s} region of sphalerite sample treated with 1×10^{-2} mol/L Fe^{2+} , followed by 1×10^{-3} M xanthate. The component at higher (I) and lower (II) binding energies are assigned to oxygen present as hydroxide and oxide, respectively.

4.3 DRIFTS

The IR spectra obtained by this method exhibit a selectivity to species that are present on the surface and complements the XPS data described above. The presence and speciation of an Fe^{3+} oxide at the surface from the above XPS results can be further investigated using DRIFTS.

DRIFTS spectra for sphalerite which has been treated with Fe^{2+} and Fe^{3+} in the absence of xanthate are presented in Fig. 4.20 (a) and (b), respectively. It is evident that the peaks in the region $1050 - 700 \text{ cm}^{-1}$ present in the Fe^{2+} treated mineral (Fig. 4.20 (a)) are not present in the Fe^{3+} treated sample (Fig. 4.20 (b)). This is consistent with the findings

from the XPS data that there is no evidence of Fe present on the surface when sphalerite is treated with Fe^{3+} .

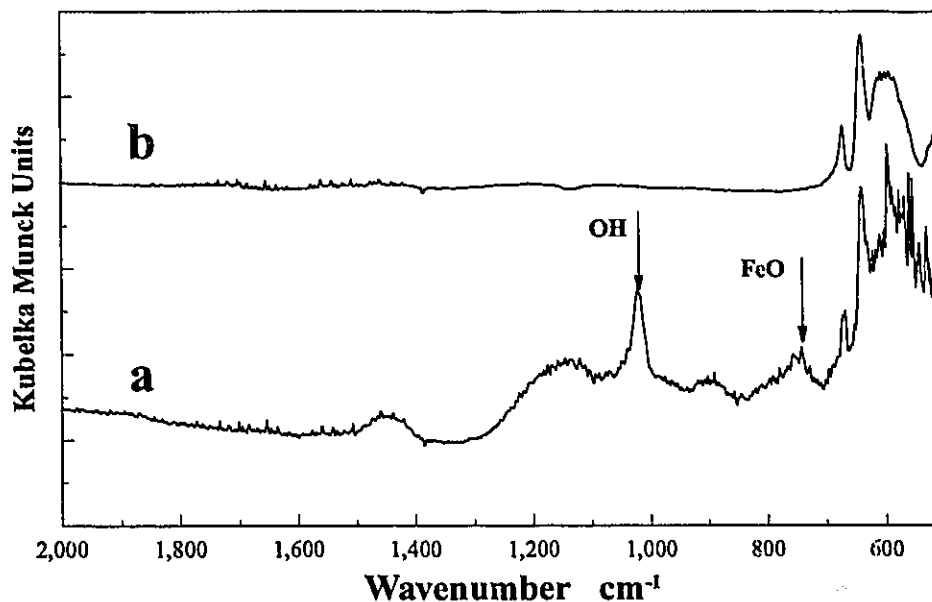


Figure 4.20 DRIFT spectra of sphalerite samples treated with: (a) 1×10^{-2} mol/L Fe^{2+} showing the presence of $\gamma\text{-FeOOH}$ and (b) sphalerite treated with 1×10^{-2} mol/L Fe^{3+} .

The identity of the product at the surface may be investigated by DRIFTS. Clean surfaces of sphalerite exhibit features (669 and 636 cm^{-1}) which are associated with the sulphide in the lattice and these features are present in similar positions for all the sphalerite samples, irrespective of the treatment conditions. Peaks at 1020 and 740 cm^{-1} for sphalerite treated with solution phase Fe^{2+} are in a similar position to those found previously for $\gamma\text{-FeOOH}$ (1025 and ca. 750 cm^{-1}) and assigned to $\delta(\text{OH})$ and $\nu(\text{FeO})$ vibrations, respectively (Barton et al., 1990 and Poling, 1969). The presence of spectral features in similar positions to that of $\gamma\text{-FeOOH}$ suggest that iron in the $3+$ oxidation state is present as a hydro-oxide on the surface for the Fe^{2+} activated sphalerite. This observation is consistent with that obtained from the above XPS characterization of Fe_{2p} (Fig. 4.17(c)) and the O_{1s} (Fig. 4.19) regions, in which for the latter, oxygen environments corresponding to both oxide and hydroxide were observed.

4.4 ATR

XPS and DRIFTS are *ex situ* techniques and therefore the results are potentially sensitive to artifacts arising from the absence of the aqueous environment. This limitation is partially overcome by use of the ATR technique. ATR spectroscopy has been used previously in the investigation of minerals (Lippenen, 1990; Lippenen et al., 1989 and Ray et al., 1973). The technique is also useful for obtaining spectra from strongly absorbing samples, such as aqueous media. The short penetration depth of the evanescent wave, exploited by this technique, allows a degree of surface sensitivity to be achieved in the presence of water (Knoll, 1991; Debe, 1987; Christensen and Hamnett, 1990).

Experiments were performed on a sphalerite ATR element and the results are presented in Fig. 4.21. All spectra have been normalized to the 1624 cm^{-1} band assigned to the bending mode of water.

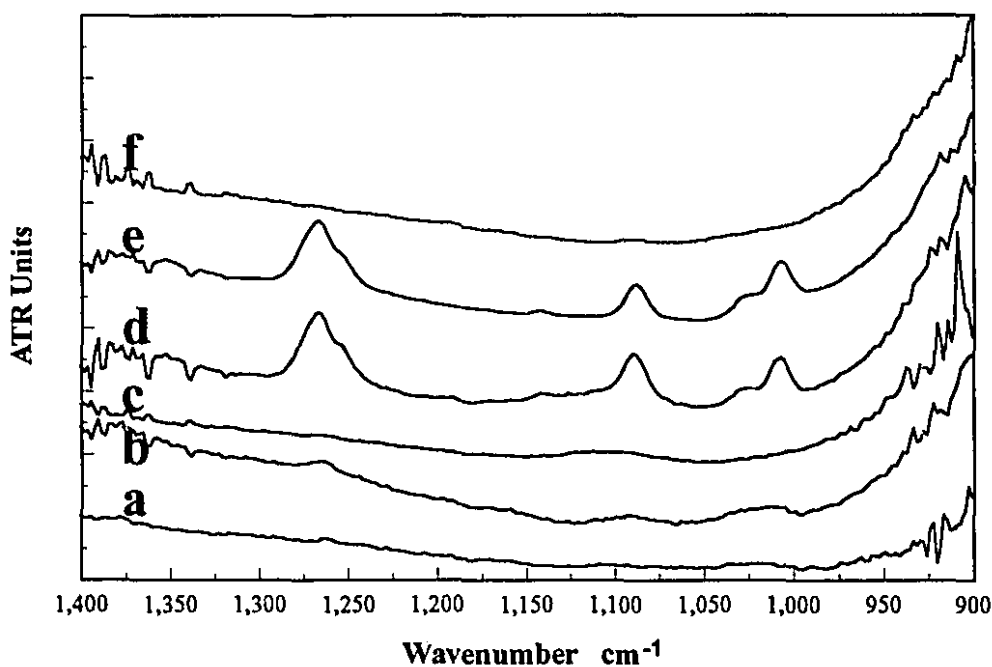


Figure 4.21 ATR spectra obtained from a sphalerite crystal treated with: (a) distilled water, (b) 1×10^{-3} mol/L xanthate, (c) washed from (b) and 1×10^{-2} mol/L Fe^{2+} added, (d) washed from (c) followed by addition of 1×10^{-3} M xanthate, (e) washing with distilled water from (d) showing the presence of intense bands due to a surface bound complex, (f) as for (e) but Fe^{3+} used in step (c) instead of Fe^{2+} showing no bands associated with a surface-bound complex.

As shown in Fig. 4.21, no evidence of adsorbed species was noted with cleaned sphalerite in the presence of distilled water. On addition of a 1×10^{-3} mol/L xanthate solution, low intensity broad peaks were observed (ca. 1265, 1080 and 1010 cm^{-1}). These broad peaks are typical of xanthate compounds in the solution phase. The position of the solution-phase peaks correspond to that of xanthate in the solid state (get resolved spectrum cm^{-1} , respectively). The frequency shifts observed are comparable to displacement observed in the IR spectra of ethyl xanthate in aqueous media (1175, 1161, 1147, 1117 and 1046 cm^{-1}) from the solid state (1172, 1159, 1139, 1117, 1100 and 1049 cm^{-1} , respectively (Leppenen et al., 1989)). These spectral features were completely removed by flushing with distilled water, which confirms that the bands arising from this compound are associated with the solution phase and are not from species adsorbed strongly onto the ATR crystal. This result is consistent with previous work which showed that xanthate does not adsorb onto sphalerite under these conditions.

Spectra collected after the addition of 1×10^{-2} mol/L Fe^{2+} shows a weak peak centered at 1089 cm^{-1} (Fig. 4.21(c)). This is in a similar position to that observed for sulphate (ca. 1100 cm^{-1}) (Nakamoto, 1970; Miller and Wilkins, 1952). This weak spectral feature disappeared after flushing with distilled water, which suggests that the compound giving rise to this band in the spectrum is associated with a solution phase species. (The absence of any discernible residual bands in the spectrum after this treatment of sphalerite, however, does not mean that the Fe^{2+} is absent from the surface, only that the Fe^{2+} is not detectable in the frequency range covered. To examine the presence of the Fe^{2+} on the surface with the ATR technique, the Far-IR region, in which lattice vibration modes are present, must be used.) Addition of 1×10^{-2} mol/L xanthate at this stage immediately caused the appearance of six sharp bands at 1267, 1253, 1140, 1089, 1028 and 1007 cm^{-1} . These bands may be provisionally assigned to the coupled vibrations of the C-O and C-S bonds in the xanthate molecule (Leppenen, 1990 and Ray et al., 1973). An important observation is that these peaks were not removed by flushing with distilled water, suggesting that the species present were strongly bound to the surface. On removal of the crystal, the surface was observed to be markedly hydrophobic, in contrast to the hydrophilic nature of the surface observed prior to treatment. No evidence was found in these studies to suggest that

bands are not due to a symmetrically coordinated xanthate complex as only three intense bands have been attributed to the ethyl xanthate complex present on Cu_2S surfaces (Leppenen, 1990; Leppenen et al., 1989; Nakamoto, 1970). The structure of this hydrophobic complex and its molecular orientation may be determined by polarisation studies.

Similar experiments with Fe^{3+} as the source of iron did not give any of the spectral features observed for Fe^{2+} in solution.

The *in situ* ATR technique indicates that the xanthate collector is bonded to the sphalerite surface after treatment with Fe^{2+} . This observation is consistent with the findings that the presence of xanthate is necessary to achieve flotation of Fe^{2+} -treated sphalerite.

4.5 ULTRA-VIOLET SPECTRA

To study the properties of surface species further, precipitates were prepared by reacting different xanthate and iron solutions. The precipitates were then treated with acetone. Approximately 70% of the bulk precipitates prepared at pH 5-6 dissolved in acetone decreasing to about 50% for those formed at pH 12.

The UV spectra of the acetone solutions derived from the bulk precipitates prepared under three conditions are shown in Fig. 4.22. All the samples showed similar UV absorption properties with maxima at 212 nm and 324 nm. Compared to the UV spectra of xanthate and dixanthogen in acetone (Fig. 4.23), the spectra in Fig. 4.22 are close to those of xanthate and show no evidence of dixanthogen.

From Fig. 4.23, the characteristic peaks of xanthate in pure acetone at 327 nm and 212 nm are shifted from the standard values in water at 301 nm and 226 nm, respectively, and the ratio of these two peak maxima is no longer 2:1 (Leja, 1982). (In a 30% acetone solution, the two peaks shift back toward the 301 nm and 226 nm values.) The slight shift of the peak at 327 nm (Fig. 4.23) to 324 nm (Fig. 4.22) could indicate the presence of an OH group in an iron xanthate (Kiselev A.V. and Lygin V.I., 1975).

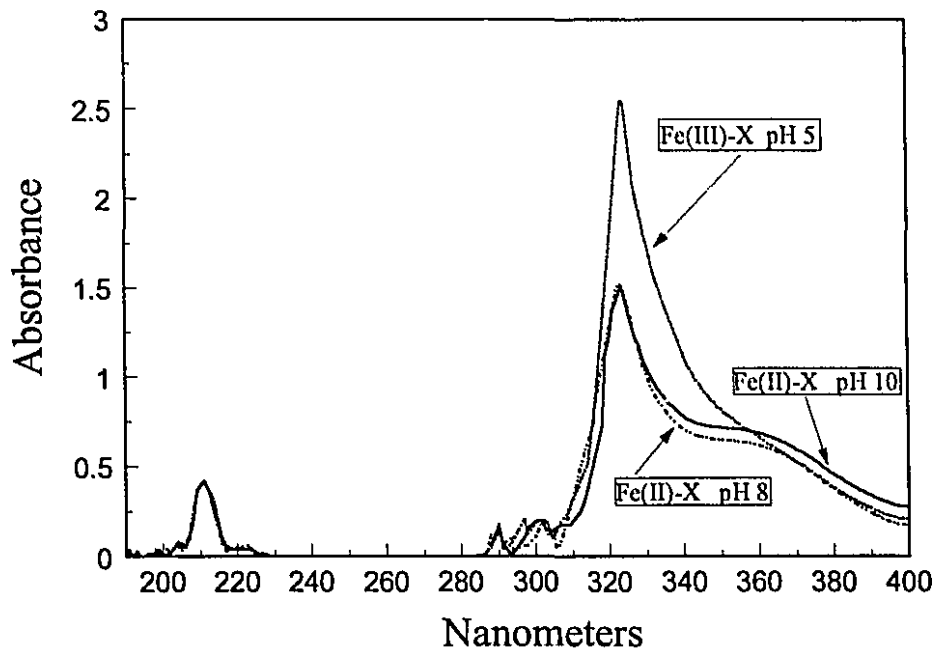


Figure 4.22 UV spectra of acetone solution derived from bulk precipitates prepared at three pHs

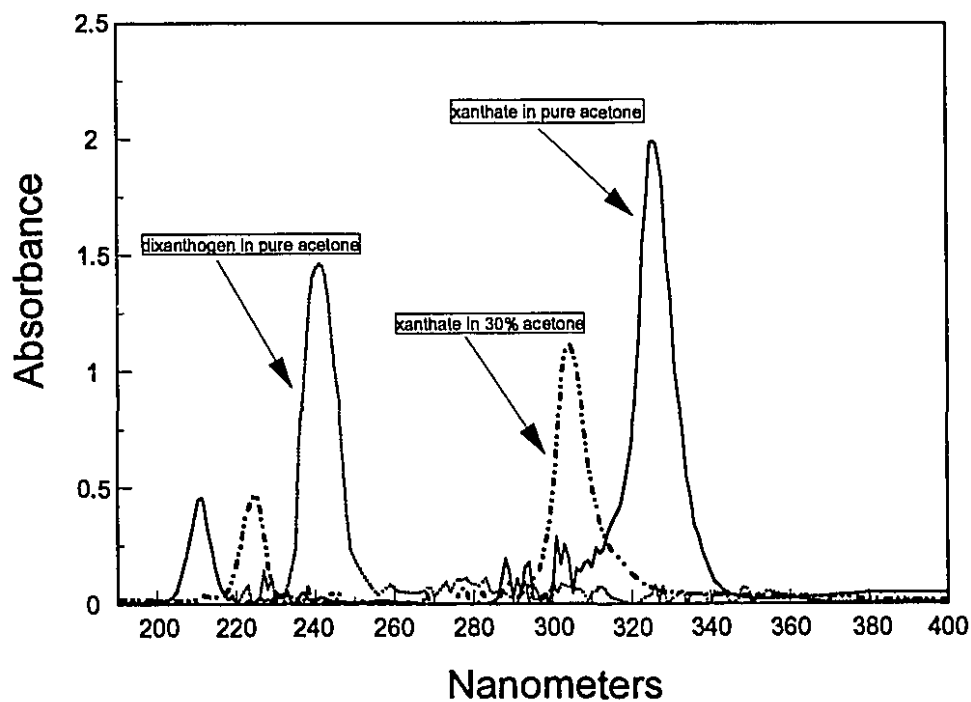


Figure 4.23 UV spectra of acetone solutions of xanthate and dixanthogen in different acetone concentrations

4.6 INFRARED ABSORPTION SPECTRA

Figure 4.24 shows the infrared spectrum of sodium isopropyl xanthate. The assignment of frequencies to specific bonds related to the xanthate group, according to Nakanishi (1977) is: the strong 1617 cm^{-1} band corresponds to vibration of the C-C-C bonds (this is also reflected in the bands at 1170 and 1145 cm^{-1}); the $1020\text{-}1070\text{ cm}^{-1}$ band is the C=S stretch; the two strong bands at 1180 cm^{-1} and 1120 cm^{-1} are vibrations of the C-O-C linkages; and, the 880 cm^{-1} band is the asymmetric stretching mode of C-S. The absorption bands at 1460 cm^{-1} , 1380 cm^{-1} and 1320 cm^{-1} , with the 1380 cm^{-1} band being the strongest, suggest C-C-O-. The absorption bands evident at less than 600 cm^{-1} indicate interactions between metal ions (Na in this case), and an organic polar group (Nakamoto, 1963). These assignments are consistent with those of Poling (1961) and Gould and Finkelstein (1969). The characteristic absorption band of dioxanthogen, at $1240\text{-}1270\text{ cm}^{-1}$ (Leja, 1982), is clearly absent.

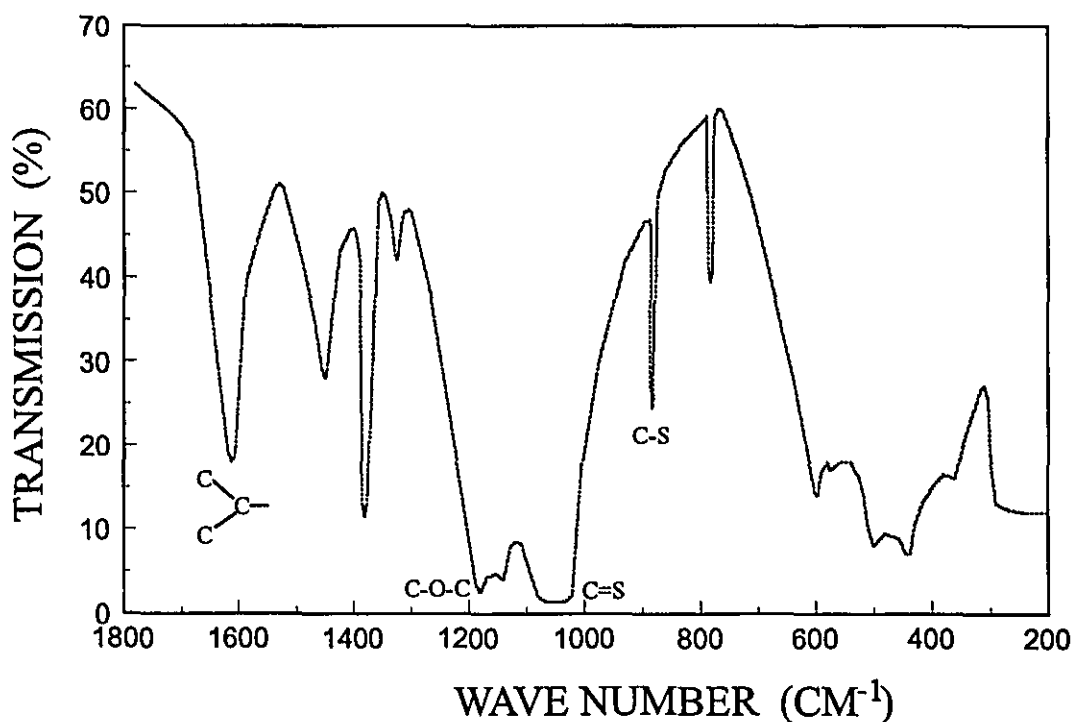


Figure 4.24 Infrared spectrum of sodium isopropyl xanthate

Figures 4.25 and 4.26 show the infrared spectra of bulk precipitates formed from ferrous sulphate and xanthate solutions at pH 8 and 10, respectively: There is not much difference between them.

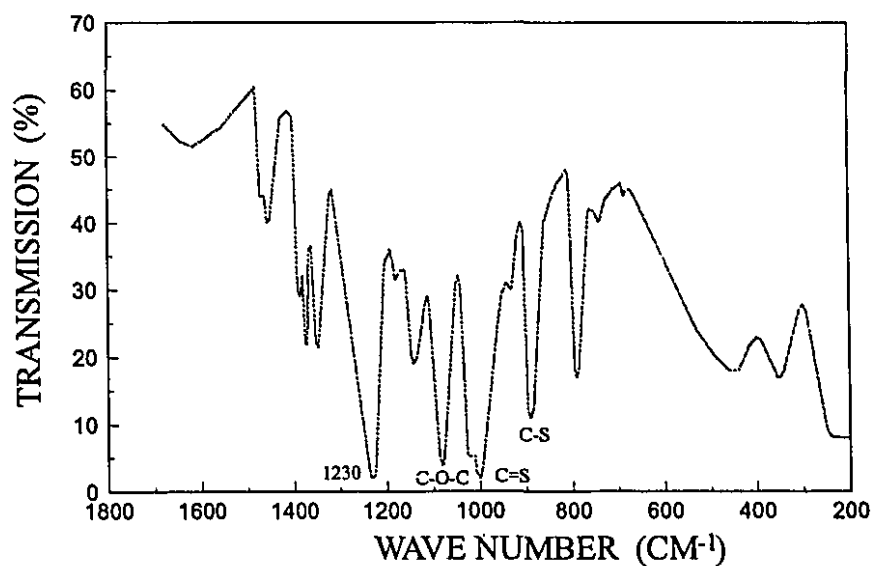


Figure 4.25 Infrared spectrum of precipitate formed from ferrous sulphate and sodium isopropyl xanthate solution at pH 8

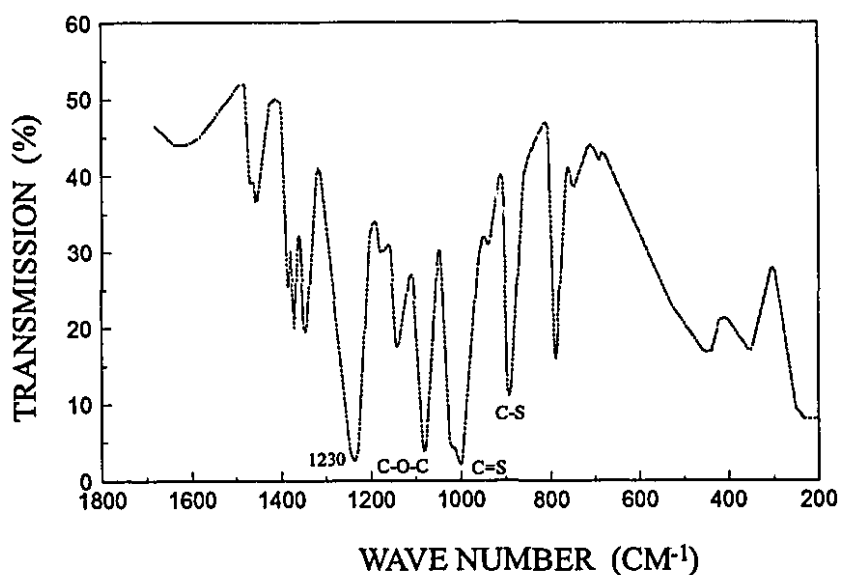


Figure 4.26 Infrared spectrum of precipitate formed from ferrous sulphate and sodium isopropyl xanthate solution at pH 10

4.7 X-RAY DIFFRACTION

Figure 4.27 shows the X-ray diffraction (XRD) patterns of the precipitates prepared from both ferrous and ferric sulphate solutions and the residue of bulk precipitate prepared from ferrous sulphate and xanthate after dissolution in acetone. It was observed that the XRD pattern of precipitate from ferrous sulphate was the combined pattern of that of the precipitate from ferric sulphate and that of the residue of the bulk precipitate.

The XRD pattern did not correspond to any of the reference patterns in the computer database (Fe_2O_3 and $\text{Fe}(\text{OH})_3$ patterns are shown to illustrate this lack of fit); thus the general designation FeO_x (Mielczarski, 1986) will be adopted.

Figure 4.28 shows the XRD pattern of bulk precipitate, the residue and, by difference, the inferred spectrum of the dissolved (i.e. organic-containing) fraction of the bulk precipitate. The XRD pattern of the latter is taken to be that of ferric hydroxy xanthate which the IR results suggest is the likely compound.

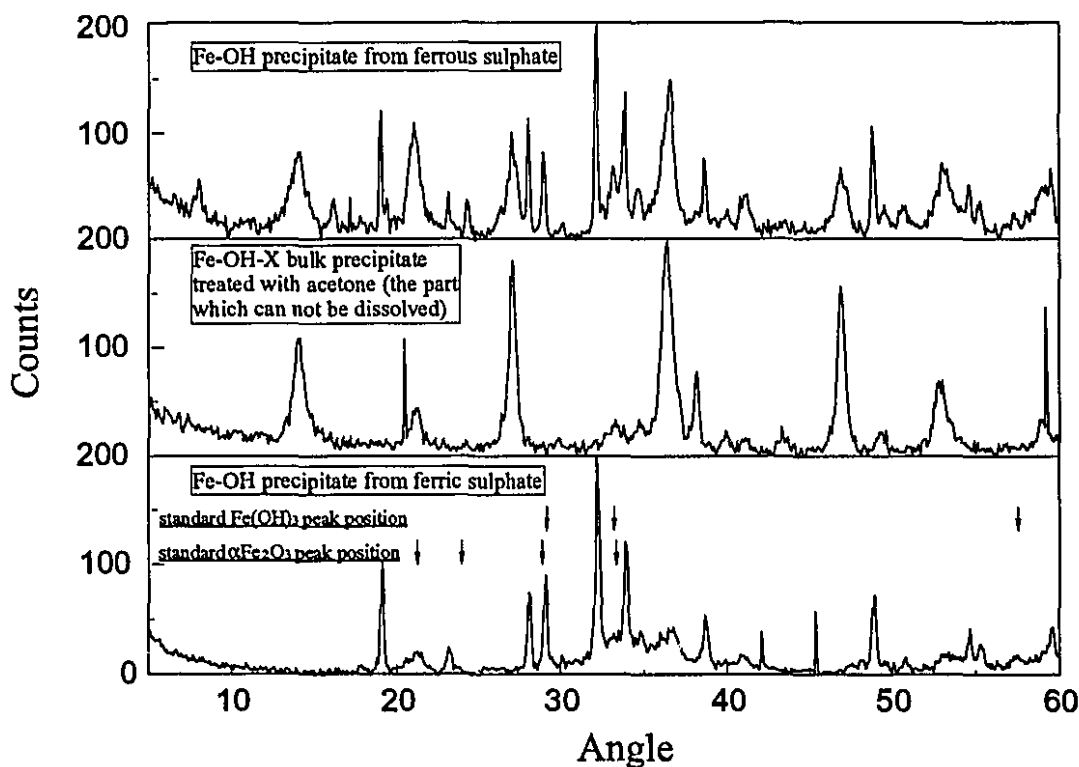


Figure 4.27 Precipitate x-ray diffraction patterns

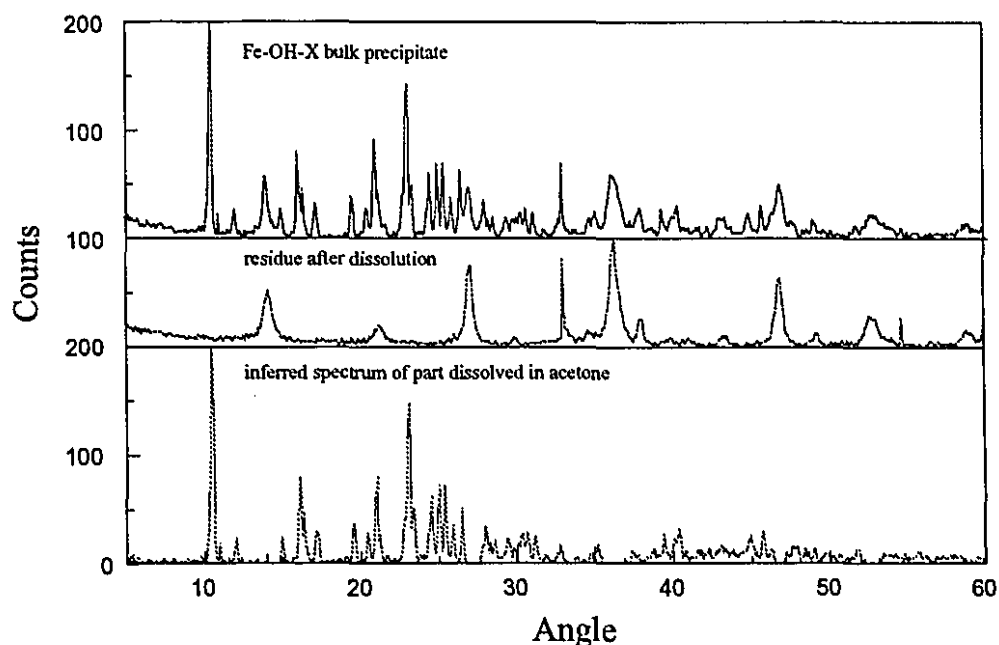


Figure 4.28. Fe-OH-X precipitate x-ray diffraction pattern

4.8 MÖSSBAUER MEASUREMENTS

Figure 4.29 shows the Mössbauer spectra of bulk precipitates prepared from ferrous sulphate and xanthate solutions at pH 6.1 and 12: They are similar. The isomer shifts are consistent with high spin Fe^{3+} compounds (Stevens and Shenoy, 1981) although the quadrupole splittings are larger than expected. From a fitting routine, the presence of three ferric compounds is suggested with the main component (over 80%) decreasing slightly as the pH increases while the other two components increase (Fig. 4.30).

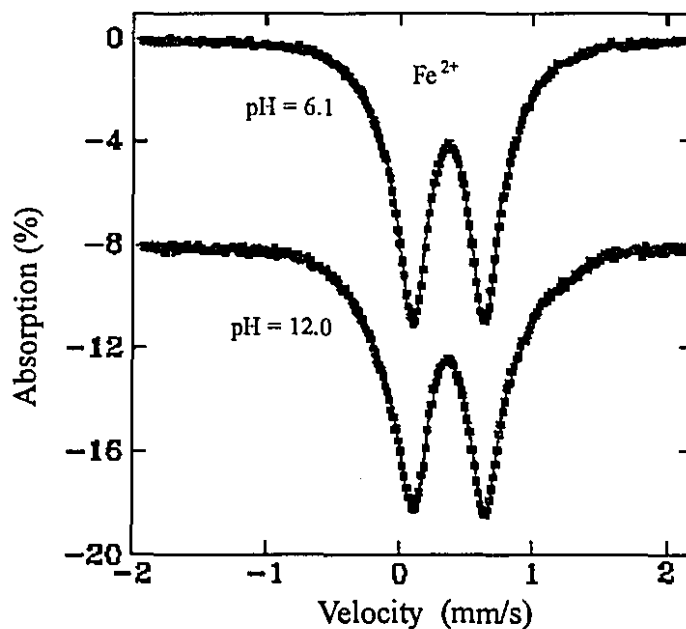


Figure 4.29 Mössbauer spectra of bulk precipitates from ferrous sulphate and xanthate solution at different pH

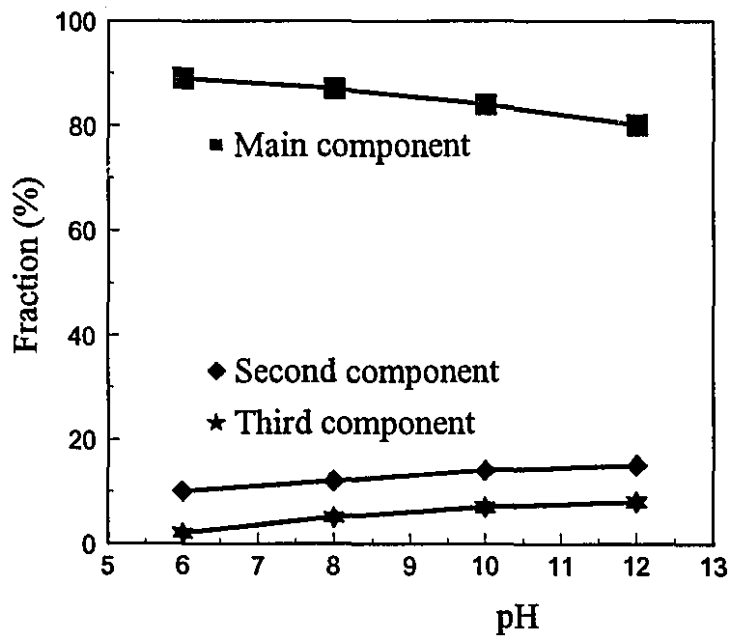


Figure 4.30 Summary of Mössbauer spectrum fits

CHAPTER 5

SURFACE IONIZATION AND COMPLEXATION AT THE SPHALERITE/WATER INTERFACE

5.1 INTRODUCTION

Complexation at the mineral/water solution interface plays an important role in both the solution and surface chemistry of sulfide mineral flotation systems. Understanding the nature of the surface functional groups is essential to elucidating the mechanism of adsorption.

The surface reactivity of a mineral in a solution derives from the chemical behavior of its surface functional groups. A surface group is a chemically reactive unit bound to a solid, which can interact with species in solution. The surface groups cannot (except by "surface diffusion") migrate like the solute molecules.

Solid surfaces in water develop an electrical double layer. Many electrical double layer and associated adsorption models have been proposed. Some emphasize the importance of the electrical double layer structure and physical interactions of major electrolyte ions with solid surfaces (James, 1972 [a, b, c]; Bowden, 1973). Others stress the specific chemical or coordinative interactions of solutes with solid surfaces (Dugger, 1964; Schindler, 1976; Hohl etc., 1976; and Stumm etc., 1976) to describe the distribution of dilute solutes between solid surfaces and solution.

In the past decade, a number of studies devoted to chemical modeling of the interfacial region between an oxide or hydroxide solid and an aqueous solution have been carried out. Those studies have produced successful quantitative models accounting for both cation and anion adsorption phenomena. However, few studies have been carried out for sulphide minerals except for some pioneering work on pyrite performed by Fornasiero and Ralston (1992). From their calculations, the mechanism of the function of iron hydroxide-xanthate complexes in pyrite flotation was obtained.

The present approach has been developed from electrical double layer properties measured under controlled conditions with single sphalerite mineral. The model is reasonably complete in that both physical and chemical interactions were considered simultaneously in the calculation of surface and solution equilibria for the major electrolyte ions and dilute solutes. An improvement in calculation over the usual approach (MIN-EQL developed by Westall et al. (1976), modified and used by some researchers (Davis, 1978[a,b]; Wood, Fornasiero and Ralston (1990); Fornasiero and Ralston (1992); Schecher, 1992)) is accomplished through the use of MATLAB^{TM†} software which made the calculations simpler and gave relatively better fitting. From the calculations, a good prediction of the surface charge - pH relationship from the zeta potential - pH experimental data can be obtained because the relationship between the surface charge and zeta potential is defined in the double layer theory, and this relationship is reflected in the calculation procedure.

5.2 SURFACE IONIZATION EQUILIBRIA AND THE ELECTRICAL DOUBLE LAYER

According to Rönngren et al. (1991), on a sphalerite surface in water three different surface species (SH_2 , ZnSH^+ and ZnOH^-) are formed with different equilibrium constants.

To obtain a reliable and accurate description of the electrical double layer, it is necessary to formulate (1) the reactions that lead to the development of surface charge on the solid, and (2) the structure of the potential and charge relationships at the interface.

Significant advances in double layer theory for ionizable surfaces have come from the formulation of the surface charge—surface potential relationship. Using an electric double layer model, experimental surface potential (i.e. zeta potential) data can yield information about (1) the stoichiometry of the surface ionization reactions, and (2) the value of the ionization constants. A model of the double layer structure is required to complete the equations necessary to relate the surface and solution equilibria. Sun (1991) studied sphalerite surface equilibria by potentiometric titration and confirmed the

† MATLAB is the trademark of MathWorks, Inc.

importance of H^+ and OH^- in controlling charge at the sphalerite/water interface. He also assumed that the hydrated ZnS surface contains both OH and SH groups that originate from a dissociative adsorption of water molecules. Based on his work, a site-binding model is developed here.

5.3 SITE-BINDING MODEL

The site-binding model describes the electrical double layer at the solid-aqueous solution interface. The electrical double layer around each particle is schematically represented in Fig. 5.1 (Hunter, 1981).

From the studies performed by Wright and Hunter (1973) and Westall and Hohl (1980), it is evident that only this triple layer model can reproduce both the σ_0/pH and the ζ/pH curves with reasonable values for the parameters. In the present study, this triple layer model is also taken to represent the electrical double

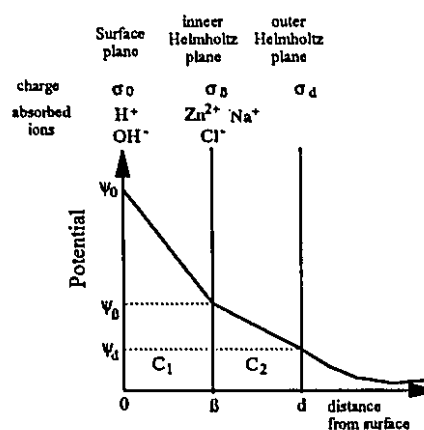
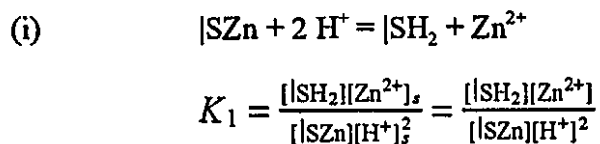


Figure 5.1 Schematic representation of the electrical double layer around the sphalerite particle

layer at the sphalerite surface. The surface is considered to be covered with specific groups or sites which can become charged by reacting with protons in a similar manner to metal oxides. Adsorption of ions occurs in the inner region with potential-determining ions, H^+ , OH^- and Zn^{2+} , adsorbing on available sites, $|SZn$ and $|ZnS$ shown in Fig. 1.1, according to (see NOMENCLATURE)



where

$$[Zn^{2+}]_s = [Zn^{2+}] \exp(-2e\psi_0/kT) \quad \text{and} \quad [H^+]_s = [H^+] \exp(-e\psi_0/kT)$$

$$\text{so that} \quad [|\text{SH}_2] = \frac{K_1[|\text{SZn}][\text{H}^+]^2}{[\text{Zn}^{2+}]} \quad (5.1)$$

$$\begin{aligned} \text{(ii)} \quad & |\text{SZn} + \text{H}_2\text{O} = |\text{SZnOH}^- + \text{H}^+ \\ & K_2 = \frac{[|\text{SZnOH}^-][\text{H}^+]_s}{[|\text{SZn}][\text{H}_2\text{O}]} = \frac{[|\text{SZnOH}^-][\text{H}^+]}{[|\text{SZn}]} \exp(-e\psi_0/kT) \end{aligned}$$

$$\text{i.e.} \quad [|\text{SZnOH}^-] = \frac{K_2[|\text{SZn}]}{[\text{H}^+]} \exp(e\psi_0/kT) \quad (5.2)$$

$$\begin{aligned} \text{(iii)} \quad & |\text{ZnS} + \text{H}^+ = |\text{ZnSH}^+ \\ & K_3 = \frac{[|\text{ZnSH}^+]}{[|\text{ZnS}][\text{H}^+]_s} = \frac{[|\text{ZnSH}^+]}{[|\text{ZnS}][\text{H}^+]} \exp(e\psi_0/kT) \end{aligned}$$

$$\text{i.e.} \quad [|\text{ZnSH}^+] = K_3[|\text{ZnS}][\text{H}^+] \exp(-e\psi_0/kT) \quad (5.3)$$

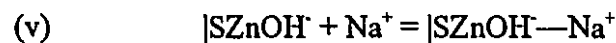
For colloids of reversible electrode systems the total potential difference between phases is determined by the equality of electrochemical potential of the potential determining ions (p.d.i.) in the interior of both phases. However, for electrochemically irreversible colloids, e.g., many oxides (Davis, James and Leckie, 1978), where ions are distributed only between the solution and surface, the surface potential results in a complex manner from the adsorption and dissociation reactions of the surface sites,

$$\begin{aligned} \text{(iv)} \quad & |\text{SZnOH}^- + \text{Zn}^{2+} = |\text{SZnOH}^- \text{---} \text{Zn}^{2+} \\ & K_4 = \frac{[|\text{SZnOH}^- \text{---} \text{Zn}^{2+}]}{[|\text{SZnOH}^-][\text{Zn}^{2+}]_s} = \frac{[|\text{SZnOH}^- \text{---} \text{Zn}^{2+}]}{[|\text{SZnOH}^-][\text{Zn}^{2+}]} \exp(2e\psi_\beta/kT) \end{aligned}$$

$$\text{i.e.} \quad [|\text{SZnOH}^- \text{---} \text{Zn}^{2+}] = K_4[|\text{SZnOH}^-][\text{Zn}^{2+}] \exp(-2e\psi_\beta/kT) \quad (5.4)$$

In addition to the affinity of the ions for the surface, these ions are also subject to an attractive or a repulsive electrical interaction following the Boltzmann distribution, e.g., $\exp(\pm ze\psi_0/kT)$.

Electrolyte ions (Na^+ and Cl^-) are also adsorbed in the inner region and form a complex with the charged surface sites according to



$$K_5 = \frac{[|\text{SZnOH}^- - \text{Na}^+]}{[|\text{SZnOH}^-][\text{Na}^+]_s} = \frac{[|\text{SZnOH}^- - \text{Na}^+]}{[|\text{SZnOH}^-][\text{Na}^+]} \exp(e\psi_\beta/kT)$$

$$\text{i.e.} \quad [|\text{SZnOH}^- - \text{Na}^+] = K_5 [|\text{SZnOH}^-][\text{Na}^+] \exp(-e\psi_\beta/kT) \quad (5.5)$$



$$K_6 = \frac{[|\text{ZnSH}^+ - \text{Cl}^-]}{[|\text{ZnSH}^+][\text{Cl}^-]_s} = \frac{[|\text{ZnSH}^+ - \text{Cl}^-]}{[|\text{ZnSH}^+][\text{Cl}^-]} \exp(-e\psi_\beta/kT)$$

$$\text{i.e.} \quad [|\text{ZnSH}^+ - \text{Cl}^-] = K_6 [|\text{ZnSH}^+][\text{Cl}^-] \exp(e\psi_\beta/kT) \quad (5.6)$$

5.4 THE CHARGE BALANCE

The formation of surface complexes readjusts the equilibrium and affects the proton balance. The surface charge defined from the proton balance, σ_0 , represents the net number of protons released or consumed by all surface reactions including ion binding reactions as well as ionization of the surface to form the species $|\text{ZnSH}^+$ and $|\text{SZnOH}^-$. For example, increases in background electrolyte concentration cause additional binding of counter-ions until equilibrium is reestablished subject to the effects of the electrostatic field. In this manner, surface complexation also provides a development of surface charge in addition to the role of protons and hydroxyl ions. Hence the surface charge is given by

$$\sigma_0 = B\{[|\text{ZnSH}^+] + [|\text{ZnSH}^+ - \text{Cl}^-] - [|\text{SZnOH}^-] - [|\text{SZnOH}^- - \text{Na}^+] - [|\text{SZnOH}^- - \text{Zn}^{2+}]\} \quad (5.7)$$

and the specifically adsorbed charge is

$$\sigma_\beta = B\{[|\text{SZnOH}^- - \text{Na}^+] + 2[|\text{SZnOH}^- - \text{Zn}^{2+}] - [|\text{ZnSH}^+ - \text{Cl}^-]\} \quad (5.8)$$

with $B = F/(Sa c')$. B is a conversion factor from surface concentration (mole per liter) to surface charge density (coulombs per square meter). These charges must be compensated by an equivalent amount of opposite charge, σ_d , in the diffuse layer to satisfy electrical neutrality i.e.

$$\sigma_0 + \sigma_\beta + \sigma_d = 0 \quad (5.9)$$

From the Gouy-Chapman-Stern diffuse layer theory, this charge can be expressed as (Hunter, 1991)

$$\sigma_d = -0.1174 z \sqrt{c} \sinh(19.46z\psi_d) \quad \text{C/m}^2 \quad (5.10)$$

where c and z are the bulk concentration and charge of the supporting electrolyte counter-ion in the diffuse layer, respectively.

5.4.1 Surface Mass Balance

The surface species are distributed among the total number of sites available, N_s sites/m².

$$N_s = [\text{SH}_2] + [\text{SZnOH}^-] + [\text{ZnSH}^+] + [\text{ZnSH}^+ \text{---Cl}^-] + [\text{SZnOH}^- \text{---Na}^+] + [\text{SZnOH}^- \text{---Zn}^{2+}] \quad (5.11)$$

where z is the elementary charge.

5.4.2 Double Layer Theories

Defining $z = z_+ = -z_-$ (i.e. z is always positive), the differential capacitance of the diffuse double layer, C_2 , can be defined by (Hunter, 1991)

$$C_2 = \frac{d\sigma_d}{d\psi_d} = 2.285z \sqrt{c} \cosh(19.46z\psi_d) \quad \text{F/m}^2 \quad (5.12)$$

in water at 25 °C, for c in mol/L and ψ_d in volts.

Potential and charge relationship in the compact double layer are given by (Hunter, 1991)

$$\sigma_0 = C_1(\psi_0 - \psi_\beta) \quad (5.13)$$

and

$$\sigma_d = C_2(\psi_d - \psi_\beta) = C_2(\zeta - \psi_\beta) \quad \text{with } \langle \psi_d = \zeta \rangle \quad (5.14)$$

where C_1 and C_2 are the integral capacitances of the inner region and outer region (see Fig. 5.1) respectively. As the inner region is more compact than the outer regions, C_1 was assumed constant while capacity C_2 changes with ψ_d as given by equation 5.12.

5.5 NUMERICAL PROCEDURES

From Eqs. 5.13 and 5.14, the following equations are obtained

$$\psi_0 = \frac{\sigma_0}{C_1} + \psi_\beta \quad \text{and} \quad \psi_\beta = \zeta - \frac{\sigma_d}{C_2} \quad (5.15)$$

Equations 5.7, 5.8 and 5.9 can be combined to give

$$\sigma_d = -B\{[ZnSH^+] - [SZnOH^-] + [SZnOH^- - Zn^{2+}]\}$$

which allows the concentration of $[SZnOH^- - Zn^{2+}]$ to be solved as

$$[SZnOH^- - Zn^{2+}] = [SZnOH^-] - [ZnSH^+] - \sigma_d/B \quad (5.16)$$

Combining Eqs. 5.7 and 5.11, the concentration of $[ZnSH^+ - Cl^-]$ can be solved from the following

$$\sigma_0 + N_s \cdot e = B\{[SZn] + [ZnS] + [SH_2] + 2[ZnSH^+] + 2[ZnSH^+ - Cl^-]\}$$

and,

$$[ZnSH^+ - Cl^-] = \frac{1}{2}\{(\sigma_0 + N_s e)/B - [SZn] - [ZnS] - [SH_2] - 2[ZnSH^+]\} \quad (5.17)$$

From Equation (8), the concentration of $[SZnOH^- - Na^+]$ can be expressed as

$$[SZnOH^- - Na^+] = \sigma_\beta/B - 2[SZnOH^- - Zn^{2+}] + [ZnSH^+ - Cl^-] \quad (5.18)$$

The entire set of equations can be solved simultaneously at any pH and electrolyte concentration by a numerical method (constrained nonlinear optimization). The algorithm employed was the Broyden-Fletcher-Goldfarb-Shanno (BFGS) updated Quasi-Newton method with a mixed quadratic and cubic line search procedure (Bazaraa et. al., 1993 and MATLAB manual, 1992). This algorithm proved to be numerically stable on large-scale problems, and capable of finding the global minimum from several local ones without the need to carefully select the initial values.

A MATLAB script program was written to fit the experimental $\zeta = F(\text{pH})$ curve using the set of equations above. In this program, ζ , pH, and [NaCl] are the variables whilst the equilibrium constants K_1 through K_6 , surface charge density σ_0 and the inner Helmholtz capacity C_1 are fitted parameters. The program simultaneously adjusts the value of the parameters and the free species concentration until a minimum is found in the sums of the squares of the deviations between the experimental and calculated curves. The strategy of the calculations is shown in Fig. 5.2.

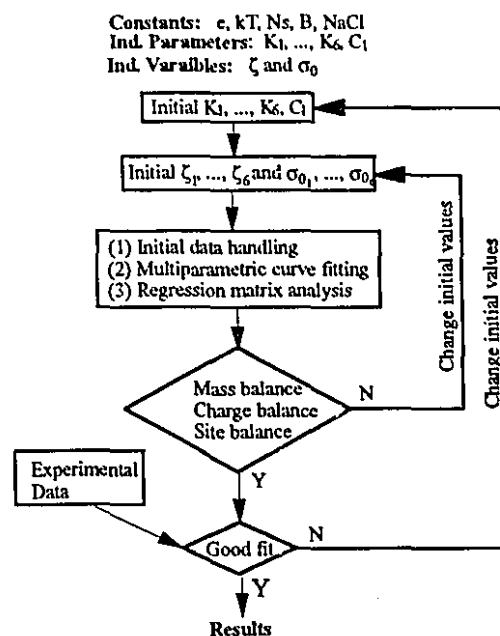


Figure 5.2 Strategy of the program

The settings of termination tolerance for X (variables) and F (objective function) are important for obtaining accurate results. Exploratory calculations showed that $< 10^{-8}$ termination tolerance was required to obtain satisfactory results. In the present work, the termination tolerance of both X and F was set to 10^{-15} .

It is worth mentioning how negative variable and independent parameters are treated: When a negative value is found, the program sets the gradient for this search step to positive and reverses the search direction.

The best-fit parameters are listed in Table 5.1, and the fitting results are shown in Fig. 5.3. The “goodness of fit” may be judged by comparing the experimental data with the calculated curve. The calculated species distribution as a function of pH is shown in Fig. 5.4.

Table 5.1 Best-fit parameters for the surface-charge and zeta-potential calculation of sphalerite using computational method with MATLAB software

Electrolyte Concentration (M)	pK ₁	pK ₂	pK ₃	pK ₄	pK ₅	pK ₆	C ₁ F/m ²
0.1	-1.45	4.53	-1.16	-3.25	-3.51	-3.05	0.7
0.01	-1.45	4.52	-1.15	-3.24	-3.49	-3.05	0.68
0.001	-1.43	4.5	-1.13	-3.23	-3.49	-3.05	0.68
0.0001	-1.43	4.51	-1.14	-2.22	-3.48	-3.06	0.67
0.000001	-1.44	4.5	-1.13	-3.24	-3.48	-3.05	0.56

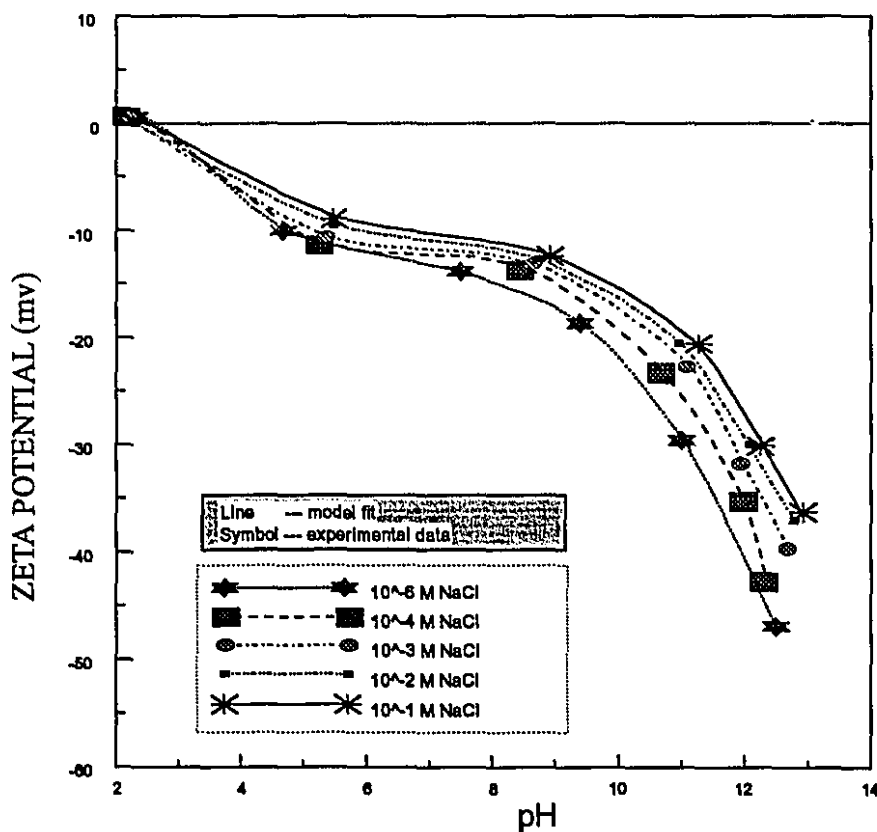


Figure 5.3 The zeta potential of sphalerite as a function of pH at different NaCl concentrations

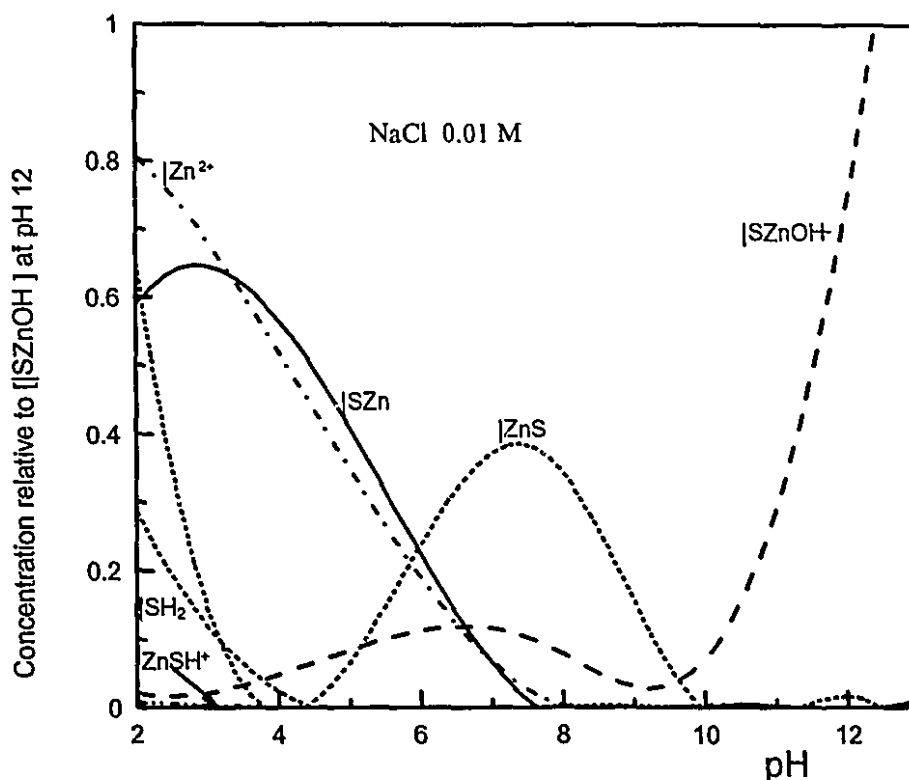


Figure 5.4 A fractional distribution diagram of the species on sphalerite surface as a function of pH

There are a few points here that need to be noted: (1) $[ZnSH^+ - Cl^-]$ is not included because its concentration is found to be not significant; (2) $[SZnOH^- - Na^+]$ and $[SZnOH^- - Zn^{2+}]$ are not included either for the purpose of clarity because the concentrations are too large to be shown on the present scale.

To check further the versatility of this approach, some experimental data on boehmite-water interface generously provided by Wood, Fornasiero and Ralston (1990) were examined. The result of fitting is given in Figure 5.5a with Figure 5.5b being the same except for a change in surface area from $44 \text{ m}^2/\text{g}$ to $0.044 \text{ m}^2/\text{g}$. (This alteration of the area was found to improve the fit and it is known that estimating a surface area relevant to modeling the zeta potential is difficult (Hunter, 1981).) The fitted parameters, compared to those given by Wood, Fornasiero and Ralston are given in Table 5.2a and Table 5.2b. The species distribution diagram is given in Figure 5.6. It can be seen that the

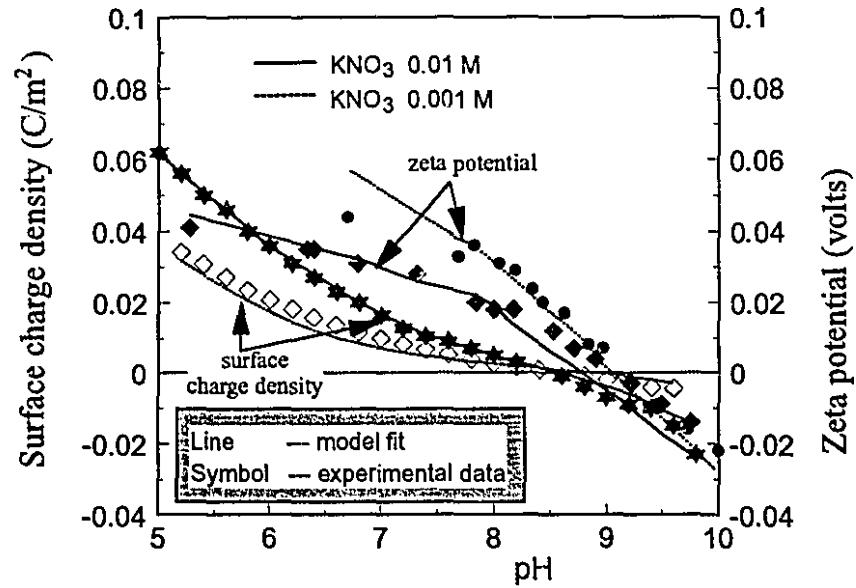


Figure 5.5a Surface charge density and zeta potential of boehmite as a function of pH (Surf. area: 44 m²/g) (The data were provided by authors (Wood, Fornasiero and Ralston, 1990))

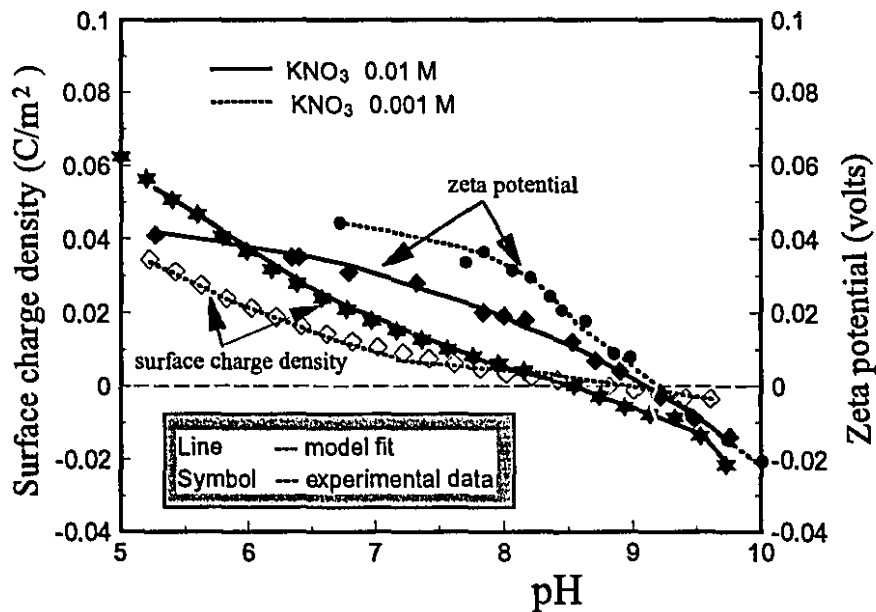


Figure 5.5b Surface charge density and zeta potential of boehmite as a function of pH (Surf. area: 0.044 m²/g) (The data were provided by authors (Wood, Fornasiero and Ralston, 1990))

σ_0 {pH, [KNO₃]} curve can be predicted from fitting the ζ {pH, [KNO₃]} curve because the relationship between σ_0 and ζ has been well defined in the equations 5.9, 5.13 and 5.14. The predicted σ_0 {pH, [KNO₃]} curve does not change with different initial values. This observation means that, with the present minimization algorithm and search method, the solution is stable and closely bound to the defined equations.

Table 5.2a Best-fit parameters for the surface-charge and zeta-potential calculation of boehmite using computational method with MATLAB software (Sa=44 m²/g)

Electrolyte Concentration (M)	pK ₁	pK ₂	p*K ₃	p*K ₄	C ₁ F/m ²
0.01	6.4	11.5	7.2	9.8	0.6
0.001	6.3	10.9	7.8	9.5	0.55
(Wood, Fornasiero and Ralston, 1990)	6.3	11.9	7.5	9.6	c1 = 0.59 c2 = 0.19

Table 5.2b Best-fit parameters for the surface-charge and zeta-potential calculation of boehmite using computational method with MATLAB software (Sa=0.044 m²/g)

Electrolyte Concentration (M)	pK ₁	pK ₂	p*K ₃	p*K ₄	C ₁ F/m ²
0.01	6.9	10.1	8.05	8.4	0.373
0.001	6.8	10.2	8.2	8.6	0.34

5.6 DISCUSSION

The agreement between experimental and calculated data, including those from Wood, Fornasiero and Ralston (1990), confirms the site-binding model and calculation procedure. The success of this approach does not preclude the applicability of other electrical double layer models (Sposito, 1983; Koopal etc., 1987; Hiemstra etc., 1989).

The equilibrium constants determined using this computational method do not agree with those obtained (pK₁ = -9.65, pK₂ = 10.29 and pK₃ = 7.14) by Sun (1991) for sphalerite using the FITEQL fitting program for the potentiometric titration curve. The difference appears to reside in the capacity values.

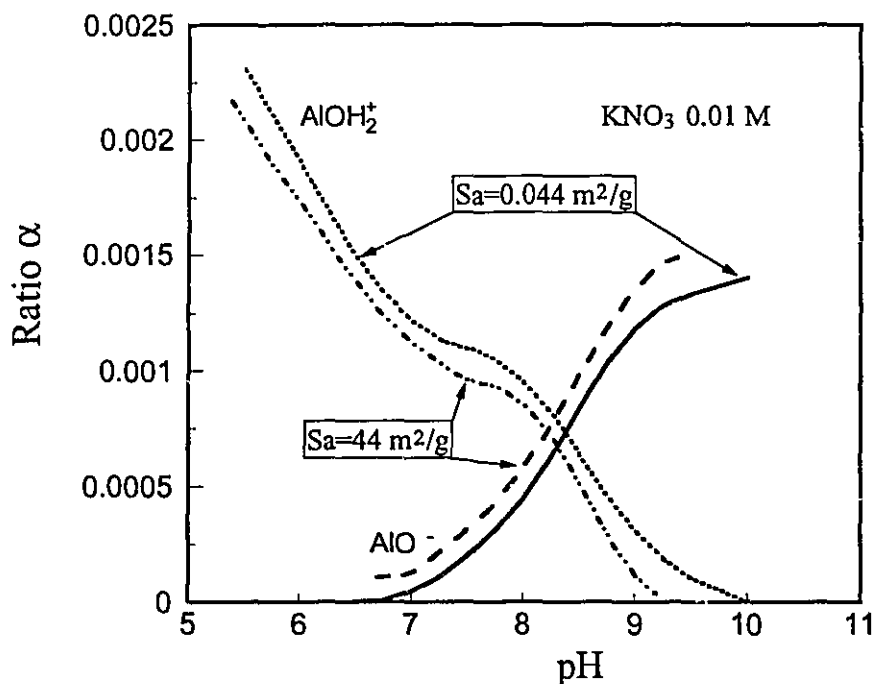


Figure 5.6 A fractional distribution diagram of the species on boehmite surface

The values of the capacitances C_1 and C_2 , are inversely proportional to the distance separating the surface from the inner Helmholtz plane, and from the inner to outer Helmholtz planes, respectively. They are also proportional to the dielectric constant of the medium between these planes. In the site-binding model, the distance between two successive planes depends on the size of the adsorbed electrolyte ions and of the water molecules surrounding them. The value of C_1 calculated in this study (0.68 F/m^2) is much smaller than that obtained by Sun ($\geq 100 \text{ F/m}^2$). The capacitance value obtained here seems more realistic being within the range (0.2 to 2.4 F/m^2) of literature values found for various oxides and hydroxides (Davis and Leckie, 1978; Koopal, etc., 1987; Gibb, et al., 1990, Wood, Fornasiero and Ralston, 1990). Fornasiero, Eijt and Ralston (1992) obtained $C_1=2.0 \text{ F/m}^2$ for pyrite in an argon environment. This value will be reduced near to the value calculated with this new approach after taking account of the dielectric coefficient of water medium.

The experimental data on boehmite-water interface provided by Wood, Fornasiero and Ralston was fitted with two different surface area settings, their surface area of $44 \text{ m}^2/\text{g}$ and one adjusted to $0.044 \text{ m}^2/\text{g}$. From comparison of the results, it can be seen that the fitting for both zeta potential and surface charge is better using $0.044 \text{ m}^2/\text{g}$ as surface area. A surface area of $44 \text{ m}^2/\text{g}$ is very large corresponding to particles about $0.045 \text{ }\mu\text{m}$ in diameter. The surface area was measured by the BET method and boehmite might be porous. It is questionable whether the area measured with the BET method is applicable to the development of zeta potential. Measurement of the surface area of a solid is by no means a trivial problem. Lyklema (1977) points out that direct (electron microscopic) measurements of average irregular particle sizes may underestimate the area because of surface roughness and may even collapse the surface on a hydrous oxide or a "spongy" organic colloid. Hunter (1981) also notes that any procedure which requires a dry sample (e.g. BET adsorption) may give an area which for all its accuracy bears little relationship to the effective area in solution. A more detailed discussion of surface area determination is given in the review by James and Parks (1980). If the resultant fit is taken as the criterion, it can be tentatively concluded that $0.044 \text{ m}^2/\text{g}$ is closer to the effective area related to the measurement of zeta potential than $44 \text{ m}^2/\text{g}$. The uncertainty associated with surface area is not a major handicap, however, as the reasonably stable fit over the 3-order of magnitude change in area here implies. In the sphalerite case, the surface area was set to $0.056 \text{ m}^2/\text{g}$ calculated from the mean particle size of $25 \text{ }\mu\text{m}$.

In the present calculations, the surface site density was taken as a constant with a crystal standard value of $5.87 \times 10^{18} \text{ sites/m}^2$. To investigate the sensitivity of the calculated parameters to the site density, calculations with $\pm 50\%$ of this value were performed. Similarly good fits were obtained with a maximum variation in the equilibrium constant of only 0.2 pK units. This agrees with the conclusion of Wood et al. (1990) that the zeta potential calculations are relatively insensitive to variations in site density. This is possibly the result of only a small proportion of available surface sites being occupied.

It is noted that the equilibrium constants for Na^+ and Cl^- are not the same. It may be possible that the point-of-zero-charge (p.z.c.) and the isoelectric point (i.e.p.) of the sphalerite are different (Somasundaran, 1975). Both experimental and calculated i.e.p.

were at pH about 2.5, which is much lower than that of 8.5 given by Sun (1991). This difference may be the result of different sample pretreatments: As mentioned by Fornasiero, Eijt and Ralston (1992), "the iso electric point has been shown to shift, as oxidation proceeds, to high pH values close to the i.e.p. of the corresponding metal oxide".

The important improvement of the numerical procedure used in present work over those previously published is that the experimental data on surface charge density is not required in calculations. This improvement is fulfilled by the use of the eq. 5.12 in which the capacitance of the outer region of compact layer is varied with the zeta potential. It is realized that the changes in counter-ion concentrations do affect the double layer charge distributions, as a consequence, the capacitances in different layers, especially the outer region of the compact layer changes. The numerical approach with a varied outer region capacitance is closer to the reality than those with a fixed outer region capacitance. This point is supported by the good fitness shown in present work. Another benefit from this approach is the prediction of the surface charge density, which was shown to fit the experimental data closely.

From the predicted species distribution on the mineral surface (sphalerite, Fig. 5.4; boehmite, Fig. 5.6), a picture of the surface sites and surface groups is obtained. This will help in understanding the surface reactions with solution reagents and species, for example, the interaction of sphalerite with Fe^{2+} ions. This information lies at the heart of modeling the chemistry of flotation, something which remains a notable challenge.

5.6 CONCLUDING REMARKS

A site-binding model provided a good description of the chemistry of the sphalerite/water interface. The calculated zeta potential values were in good agreement with the experimental data. The equilibrium constants of the surface reaction and the site-binding parameters were obtained using a computational method. The BFGS Quasi-Newton method with a mixed quadratic and cubic line search procedure has been shown to be effective for solving surface and solution equilibria including charge and mass balances. However, with the present approach, a unique zeta potential, surface charge and

surface species' concentrations at a certain pH can be solved. Further information about the surface (i.e. σ_0) is required to confirm the parameters obtained. By observing the fit of the experimental data of Wood, Fornasiero and Ralston (1990), good agreement between the predicted $\sigma_0\{\text{pH}, [\text{KNO}_3]\}$ curve and experimental data was obtained. This self-consistent calculation for the surface and solution equilibria simultaneously allows the prediction of surface charge, diffuse layer potential and distribution of solution and surface species by fitting the $\zeta\{\text{pH}, [\text{NaCl}]\}$ curve using double layer theory. This integrated approach provides a better understanding of the effects of supporting electrolyte ions on the development of surface charge and provides a background model for the consideration of dilute ion adsorption on sulphide surfaces. This method also reveals which parameters are sensitive in controlling the zeta potential. The different affinities of the electrolyte cations and anions for the sphalerite surface may contribute to a suspected difference between p.z.c and i.e.p.

CHAPTER 6

DEVELOPMENT OF MECHANISM OF IRON ACTIVATION OF SPHALERITE

6.1 FLOTATION

The flotation results have established that: (i) iron must be in the ferrous not ferric state (Fig. 4.1), (ii) oxygen must be present (Fig. 4.3), and (iii) xanthate is required.

The results clearly re-confirm the observation of Leroux et al. (1987) that ferrous ions can 'activate' sphalerite at moderately alkaline pH. Leroux et al. suggested $\text{Fe}(\text{OH})_2$ as a possible activating species, but they did not confirm this. The concentration of ferrous hydroxy species over a pH range 6-12 has been determined by Fuerstenau (1976) and more recently by Acar and Somasundaran (1992). The latter results (Fig. 6.1) show that FeOH^+ is the dominant species around pH 8-11 over a total iron concentration from 10^{-5} M to 10^{-2} M (i.e. 0.56~560 mg/l), which covers the range in this work. It is suggested that FeOH^+ is the activating species between pH 8-11.

The flotation results show that Fe^{3+} ions do not activate sphalerite. The reason is probably because Fe^{3+} is precipitated as $\text{Fe}(\text{OH})_3$ at $\text{pH} > 3.5$ (Fig. 6.2) and so Fe^{3+} is effectively removed from solution.

The role of oxygen in the flotation is discussed below along with the interpretation of the surface charge data.

6.2 SURFACE CHARGE

The surface charge of sphalerite alone was negative for most of the pH range with a pzc ~ pH 2.5. Published values of pzc show a wide variation of results (Bender and Mouquin, 1952; Popov et al., 1989). This variation in part reflects the different Fe content of the sphalerite samples (Gigowski et al., 1991). The actual pzc of sphalerite does not, however, affect the interpretation of the results in the pH range 6-12 which is the focus

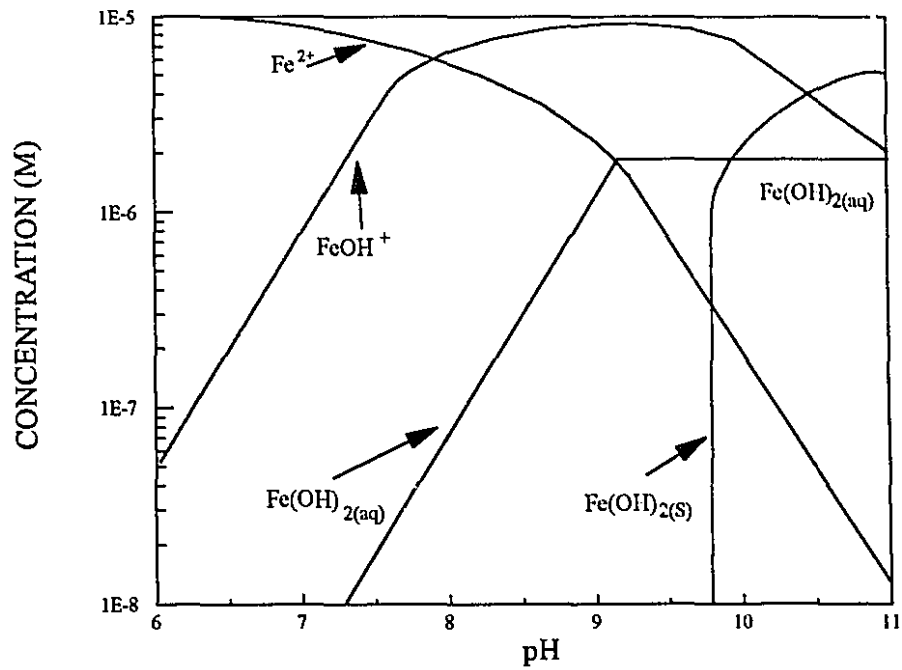


Figure 6.1 Logarithmic concentration diagram for $1 \times 10^{-5} \text{ M Fe}^{2+}$ from Acar and Somasundaran, 1992

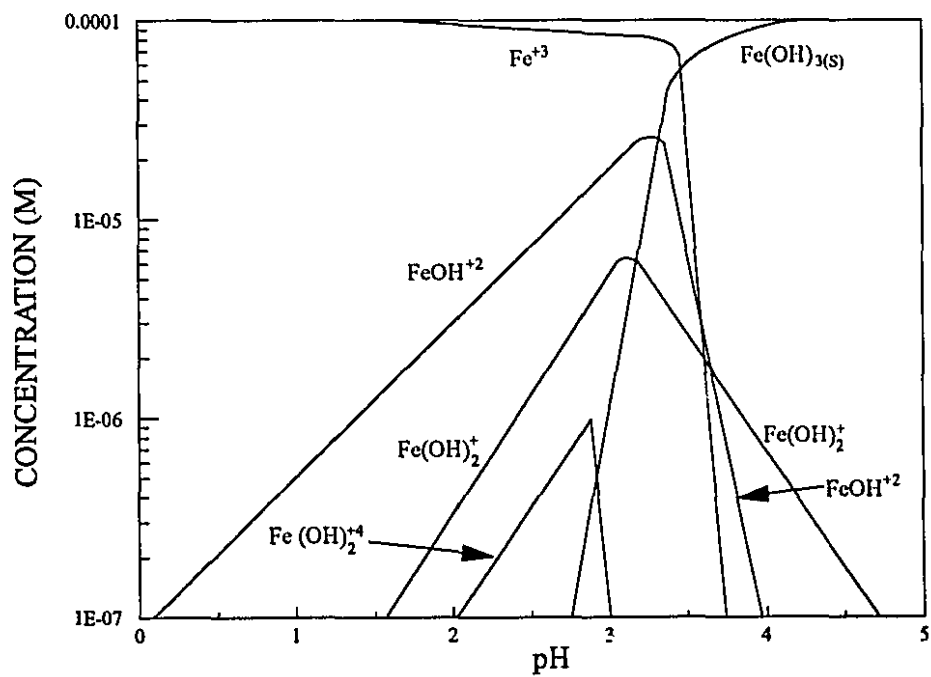


Figure 6.2 Logarithmic concentration diagram for $1 \times 10^{-4} \text{ M Fe}^{3+}$ Equilibrium data from Butler, 1964.

of this work.

The variation in surface charge over the pH range of interest can be summarized as follows:

- 1 The surface charge increases with Fe^{2+} and oxygen concentration.
- 2 It decreases with increasing xanthate ion (X^-) concentration and excess Fe^{2+} in the absence of oxygen.
- 3 It changes insignificantly with Fe^{3+} ions.
- 4 After Fe^{2+} /xanthate treatment, it is similar to the surface charge of iron xanthate precipitate.

Adsorption of $\text{Fe}(\text{OH})^+$ into the electrical double layer is a reasonable explanation of the increase in charge. Certainly Fe^{2+} ions are extracted from solution (without release of Zn^{2+} ions, Fig. 4.13). The role of oxygen may be to oxidize this species to $\text{Fe}(\text{OH})^{2+}$ which would explain the further increase in charge (Fig. 4.12); it is evident that oxygen is consumed (Fig. 4.13). The decrease in charge with excess Fe^{2+} concentration may be related to: (i) the change in predominant species from $\text{Fe}(\text{OH})^+$ to $\text{Fe}(\text{OH})_2$ when ferrous ion concentration is greater than about 5×10^{-5} M (2.8 mg/l) (Baes et al., 1976); and/or (ii) the consumption of oxygen by oxidation of Fe^{2+} to Fe^{3+} species in solution and thus depletion of the oxygen available for the $\text{Fe}(\text{OH})^+$ to $\text{Fe}(\text{OH})^{2+}$ reaction on the surface. Subsequent reaction of $\text{Fe}(\text{OH})^{2+}$ with xanthate ion (X^-) to form a neutral species, for example, $\text{Fe}(\text{OH})_2\text{X}$ (Wang et al. 1989), could account for the decrease in charge upon adding xanthate. No particular significance is attached to the fact that the Fe^{2+} /xanthate treatment returns the surface charge to that of untreated sphalerite; it may reflect the neutralization of the $\text{Fe}(\text{OH})^+$ by X^- thus leaving the surface charge dictated by the other ions/species which remain present. Indirect evidence supporting formation of $\text{Fe}(\text{OH})^{2+}$ is that the solubility product of $\text{Fe}(\text{OH})_2\text{X}$ is lower than the corresponding ferrous compound (Wang et al. 1989).

The lack of response of surface charge to Fe^{3+} ions is again probably related to their removal as $\text{Fe}(\text{OH})_3$ precipitates. The pzc of $\text{Fe}(\text{OH})_3$ precipitates is about pH 7-8 (Parks, 1967) so heterocoagulation with sphalerite at pH < 7, with a consequent effect on

surface charge, may be expected. The small concentration of Fe^{3+} ions, however, may mean any effect is negligible.

The similarity to the surface charge of the iron xanthate precipitate prepared at alkaline pH strongly suggests it is the species responsible for the surface charge variations of sphalerite in the presence of Fe^{2+} ions and xanthate.

6.3 IRON XANTHATE PRECIPITATE

6.3.1 Infrared Studies

From the infrared spectra of pure xanthate (Fig. 4.24) and iron xanthate precipitates (Figs. 4.25, 4.26), some observations can be made:

- ♦ The absorption peak at 1617 cm^{-1} is suppressed.
- ♦ The 1380 cm^{-1} band is split indicating the effect of OH on a dialkyl group, i.e. isopropyl in this case; this is supported by the enhancement of 1140 cm^{-1} band absorption and the skeletal vibrations at 1175 and 1120 cm^{-1} with a reduced intensity (Nakanishi, 1977).
- ♦ The absorption peak at 1230 cm^{-1} is enhanced suggesting a covalent bond with a trivalent metal (for divalent metals the band is at 1200 cm^{-1} .) (Farmer, 1975; Leja, 1982).
- ♦ The dixanthogen characteristic absorption band at 1270 cm^{-1} is not seen.
- ♦ The absorption peak at 355 cm^{-1} became more prominent suggesting introduction of OH into the xanthate structure (Ferraro, 1971). Absorption at 464 cm^{-1} is the M-O (Fe^{3+} -O in this case, Nakamoto, 1963) stretching vibration coupled weakly with the C-S stretching vibration.

From the above, it can be concluded that the precipitates formed from interaction of ferrous sulphate with sodium isopropyl xanthate at pH 8 and 10 are the same in molecular structure and different from that of xanthate alone in that: (1) the precipitates have a stronger polar group (from the suppression of 1617 cm^{-1} band, splitting of 1380 cm^{-1} band and the sharpness of C=S peak); (2) there are ionically bonded trivalent metal

ions in the precipitates (1230 cm^{-1} band); and, (3) there are OH^- groups in the precipitates. These observations are consistent with ferric hydroxy xanthate.

6.3.2 Other Studies (Mössbauer, UV and XRD)

The Mössbauer spectra of the bulk precipitate are essentially the same as those of Sheikh and Leja (1977) (whose sample preparation procedure was followed). They however, interpreted the spectra as only one compound, ferric hydroxy xanthate. In our case the spectra show three components are presented. UV spectra results showed presence of xanthate and OH^- group but no sign of dixanthogen. The XRD patterns revealed a complex picture of these precipitates but gave no clear interpretation.

6.3.3 Suggested Compounds

The characteristics of the bulk precipitate formed at alkaline pH from ferrous sulphate and xanthate solutions appear to be as follows:

- 1 There are three compounds present: The evidence is from (a) the Mössbauer and (b) the XRD which shows at least two compounds.
- 2 There is xanthate in at least one compound (from UV and IR spectra) and one compound is an iron oxide (FeO_x) (from XRD).
- 3 The iron in the compounds is in the ferric state. This can be seen from (a) the absorption peak at 1230 cm^{-1} in the IR spectra and, (b) the Mössbauer spectra.
- 4 There are OH^- groups in the ferric/xanthate compound. This is shown in (a) the slight shift in the 327 nm peak to 324 nm in the UV spectra and, (b) the splitting of 1380 cm^{-1} in the IR spectra.
- 5 There is no dixanthogen. The evidence is the lack of corresponding peak in either the UV or IR spectra.

The bulk precipitate from the interaction of ferrous sulphate and xanthate, formed under conditions similar to those used in sphalerite flotation, is tentatively concluded to be a mixture of Fe(III)O_x , $\text{Fe(OH)}_2\text{X}$ and Fe(OH)X_2

Regardless of its exact nature, the precipitate is shown to be hydrophobic and have a surface charge similar to that of Fe/X treated sphalerite (Fig. 4.14). This provides strong circumstantial evidence that a ferric hydroxy xanthate is responsible for the observed flotation of sphalerite.

6.3.4 Hydrophobicity

The hydrophobicity of ferric hydroxy xanthate is controversial. Critchley and Hunter (1986) considered them ($\text{Fe}(\text{OH})_2\text{X}$ specifically) to be not hydrophobic and unimportant as a collector species. Leja (1982) suggested they were weakly hydrophobic and possibly responsible for flotation of pyrite at alkaline pH. Others have suggested the ferric hydroxy xanthate, while weakly hydrophobic itself, could act as a contact site for adsorption of xanthate ions (Wang and Forssberg, 1991) and/or dixanthogen (Wang and Forssberg, 1991; Hodgson and Agar, 1989), the resulting species being strongly hydrophobic. This possibility is not ruled out here, but as far as the authors can determine, the degree of hydrophobicity of ferric hydroxy xanthates is not actually known so invoking co-adsorption may not be necessary. The suggestion from this work is they are hydrophobic enough to cause the flotation observed.

From the results above, a mechanism of sphalerite flotation in the presence of ferrous ions can be proposed.

6.4 PROPOSED MECHANISM

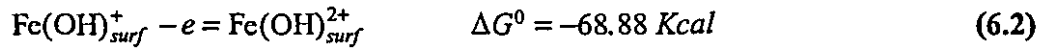
The mechanism suggested comprises three steps:

Step 1. Adsorption of FeOH^+ , the dominant ferrous species in solution at pH 8-11, resulting from:



(the value of pK is selected from Baes, 1976).

Step 2. After adsorption, FeOH^+ undergoes anodic oxidation at the mineral surface:



(the value of ΔG^0 is from *Natl. Bur. Standards Circ. 500*, U.S. Dept. Commerce (1952)).

The corresponding cathodic reaction is:



Another possible reaction is:

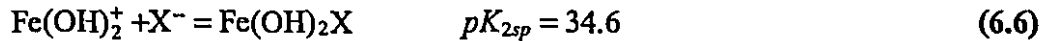


(the value of G^0 is from *Natl. Bur. Standards Circ. 500*, U.S. Dept. Commerce (1952)).

Step 3. The xanthate reacts with the ferric hydroxy species forming ferric hydroxy xanthate:



or



(the values of pK_1 and pK_2 are from Wang et al. (1989) and Pålsson et al. (1989)).

A fourth step, adsorption of X^- or X_2 onto the ferric hydroxy xanthate is not included, although the possibility is recognized.

The three-step mechanism can now be analysed in view of the surface analysis results.

6.5 THE MECHANISM AND SURFACE ANALYSIS

The incorporation of iron into the surface of sphalerite was observed by XPS and DRIFTS only when solution phase Fe^{2+} was used. This is consistent with the first step of the mechanism which requires adsorption of Fe^{2+} . The XPS and ATR spectra showing no xanthate on the surface unless Fe^{2+} was used is further support. The reason Fe^{3+} does not adsorb is consistent with its removal from solution as the hydroxide. The presence of Fe^{3+} (XPS, ATR), in the form of $-\text{FeOOH}$ (DRIFTS) on the surface of sphalerite that had been treated with Fe^{2+} suggests that oxidation of the iron takes place on the mineral surface. This observation is consistent with the second step of the mechanism, namely that an oxidizing medium is required for flotation to occur. (A note of caution is worth

introducing, however, that the *ex situ* techniques may have contributed to the oxidation as an artifact of the sample presentation technique.)

The role of the collector was demonstrated in the *in situ* ATR technique in which xanthate was shown to form an insoluble, surface-bound complex only on the sphalerite treated with Fe^{2+} . This result is consistent with part of the third step, namely the finding that the presence of xanthate is essential to achieve flotation. The spectra, however, do not permit the nature of the species to be determined.

The surface analysis findings here are in good agreement with the proposed mechanism of iron activation of sphalerite.

Understanding the mechanism may lead to deliberate exploitation but more likely it will be of concern as a possible source of unintentional activation. One remedy, if this occurs, is to ensure that the iron in solution is oxidized to Fe^{3+} prior to contact with sphalerite. This may require, for example, maintaining oxidizing conditions during size-reduction (usually by wet-grinding) where most iron (and other) ions appear to be released into solution.

CHAPTER 7

CONCLUSIONS AND SUGGESTIONS FOR FUTURE WORK

7.1 CONCLUSIONS

7.1.1 Flotation

1. Sphalerite can be floated with xanthate in the pH range 8-11 in the presence of ferrous (but not ferric) ions and oxygen.

7.1.2 Bulk Flotation and Analysis

1. The iron-xanthate precipitates formed over the pH range 6-12 are hydrophobic.
2. The flotation properties of Fe^{2+} /xanthate-treated sphalerite are almost the same as those of the iron-xanthate precipitates.
3. There are three compounds present in the iron-xanthate bulk precipitates: The evidence is from (a) Mössbauer and (b) XRD which shows at least two compounds.
4. In the iron-xanthate precipitates, there is xanthate in at least one compound (from UV and IR spectra) and one compound is an iron oxide (FeO_x) (from XRD).
5. The iron in the iron-xanthate precipitates is in the ferric state. This can be seen from (a) the absorption peak at 1230 cm^{-1} in the IR spectra and, (b) the Mössbauer spectra.
6. There are OH^- groups in the iron-xanthate precipitates. This is shown in (a) the slight shift in the 327 nm peak to 324 nm in the UV spectra and, (b) the splitting of 1380 cm^{-1} in the IR spectra.

7. There is no dixanthogen. The evidence is the lack of corresponding peak in either the UV or IR spectra.
8. The precipitate formed from the interaction of ferrous sulphate and xanthate, under conditions similar to those used in sphalerite flotation, is tentatively concluded to be a mixture of Fe(III)O_x , $\text{Fe(OH)}_2\text{X}$ and Fe(OH)X_2

7.1.3 Surface Analysis

1. The surface charge of sphalerite increases with a low concentration of Fe^{2+} ions (less than 2 ppm), but decrease at higher concentration unless oxygen is introduced; the surface charge decreased upon xanthate addition after Fe^{2+} ion additions.
2. The surface charge of Fe^{2+} /xanthate-treated sphalerite is almost the same as that of the ferric xanthate precipitate.
3. Solution phase Fe^{2+} but not Fe^{3+} is adsorbed onto the surface of sphalerite at pH 10.
4. The conversion of Fe^{2+} to Fe^{3+} on the surface, possibly as the oxide-hydroxide, is suggested by the XPS and DRIFTS experiments.
5. On the basis of the in situ ATR results, xanthate forms an insoluble hydrophobic surface species with Fe^{3+} .

7.1.4 Proposed Mechanism of Sphalerite Flotation with Fe^{2+} Ions

1. Adsorption of Fe(OH)^+ (the dominant Fe^{2+} species at pH 8-11).
2. Oxidation to Fe(OH)^{2+} on the surface (explaining the need for oxygen).
3. Reaction with xanthate (X^-) to form $\text{Fe(OH)}_2\text{X}$ or Fe(OH)X_2 (which are insoluble and shown to be hydrophobic).

7.1.5 Surface Complexation at Sphalerite/Water Interface

1. The equilibrium constants of the surface complexes at the sphalerite/water interface and the site-binding parameters can be obtained using a computational method.

2. The BFGS Quasi-Newton method with a mixed quadratic and cubic line search procedure was shown to be effective for solving surface and solution equilibria including charge and mass balance.
3. Only experimental zeta potential data was needed to characterize the sphalerite surface complexation.
4. The surface charge density can be predicted and was shown in the case of boehmite to be close to that experimentally determined.
5. Surface ion species distribution can be pictured in different conditions with calculated equilibrium constants of the surface complexes.

7.2 CLAIMS FOR ORIGINAL RESEARCH

1. The effect of iron ions on the flotation of sphalerite was interpreted.
2. Powerful mathematic tools and double layer theories were combined to characterize the sphalerite complexes at the surface/water interface. This technique gave a picture of the surface ion species distribution at the mineral surface as a function of pH.
3. An improvement was made to the surface complexation model by choosing a variable outer Helmholtz region capacitance which is more realistic than in prior modelling where it was treated as constant.

7.3 SUGGESTIONS FOR FUTURE WORK

1. Study of Fe interaction with pyrite should be done to complete the picture of the role of Fe ions in sphalerite / pyrite selective flotation.
2. Other metal ion effects need to be investigated, especially those of copper and calcium.
3. The iron, xanthate species need to be included in the complexation model to complete the modeling of the sphalerite system.
4. The means to control the iron, or other metal ion concentrations to the benefit of mineral separation should be investigated.

REFERENCES

- Acar S. and Somasundaran P., 1992, Effect of dissolved mineral species on the electrokinetic behaviour of sulfides, *Minerals Engineering*, Vol. 5, No. 1, p.27-40.
- Allison S.A., Goold L.A., Nicol M.J. and Granville A., 1972, Determination of the products of reaction between various sulfide minerals and aqueous xanthates solutions, and a correlation of the products with electrode rest potentials, *Metall. Trans.*, Vol. 3, No. 10, p.2613-2618.
- Baes C.F. and Mesmer R.E., 1976, Chapter 10, *The Hydrolysis of Cations*, Wiley, New York, NY, p.226-237.
- Barton T.F., Price T. and Dillard J.G., 1990, The production of γ -FeOOH from FeSO₄ in the presence of EDTA, *J. Colloid Interfac. Sci.*, Vol. 138, p.122-127.
- Bazaraa M.S., Sherali H.D. and Shetty C.M., 1993, Nonlinear programming: Theory and algorithms, second edition, Charity Robey (Editor), John Wiley & Sons, Inc.
- Bender M. and Mouquin H., 1952, Brownian movement and electrical effects, *J. Phys. Chem.*, Vol. 56, p.272-278.
- Blaha J.J., Rosasco G.J. and Etz E.S., 1978, Raman microprobe characterization of residual carbonaceous material associated with airborne particulates, *Appl. Spectrosc.*, Vol. 32, p.292-297.
- Bogdanov O.S., Podnek A.K. and Semenova E.A., 1965, Issledovanie flotacii raznovidnostiei sfalerita (Flotation study of different sphalerite forms), *Trudy Inst. Mecha-nobr*, Vypusk, p.135 (in Russian).
- Bogdanov O.S., Yeropkin Yu.I., Leonov N.B., Mikhailova N.S., Satayev I.Sh. and Fyodorov L.D., 1991, The use of antioxidants and nitrogen in complex sulfide ore flotation, XVII International Mineral Processing Congress, Dresden, Vol. 2, p.83-92.

- Bowden J.W. and Bolland M.D.A., Posner A.M. and Quirk J.P., 1973, Generalized model for anion and cation adsorption at oxide surface, *Nature Phys. Sci.*, Vol. 245, p.81-83.
- Bowden J.W., Posner A.M. and Quirk J.P., 1974, in "Transaction of the 10th International Congress of Soil Science II", p.29.
- Boyce J.H., Venter W.J. and Adam J., 1970, Beneficiation practice at the Tsumeb concentrator, *Proc. World Sym. Min. Metal. Lead and Zinc*, AIME, New York, N.Y., p.542.
- Briggs D. and Riviere J.C., 1983, Spectral interpretation, In: *Practical Surface Analysis by Auger and X-ray Photoemission Spectroscopy*, D. Briggs and M.P. Seah (Editors), Wiley, Chichester, p.87-137.
- Brion D., 1980, Etude par spectroscopie de photoélectrons de la dégradation superficielle de FeS₂, CuFeS₂, ZnS et PbS à l'air et dans l'eau, *Appl. Surface Sci.*, Vol. 5, p.133-152.
- Buckley A.N. and Woods R., 1990, X-ray photoelectron spectroscopic and electrochemical studies of the interaction of xanthate with galena in relation to the mechanism proposed by Page and Hazell, *Int. J. Miner. Process.*, Vol. 28, p.301-311.
- Buckley A.N. and Woods R., 1991, Adsorption of ethyl xanthate on freshly exposed galena surface, *Colloids Surfaces*, Vol. 53, p.33-45.
- Butler J.N., 1964, *Ionic Equilibrium*, Addison-Wesley, Reading, MA. p.364.
- Calas G., Bassett W.A., Petiau J., Steimberg M., Tchoubar D. and Zarka A., 1984, Some mineralogical applications of synchrotron radiation, *Phys. Chem. Miner.*, Vol. 11, p.17-36.
- Cases J.M., De Donato P., Kongolo M. and Michot L, 1989, An infrared investigation of amyloxanthate adsorption by pyrite after wet grinding at natural and acid pH. *Colloid Surf.*, Vol. 36, p.323-338.

- Cases J.M., Kongolo M., De Donato P., Michot L. and Erre R., 1990a, Interaction between finely ground galena and potassium amylxanthate in flotation, 1. Influence of alkaline grinding, *Int. J. Miner. Process.*, Vol. 28, p.313-337.
- Cases J.M., Kongolo M., De Donato P., Michot L. and Erre R., 1990b, Interaction between finely ground galena and pyrite with potassium amylxanthate in relation to flotation, 2. Influence of grinding media at natural pH, *Int. J. Miner. Process.*, Vol. 30, p.36-37.
- Cases J.M., Kongolo M., De Donato P., Michot L. and Erre R., 1993, Interaction between finely ground pyrite and potassium amylxanthate in flotation: 1. Influence of alkaline grinding, *Int. J. Miner. Process.*, Vol. 38, p.267-299.
- Cecile J.L., Bloise R. and Barbery G., 1980, Galena depression with chromate ions after flotation with xanthates: a kinetic and spectrometry study, *Complex Sulphide Ores*, Jones M.J. (Editor), The Institution of Mining and Metallurgy, London, P.159-170.
- Chadwick D. and Hashemi T., 1979, Electron spectroscopy of corrosion inhibitors: Surface films formed by 2-Mercaptobenzthiazole and 2-Mercaptobenzimidazole on copper. *Surface Sci.*, Vol. 89, p.649-659.
- Chesters M.A. and Sheppard N., 1981, Vibrational spectroscopy and chemisorbed species. *Chem. Britain*, Vol. 17, p.521-532.
- Childers J.W., Röhl R. and Palmer R.A., 1986, Direct comparison of the capabilities of photoacoustic and diffuse reflectance spectroscopies in the Ultraviolet, Visible, and Near-Infrared regions, *Anal. Chem.*, Vol. 58, p.2629-2636.
- Christensen P.A., Hamnett A., 1990, *Chemical Kinetics*, Compton R.G. (Editor), Elsevier, Amsterdam, Vol. 30, p.245.
- Chrysoulis S.L., Stowe K.G. and Reich F., 1992, Characterization of composition of mineral surfaces by laser-probe microanalysis, *Trans. IMM (Sect. C: Mineral Process. Extr. Metall.*, Vol. 101, p.C1-C6.

- Clifford K.L., 1971, Mechanism of flotation of unactivated sphalerite with xanthates, Ph. D. Thesis, University of Utah.
- Clifford R.K., Purdy K.L. and Miller J.D., 1975, Characterization of sulfide mineral surfaces in froth flotation systems using electron spectroscopy for chemical analysis, *AIChE, Symp. Ser.*, 71, Vol. 150, p.138-147.
- Critchley J.K., 1981, Reaction of ethyl xanthate at an iron electrode, *Trans. IMM*, Section C, Vol. 95, p.C42-C44.
- Critchley J.K. and Hunter C.J., 1986, Solubility products of ferric xanthate, *Trans. IMM*, Section C, Vol. 95, p.C173-C175.
- Cross W.M., Kellar J.J. and Miller J.D., 1991, Conformation of adsorbed surfactant species in the alumina/sodium dodecylsulfate/water system as determined by in-situ FTIR/IRS, *XVII Int. Miner. Process. Congr.*, Dresden. Polygraphischer Bereich, P.319-339.
- Davis J., James R.O. and Leckie J.O., 1978a, Surface ionization and complexation at the oxide/water interface I. Computation of electrical double layer properties in simple electrolytes, *J. Colloid Interface Sci.*, Vol. 63, No. 3, p.480-499.
- Davis J., and Leckie J.O., 1978b, Surface ionization and complexation at the oxide/water interface II. Surface properties of amorphous iron oxyhydroxide and adsorption of metal ions, *J. Colloid Interface Sci.*, Vol. 67, No. 1, p.90-107.
- Debe M.K., 1987, Optical probes of organic thin films: Photons-in and photons-out, *Prog. Surf. Sci.*, Vol. 24(1-4), p.1-282.
- De Donato P., Cases J.M., Kongolo M., Michot L. and Burneau A., 1990, Infrared investigation of amylxanthate adsorption on galena: Influence of oxidation, pH and grinding, *Colloids Surfaces*, Vol. 44, p.207-228.
- Dhamelincourt P., Wallart F., Leclercq M., N'Guyen A.T. and Landon D.O., 1979, Laser Raman molecular microprobe, *Anal. Chem.*, Vol. 51, p.414A-421A.

- Dugger D.L., Stanton J.H., Irby N., McConnell B.L., Cummings W.W. and Maatman R.W., 1964, The exchange of twenty metal ions with the weakly acidic silanol group of silica gel, *J. Phys. Chem.* Vol. 68, p.757.
- Etz e.S., 1979, Raman microprobe analysis: principles and applications, *Scanning Electron Microsc.*, p.67-82.
- Farmer V.C., (Editor), 1974, *The Infrared Spectra of Minerals*, Mineralogical Society, London.
- Farmer V.C., 1975, Infrared spectroscopy in mineral chemistry, *Physicochemical Methods of Mineral Analysis*, (Ed: A.W. Nicol) Chapter 9, Plenum Press: New York).
- Ferraro J.R., 1971, *Low-frequency Vibrations of Inorganic and Co-ordination Compounds*, Plenum Press: New York.
- Finkelstein N.P. and Allison S.A., Lovell V.M. and Stewart B.V., 1975, Natural and induced hydrophobicity in sulphide mineral systems, *Am. Inst. Chem. Eng. Sym. Ser.*, Vol. 71, p.165-175.
- Finkelstein N.P. and Allison S.A., 1976, The chemistry of activation, deactivation and depression in the flotation of zinc sulfide: a review. *FLOTATION: A.M. Gaudin Memorial volume*, Vol. 1, p.414.
- Fornasiero D., Eijt V. and Ralston J., 1992, An electrokinetic study of pyrite oxidation, *Colloid and Surfaces*, Vol. 62, p.63-73.
- Fredericks P.M., Tattersall A. and Donaldson R., 1987, Near-infrared reflectance analysis of iron ores, *Appl. spectrosc.*, Vol. 41, p.1039-1042.
- Fuerstenau D.W., 1982. *PRINCIPLES OF FLOTATION*. In: R.P. King (Editor), Chapter 9.
- Fuerstenau D.W., Metzger P.H. and Seele G.D., 1957, How to use the modified Hallimond tube for better flotation testing, *Eng. Min. J.* Vol. 158 (3), p.93.

- Fuerstenau D.W. and Mishra R.K., 1980, On the mechanism of pyrite flotation with xanthate collectors, *Complex Sulphide Ores*, (Editor: Jones M.J.), IMM, London, p.271-278.
- Fuerstenau M.C., Clifford K.L. and Kuhn M.C., 1974, The role of zinc xanthate precipitation in sphalerite flotation, *Int. J. Miner. Process.*, Vol. 1, p.307.
- Fuerstenau M.C., Kuhn M.C. and Elgillani D.A., 1968, The role of dixanthogen in xanthate flotation of pyrite, *Trans. AIME*, Vol. 241, p.148-156.
- Fuerstenau M.C. and Sabacky N.J., 1981, On the natural floatability of sulphides, *Int. J. Miner. Process.*, vol. 8, p.79-84.
- Garbassi F. and Marabini A.M. 1986, Spectroscopic investigation of sulphidation of zinc and lead carbonates, *J. Chem. Soc. Faraday Trans.*, 82, p.2043-2055.
- Gardella J.A. and Hercules D.M, 1981, Comparison of static secondary ion mass spectrometry, ion scattering spectroscopy, and X-ray photoelectron spectroscopy for surface analysis of acrylic polymers, *Anal. Chem.*, Vol. 53, p.1879-1884.
- Gardner J.R. and Woods R., 1979, An electrochemical investigation of the natural floatability of chalcopyrite, *Int. J. Miner. Process.* vol. 6, p.1-16.
- Gaudin A.M., 1930, The effect of xanthates, copper sulfate and cyanides on the flotation of sphalerite, *Trans. AIME*, vol. 87, p.417
- Gaudin A.M., 1957, *FLOTATION*. McGraw-Hill, London, p.254.
- Gaudin A.M., Dewey W.E., Duncan E., Johnson R.A. and Tangel O.F., 1934, Reactions of xanthate with sulphide minerals, *Trans. AIME*, Vol. 112, p.319-347.
- Gaudin A.M., Fuerstenau D.W. and Mao G.W., 1959, Activation and deactivation studies with copper on sphalerite, *Min. Eng.*, vol. 11, p.430.
- Gaudin A.M. and Schuhmann R., 1936, The action of potassium n-amyl xanthate on chalcocite, *J. Phys. Chem.*, vol. 40, p.257.

- Gibb A.W.M. and Koopal L.K., 1990, Electrochemistry of a model for patchwise heterogeneous surfaces: The rutile-hematite system, *J. Colloid Interface Science*, Vol. 134, No. 1, p.122-13
- Gigowski B., Vogg A., Wiercer K. and Dobias B., 1991, Effect of Fe-lattice ions on adsorption, electrokinetic, calorimetric and flotation properties of sphalerite, *Int. J. Miner. Process.*, Vol. 33, p.103-120.
- Girczys J. and Laskowski J., 1972, Mechanism of flotation of unactivated sphalerite with xanthates, *Trans. Inst. Min. Metall.* Vol. 81, C118.
- Giesekke E.W., 1983, A review of spectroscopic techniques applied to the study of interactions between minerals and reagents in flotation systems, *Int. J. Miner. Process.*, Vol. 11, p.19-56.
- Goold L.A. and Finkelstein N.P., 1969, An infrared investigation of the potassium alkyl xanthate and alkyltrimethylammonium bromide mixed-collector system, *National Institute for Metallurgy, Report 498*, Johannesburg, South Africa.
- Greeler R.G., 1962, An infrared investigation of xanthate adsorption by lead sulfide, *J. Phys. Chem.*, vol. 66, p.879.
- Griffiths P.R. and Haseth J.A., 1986, *Fourier Transform Infrared Spectrometry*. Wiley, New York.
- Hagihara H., 1952, Mono and multilayer adsorption of aqueous xanthate on galena surfaces, *J. Phys. Chem.*, vol. 56, p.616.
- Hair M.L., 1967, *Infrared Spectroscopy in Surface Chemistry*, Marcel Dekker, New York, N.Y., 315 pp.
- Hall C.I., Johnson N.W. and Quast K.B., 1990, The interaction of ethyl xanthate and cyanide in the lead roughing of a Mount Isa ore, *Proc. Aust. Inst. Min. Metall.*, Vol. 2, p.39-43.

- Hall S.T., Finch J.A. and Rowlands N., 1985, Enhancement of magnetic susceptibility of pyrite by oxidative pressure leaching, *Trans. Instn Min. Metall. (Sect. C: Mineral Process. Extr. Metall.)*, Vol. 94, p.C35-C39.
- Harrick N.J., 1967, *Internal Reflection Spectroscopy*, Wiley, New York.
- Hawthorne F.C. (Editor), 1988, *Spectroscopic methods in mineralogy and geology*, Review in Mineralogy, Vol. 18, Mineralogy Society of America, Michigan.
- Haycs R.H. and Ralston J., 1988, the collectorless flotation and separation of sulphide minerals by E_p control, *Int. J. Miner. Process.*, vol. 23, p.55-84.
- Heyes G.W. and Trahar W.J., 1977, The natural floatability of chalcopyrite, *Int. J. Miner. Process.*, vol. 4, p.317-331.
- Hiemstra T., Van Riemsdijk W.H. and Bolt G.H., 1989, Multisite proton adsorption modeling at the solid/solution interface of (hydr)oxides: A new approach, *J. Colloid and Surface Sci.*, Vol. 133, No. 1, p.91-117.
- Hodgson M. and Agar G.F., 1989, Electrochemical investigations into the flotation chemistry of pentlandite and pyrrhotite: Process water and xanthate interactions, *Canadian Metallurgical Quarterly*, Vol. 28, No. 3, p.189-198.
- Hohl H. and Stumm W., 1976, Interaction of Pb^{2+} with hydrous $\gamma-Al_2O_3$, *J. Colloid and Interface Sci.*, Vol. 55, p.281-288.
- Hu J.S., Misra M. and Miller J.D., 1986, Characterization of adsorbed oleate species at the fluorite surface by FTIR spectroscopy, *Int. J. Miner. Process.*, Vol. 18, p.73-84.
- Hunter R.J., 1981, *Zeta Potential in Colloid Science (Principles and Applications)*, R.H. Ottewill and R.L. Rowell (Editors.), p.35, Academic Press, London.
- Hunter R.J., 1991, *Foundations of Colloid Science*, p.337, Clarendon Press, Oxford, New York.

- Ibach H., Hopster H. and Sexton B., 1977, Analysis of surface reactions by spectroscopy of surface vibrations. *Appl. Surface Sci.*, Vol. 1, p.1-24.
- James R.O. and Healy T.W., 1972, Adsorption of hydrolyzable metal ions at the oxide-water interface, *J. Colloid and Interface Sci.*, Vol. 40, (a) Co(II) adsorption on SiO₂ and TiO₂ as model systems, p.42-52; (b) Charge reversal of SiO₂ and TiO₂ colloids by adsorbed Co(II), La(III) and Th(IV) as model systems, p.53-64; (c) A thermodynamic model of adsorption, p.65-81.
- James R.O. and Parks G.A., 1980, *Surface and Colloid Science*, Vol. II (E. Matijevic editor), John Wiley, New York.
- Johansson L.S., Juhanaja J., Laajalahti K. and Suoninen E., 1986, XPS studies of xanthate adsorption on metals and sulphides, *Surf. Interface Anal.*, Vol. 9, p.501-505.
- Kiselev A.V. and Lygin V.I., 1975, Ultraviolet spectra of adsorbed molecules and their interaction with a silica surface, *Infra-red Spectra of Surface Compounds*, Halsted Press, a division of JOHN WILEY & SONS, INC., New York. Chapter VII.
- Kizilirmakli A.V., 1989, Application of reverse pyrite flotation at Kidd Creek Mines Ltd., *Processing of Complex ores*, Proceedings of the International Symposium, G.S. Dobby and S.R. Rao (Editors), Vol. 12, Pergamon Press, p.215-226.
- Klimpel R.R. and Fee B.S., 1993, Some new collector products for improving the performance of industrial flotation circuits, *XVIII International Mineral Processing Congress*, The Australasian Institute of Mining and Metallurgy, Sydney, Australia, Vol. 3, p.569-576.
- Knoll W., 1991, Optical characterization of organic thin films and interfaces with evanescent waves, *M.R.S. Bull.* July, p.29-39.
- Kongolo M., Cases J.M., De Donato P., Michot L. and Erre R., 1990, Interaction of finely ground galena and potassium amylxanthate in relation to flotation, 3. Influence of acid and neutral grinding, *Int. J. Miner. Process.*, Vol. 30, p.195-215.

- Koopal L.K., Van Riemsdijk W.H. and Roffey M.G., 1987, Surface ionization and complexation models: A comparison of methods for determining model parameters, *J. Colloid and Interface Sci.*, Vol. 118, No. 1, p.117-136.
- Kortüm G., 1969, *Reflectance Spectroscopy*, Springer-Verlag, New York.
- Kostov I. and Minčeva-Stefanova J., 1982a, *Sulphide minerals crystal chemistry parageneses and systematics*, E. Schweizerbart'sche Verlagsbuchhandlung, (Nägele u. Obermiller). Stuttgart.
- Kostov I., 1982b, *Sulphide Mineral: Crystal chemistry parageneses and systematics*, E. Schweizerbart'sche Verlagsbuchhandlung, (Nägele u. Obermiller). Stuttgart.
- Laajalehto K., Johansson L.S., Mielczarski J., Anderson S. and Suoninen E., 1988, Electron spectroscopic studies of interaction of xanthate collectors with different substrates, *XVI Int. Miner. Process. Congr.*, Amsterdam, Forssberg E. (Editor), Elsevier, Amsterdam, p.691-702.
- Laajalehto K., Nowak P. and Suoninen E., 1993, On the XPS and IR identification of the products of xanthate sorption at the surface of galena, *Int. J. Miner. Process.*, Vol. 37, p.123-147.
- Labonté G., Leroux M., Sandoval I., Rao S.R. and Finch J.A., 1989, Some observations on copper-zinc separation from complex sulphide ores, *Processing of Complex Ores*, Proceedings of the International Symposium, G.S. Dobby and S.R. Rao (Editors), Vol. 12, Pergamon Press, p.193-202.
- Leja J., 1982, *Surface Chemistry of Froth Flotation*, Plenum Press, New York.
- Lepetic V., 1973, Flotation of chalcopyrite without a collector after dry, autogenous grinding, *75TH ANNU. MEET. CAN. INST. MIN.*
- Leppinen J.O., 1990, FTIR and flotation investigation of the adsorption of ethyl xanthate on activated and non-activated sulfide minerals, *Int. J. Miner. Process.*, Vol. 30, p.245-263.

- Leppinen J.O., Basilio C.I. and Yoon R.H., 1989, In-situ FTIR study of ethyl xanthate adsorption on sulfide minerals under conditions of controlled potential, *Int. J. Miner. Process.* Vol. 26, p.259-274.
- Leroux M, Rao S.R., Finch J.A., Gervais V. and Labonté G., 1989, Collectorless flotation in the processing of complex sulphide ores, *Advances in Coal and Mineral Processing Using Flotation*, S. Chander and R.R. Klimpel, Editors, 1989, Colorado, p.65-70.
- Leroux M, Rao S.R. and Finch J.A., 1987, Selective flotation of sphalerite from Pb-Zn ore without copper activation, *CIM Bulletin*, June, Vol. 80, p.41-44.
- Limouzin-Maire Y, 1981, Étude par spectroscopie ESCA de sulfures et sulfates de manganèse, fer, cobalt, nickel, cuivre et zinc, *Bull. Soc. Chim.*, France, Vol. 9-10, p.I-340.
- Little L.H., 1966, *Infrared Spectra of Adsorbed Species*, Academic Press, London
- Low M.J.D. and Parodi G.W., 1989, Infrared photoacoustic spectroscopy of solids and surface species, *Appl. Spectrosc.*, Vol. 34, p.76-80.
- Lozyk G.M., 1978, The surface chemistry of sphalerite flotation, Thesis (M. Eng.), McGill University.
- Luttrel G.H. and Yoon R.H., 1984, Surface studies of collectorless flotation of chalcopyrite, *Colloids Surfaces*, Vol. 12, p.239.
- Lyklema J., 1977, Trends in Electrochemistry, (Bochris J.O'M., Rand D.A.J. and Welch B.J. Editors), Plenum Publishing Corp, New York, p.159.
- Manceau A. and Combes J.M., 1988, Structure of Mn and Fe oxides and oxyhydroxides: a topological approach by EXAFS, *Phys. Chem. Miner.*, Vol. 15, p.283-295.
- Marabini A., Alesse V. and Belardi G., 1993, A new reagent for selective flotation of copper sulphides, *XVIII International Mineral Processing Congress*, The Australasian Institute of Mining and Metallurgy, Sydney, Australia, Vol. 3, p.561-567.

- Marabini A.M. and Cozza C., 1988, A new technique for determining mineral-reagent chemical interaction products by transmission IR spectroscopy: Cerussite-xanthate system, *Colloids Surfaces*, 33, p35-41.
- Marabini A.M. and Rinelli G., 1982, Development of specific reagent for rutile flotation, *Trans. Soc. Min. Eng. AIME*, 274, p1822-1827.
- Mason B. and Berry L.G., 1968, *Elements of Mineralogy*, W.H. Freeman and Company, San Francisco.
- Maulhardt H. and Kunath D., 1982, Diffuse-reflectance spectroscopy in the infrared, *Talanta*, Vol. 29, p.237-241.
- McIntyre N.S., Zetaruk D.G., 1977, X-ray photoelectron spectroscopic studies of iron oxides, *Anal. Chem.*, Vol. 49, No.11, p.1521-1529.
- McTavish S., 1980, Flotation practice at Brunswick Mining, *CIM Bull.* p.115-120.
- Mellberg, F., 1982, Operating experience at a new lead zinc flotation plant of the Vieille-Montagne Company, Preprint, Paper IV-2 at *14th Int. Miner. Process. Congr.*, Toronto, 20pp.
- Mielczarski J., 1986a, The role of impurities of sphalerite in the adsorption of ethyl xanthate and its flotation, *Int. J. Miner. Process.*, Vol. 16, p.179-194.
- Mielczarski J. 1986b, In situ ATR-IR spectroscopic study of xanthate adsorption on marcasite, *Colloids Surfaces*, Vol. 17, p.251-271.
- Mielczarski J. and Minni E., 1984, The adsorption of diethyldithiophosphate on cuprous sulphide, *Surf. Interface Anal.* Vol. 6, p.221-226.
- Mielczarski J., Nowak P., Strojek J.W. and Pomianowski A., 1979, Infra-red internal reflection spectrophotometric investigations of the products of potassium ethyl xanthate sorption on sulphide minerals, *Proc. XIII Int. Miner. Process. Congr.*, Laskowski J. (Editor), Warsaw, Preprints, Vol. 1, p.33-53.

- Mielczarski J., Nowak P. and Strojek J.W., 1983, Correlation between the adsorption of sodium dodecyl sulphate on calcium fluoride (fluorite) and its floatability—an infra-red internal reflection spectrophotometric study, *Int. J. Miner. Process.*, Vol. 11, p.303-317.
- Mielczarski J., and Suoninen E., 1984, The adsorption of diethyldithiophosphate on cuprous sulphide, *Surf. Interface Anal.*, Vol. 6, p.221-226.
- Mielczarski J., Suoninen E., Johanson L.S. and Leejalehto K., 1989, An XPS study of adsorption of methyl and amyl xanthates on copper, *Int. J. Miner. Process.*, Vol. 26, p.181-191.
- Miller F.A. and Wilkins, 1952, Infrared spectra and characteristic frequencies of inorganic ions: Their use in qualitative analysis, *Anal. Chem.*, Vol. 24, p.1253-1294.
- Morris r.V., Lauer Jr. H.V., Lawson C.A., Gibson Jr. E.K., Nace G.A. and Stewart C., 1985, Spectral and other physicochemical properties of submicron powders of Hematite (α -Fe₂O₃), Maghemite (γ -Fe₂O₃), Magnetite (Fe₃O₄), Goethite (α -FeOOH) and Lepidocrocite (γ -FeOOH), *J. Geophys. Res.*, Vol. 90 (B4), p.3126-3144.
- Morrison T.I., Iton L.E., Shenoy G.K., Stucky G.D. and Suib S.L., 1981, EXAFS study of hydrated manganese-exchanged A and Y zeolites, *J. Chem. Phys.*, Vol. 75, p.4086-4089.
- Morrow B.A., 1977, The Raman spectrum of chemisorbed methanol on silica: A comparison with the infrared technique, *J. Phys. Chem.*, Ithaca, Vol. 81, p.2663—2666.
- Mukherjee A.D. and Sen P.K., 1976, Floatability of sphalerite in relation to its iron content, *J. Mines, Metals, Fuels*, October: p.327.
- Nakamoto K., 1963, *Infrared Spectra of Inorganic and Co-ordination Compounds*, 2nd Edition, Wiley Interscience, New York.

- Nakanaga T. and Takenaka T., 1977, Resonance Raman spectra of monolayers of a surface-active dye absorbed at the oil-water interface, *J. Phys. Chem.*, Ithaca, Vol. 81, p.645-649.
- Nakanishi K. and Solomon P.H., 1977, *Infrared absorption spectroscopy*, 2nd edition, Holden-Day Inc. San Francisco, USA.
- Nowak P. and Strojek J.W., 1977, Spectrophotometric study of surface compounds formed on sulfide electrodes during anodic polarization in solutions of potassium ethyl xanthate, *Proceed. IVTH ELECTROCHEM. SYMP. POLISH CHEM. SOC.*, Jabgonna, Ed. Galus Z., Pub. 1980, p.253.
- Otten M.T., Miner B., Rask J.H. and Busek P.R., 1985, The determination of Ti, Mn, and Fe oxidation states in minerals by electron energy-loss spectroscopy, *Ultramicroscopy*, Vol. 18, p.285-290.
- Otto A., 1980, Surface enhanced Raman scattering (SERS): What do we know? *Appl. Surface Sci.*, Vol. 6, p.309-355.
- Page P.W. and Hazell L.B., 1989, X-ray photoelectron spectroscopy (XPS) studies of potassium amyl xanthate (KAX) adsorption on precipitated PbS related to galena flotation, *Int. J. Miner. Process.*, Vol. 25, p.87-100.
- Pålsson B.I. and Forssberg K.S.E., 1989, Computer-assisted calculations of thermodynamic equilibria in sphalerite-xanthate systems, *Int. J. Miner. Process.*, Vol. 26, p.223-258.
- Pao Y.H. (Editor), 1977, *Optoacoustic Spectroscopy and Detection*, Academic Press, New York.
- Parks G.A., 1967, Aqueous surface chemistry of oxides and complex oxide minerals, *Equilibrium Concepts in Natural Water System*, American Chemical Society, Washington, D.C.

- Paul R.L. and Hendra P.J., 1976, Laser Raman spectroscopy in surface chemical problems, *Miner. Sci. Eng.*, Vol. 8, p.171-186.
- Persson I., Persson P., Valli M., Fözö S. and Malmensten B., 1991, Reactions on sulfide mineral surfaces in connection with xanthate flotation studied by diffuse reflectance FTIR spectroscopy, atomic absorption spectrophotometry and calorimetry, In: K.S.E. Forssberg (Editor), Flotation of Sulphide Minerals, 1990. *Int. J. Miner. Process.*, Vol. 33, p.67-81.
- Pillai K.C., Young V.Y. and Bockris J.O'M., 1983, XPS studies of xanthate adsorption on galena surfaces. *Appl. Surf. Sci.*, Vol. 16, p.322-344.
- Pillai K.C., Young V.Y. and Bockris J.O'M., 1985, X-ray photoelectron spectroscopy studies of xanthate adsorption on pyrite mineral surfaces, *J. Colloid Interface Sci.*, Vol. 103, p.145-153.
- Poling G.W., 1969, Infrared reflection studies of the oxidation of copper and iron, *J. Electrochem. Soc.*, Vol. 116, No. 7, p.958-963.
- Poling G.W., 1961, Infrared spectroscopy of xanthate compounds in the solid, solution and the absorbed states, M. Sc. Thesis, University of Alberta, Edmonton, Canada.
- Poling G.W. and Leja J., 1963, Infrared study of xanthate adsorption on vacuum deposited films of lead sulfide and metallic copper under conditions of controlled oxidation, *J. Phys. Chem.* vol. 67, p.2121.
- Pomianowski A. and Leja J., 1964, Equimolar solutions of xanthate and alkyl trimethyl ammonium bromide adsorption on copper, nickel and sphalerite powders, *Trans. AIME*, vol. 229, p.307.
- Pomianowski A., Szczypa J., Poling G. and Leja J., 1975, Influence of iron content in sphalerite-marmatite on copper ion activation in flotation, *11TH INT. MINER. PROCESS. CONGRESS*. Cagliari, paper 23.

- Predali J.J., Brion D., Hayer J. and Pellettier B., 1979, Characterization by ESCA spectroscopy of surface compounds on the fine sulphide minerals in the flotation. *Preprints 13th Int. Miner. Process. Congr.*, Laskowski J. (Editor), Warsaw, Polish Scientific Publisher,, Vol. 1, p.134-156.
- Primet M., Fouilloux P. and Imelik B., 1979, Propene-V₂O₅ interaction studied by infrared emission spectroscopy, *Surf. Sci.*, Vol. 85, p.457-470.
- Ralston O.C., King C.R. and Tartaron F.X., 1930, Copper sulfate as flotation activator for sphalerite, *Trans. AIME*, vol. 87, p.389.
- Ranta L., Minni E., Suoninen E. Heimala S., Hintikka V., Saari M. and Rastas J., 1981, XPS studies of adsorption of xanthate on sulphide surfaces, *Appl. Surface Sci.*, Vol. 7, p.393-401.
- Rao S.R., 1971, Xanthates and related compounds, Marcel Dekker, New York, p.15-18.
- Rask J.H., Miner B.A. and Buseck P.R., 1987, Determination of manganese oxidation states in solids by electron energy-loss spectroscopy, *Ultramicroscopy*, Vol. 21, p.321-326.
- Ray A., Sathyanarayana D.N., Prasad G.D. and Patel C.C., Infrared spectral assignments of methyl and ethyl xanthato complexes of nickel (II), *Spectrochim. Acta*, Part A, 1973, Vol. 29, p.1579.
- Rey M. and Formanek V., 1960, Some factors affecting selectivity in the differential flotation of lead-zinc ores, *5TH INT. MINER. PROCESS. CONGR.*, Inst. Min. Metall., London, p.343-354.
- Rochley M., 1980, Fourier-transformed infrared photoacoustic spectroscopy of solids, *Appl. Spectrosc.*, Vol. 34, p.405-406.
- Rochley M. and Delvin J.P., 1980, Photoacoustic infrared spectra of aged and fresh cleaved coal surfaces, *Appl. Spectrosc.*, Vol. 34, p.407-408.

- Rönngren L., Sjöberg S., Sun Z., Forsling W. and Schindler P.W., 1991, Surface reaction in aqueous metal sulfide systems 2. Ion exchange and acid/base reactions at the ZnS-H₂O interface, *J. Colloid and Interface Sci.*, Vol. 145, No. 2, p.396-404.
- Rosasco G.J., 1980, Raman microprobe spectroscopy, *Adv. Infrared Raman Spectrosc.*, Vol. 7, p.223-282.
- Schecher W.D., and McAvoy D.C., 1992, MINEQL+: A software environment for chemical equilibrium modeling, *Comput. Environ. and Urban Systems*, Vol. 16, p.65-76.
- Schindler P.W., Fürst B., et al., 1976, Ligand properties of surface silanol groups I. Surface complex formation with Fe²⁺, Cu²⁺, Cd²⁺ and Pb²⁺, *J. Colloid and Interface Sci.*, Vol. 55, p.469.
- Sen P.K., Ray K.C. and Ray S., 1975, Role of semiconductor properties of galena in flotation, *Trans. Indian Inst. Met.*, vol. 28, p.337-342.
- Sheikh N., 1974, The chemical stability of heavy metal xanthates, Ph. D. thesis, University of British Columbia.
- Sheikh N. and Leja J., 1977, Mössbauer spectroscopy of Fe xanthates, *Sep. Sci.*, Vol. 15 (5), p.529-540.
- Sheppard N., Egerton T.A., Hardin A.H. and Kozirovski Y., 1971, Raman spectra of molecules adsorbed on porous Vycor glass: Elimination of the fluorescent background, *J. Chem. Soc., D.*, p.887-889.
- Shuey R.T., 1975, *Semiconducting Ore Minerals*, elsevier, Amsterdam.
- Smart R.St.C., 1991, Surface layers in base metal sulphide flotation, *Minerals Engineering*, Vol. 4, Nos 7-11, p.891-909.
- Somasundaran P., 1975, Interfacial chemistry of particulate flotation, *Advances in Interfacial Phenomena*, AIChE Symposium Series, No. 150, Vol. 71, p.1-15.

- Sposito G., 1983, On the surface complexation model of the oxide-aqueous solution interface, *J. Colloid and Interface Sci.*, Vol. 91, No. 2, p.329-340.
- Steininger J., 1968, Collector ionization in sphalerite flotation with sulfhydryl compounds, *Trans. AIME*, vol. 241, p.251.
- Stevens, J.G. and Shenoy G.K., Editor, *Mössbauer spectroscopy and its chemical applications*, American Chemical Society, Washington, D.C., 1981.
- Stewart B.V. and Finkelstein N.P., 1973, A preliminary investigation of the flotation of copper activated sphalerite without the use of collectors, *Nat. Inst. Metall., Repub. S. Afr.*, p.1587.
- Stumm W., Hohl H. and Dalang F., 1976, Interaction of metal ions with hydrous oxide surfaces, *Croat. Chem. Acta*, Vol. 48, p.491.
- Sun Z., Forsling Willis, Rönngren Lars and Sjöberg Staffan, 1991, Surface reactions in aqueous metal sulfide systems. 1. Fundamental surface reaction of hydrous PbS and ZnS, *Int. J. Miner. Process.*, Vol. 33, p.83-93.
- Sutherland K.L. and Wark I.W., 1955, *PRINCIPLES OF FLOTATION*. Astralas. Inst. Min. Metall. Melbourne.
- Takenaka T., 1979, Application of Raman spectroscopy to the study of surface chemistry, *Adv. Colloid Interface Sci.*, Vol. 11, p.291-313.
- Takenaka T. and Nakanaga T., 1976, Resonance Raman spectra of monolayers adsorbed at the interface between carbon tetrachloride and an aqueous solution of a surfactant and a dye, *J. Phys. Chem.*, Ithaca, Vol. 80, p.475-480.
- Termes S.C. and Richardson P.E., 1986, Application of FR-IR spectroscopy for in situ studies of sphalerite with aqueous solutions of potassium ethylxanthate and diethyldixanthogen, *Int. J. Miner. Process.*, Vol. 18, p167-178.
- Vidrine D.W., 1980, Photoacoustic Fourier transform infrared spectroscopy of solid samples, *Appl. Spectrosc.*, Vol. 34, p.314-319.

- Wagner C.D., Rids W.N., Davis L.E., Moulder J.F. and Muilenberg G.E. (Editors), 1979, *Handbook of X-ray Photoelectron Spectroscopy*, Physical Electronic Division, Perkin Elmer, Eden Prairie, MN, 190pp.
- Walker G.W., Walters C.O. and Richardson P.E., 1986, Hydrophobic effects of sulphur and xanthate on metal and mineral surfaces, *Int. J. Miner. Process.*, vol. 18, p.119-137.
- Wang Z.L. and Cowley J.M., 1988, Reflection electron energy loss spectroscopy (Recls): a technique for the study of surfaces, *Surf. Sci.*, Vol. 193, p.501-512.
- Wang X. and Forssberg K.S.E., 1991, Mechanisms of pyrite flotation with xanthates, *Int. J. Miner. Process.*, Vol. 33, p.275-290.
- Wang X., Forssberg K.S.E. and Bolin N.J., 1989, Thermodynamic calculations on iron-containing sulphide mineral flotation systems. I: The stability of iron xanthate, *Int. J. Miner. Process.*, Vol. 27, p.1-20.
- Wark E.E. and Wark I.W., 1936, The physical chemistry of flotation. VIII. The process of activation, *J. Phys. Chem.*, vol. 40, p.799.
- Waychunas G.A., Brown Jr. G.E. and Apter M.J., 1986, X-ray K-edge absorption spectra of Fe minerals and model compounds: II. EXAFS, *Phys. Chem. Miner.*, Vol. 13, p.31-47.
- Wendlandt W.W., Hecht H.G., 1966, *Reflectance Spectroscopy*, Wiley-Interscience, New York.
- Westall J.C. and Hohl H., 1980, A comparison of electrostatic models for the oxide / solution interface, *Adv. Colloid Interface Sci.*, No. 12, p.265-294.
- Westall J.C., Zachary J.L. and Morel F.M.M., MINEQL, 1976, A computer program for the calculation of chemical equilibrium composition of aqueous systems, *Civil Engineering Technical Note 18*, Cambridge, MA, Massachusetts Institute of Technology.

- Wilkinson W.D., 1935, Untersuchungen über die Wirkung des Xanthogenates auf Bleiglanz. Konrad Tritsch, Würzburg.
- Wood R., Fornasiero D. and Ralston J., 1990, Electrochemistry of the boehmite-water interface, *Colloid and Surface*, Vol. 51, p.389-403.
- Wright H.J.L. and Hunter R.J., 1973, Adsorption at solid-liquid interfaces *Austral. J. Chem.*, No. 26, I. Thermodynamics and the adsorption potential, p.1183-1190. II. Models of the electrical double layer at the oxide-solution interface, p.1191-1206.
- Xu M., Zhang Q., Rao S.R. and Finch J.A., 1991, Miniflotation test of sphalerite flotation without Cu activation, *Can. Min. Process. Ann. Meet.*, Paper 14, Ottawa.
- Xu M., Finch J.A. and Rao S.R., 1992, Sphalerite reverse flotation using nitrogen, Proceeding of the Third International Symposium on *ELECTROCHEMISTRY IN MINERAL AND METAL PROCESSING III*, Vol. 92-17, p.170-179.
- Yamamoto T., 1980, Mechanism of pyrite depression by sulphite in the presence of sphalerite, *Complex Sulphide ores*, Jone M.J. (Editor), Institution for Mining and Metallurgy, London, p.71-78.
- Yelloji Rao M.K. and Natarajan K.A., 1989, Effect of galvanic interaction between grinding media and minerals on sphalerite flotation. *Int. J. Miner. Process.*, Vol. 27, p.95-109.
- Yonezawa T., 1961, Experimental study of adsorption and desorption of xanthate by sphalerite, *Bull. Inst. Min. Metall.*, Vol. 70, p.329.
- Yoon R.H., 1981, Collectorless flotation of chalcopyrite and sphalerite ores by using sodium sulfide, *Int. J. Miner. Process.*, vol. 8, p.31-48.
- Zhang Q., Rao S.R. and Finch J.A., 1992, Flotation of sphalerite in the presence of iron ions, *Colloid and Surfaces*, Vol. 66, p.81-89.

APPENDIX 1

DETERMINATION OF ELECTROPHORETIC MOBILITIES USING MASS TRANSPORT METHOD: THE ZETA POTENTIAL ANALYZER

GENERAL DESCRIPTION

The Zeta Potential Analyzer consists of a special container cell for the particle-liquid system under investigation and an electronic control module. Two electrodes are located opposite one another in the mass-transport chamber. One electrode, shown on the left in the exploded view of the mass-transport chamber (Fig. A1), is accessible to the bulk of the particle-liquid system. The electrode on the right is located at the closed end of a cell that has a restricted tubular opening located directly between the two electrodes. The electrode in the cell is electrolytically reversible. Standard electrodes are made of zinc. During a test, the suspension container is usually rotated (25 or 30 rpm) to minimize the gravitational settling of coarse particles.

To measure electrophoretic mobility of suspended particles with the device, the cell and chamber reservoir are filled with the colloid or suspension to be studied. When a potential difference is applied between the two electrodes, particles having an electric charge (\pm) will migrate either into, or out of the cell, de-

pending on the polarity of the cell electrode. After a certain time period, there will be a change in the particle concentration of the cell contents because of their migration from the reservoir toward the electrodes. This charge can be determined by analysis (usually

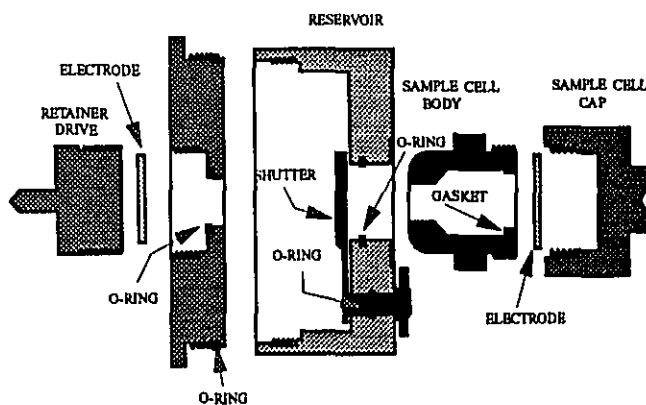


Figure A1. Exploded view of mass-transport chamber

gravimetrically), and from it, the mobility and the zeta potential are calculated. Typically, the time of the voltage gradient application is a few minutes.

THEORY

The electrophoretic mobility of particles is measured with the Zeta Potential Analyzer by determining the rate at which particles migrate into or out of the sample cell. Usually, the particles have a significantly different density from that of the suspending liquid, and the change of their concentration in the cell with time is most easily determined gravimetrically. The following derivation is based on a gravimetric determination. Changes necessitated by use of other analytical techniques will become readily apparent. In this derivation, it is also assumed that particles migrate into the cell rather than out of it. Again, it will become readily apparent how the treatment should be altered when the opposite is the case.

The particles of mass W_p entering the cell per unit time t due to electrophoretic migration can be expressed by

$$\frac{W_p}{t} = v \cdot A \cdot C \quad (\text{A1.1})$$

where

v = velocity of migration;

A = cross sectional area of the entry passageway (hole);

C = mass concentration of particles in the slurry.

Particles entering the cell displace an equivalent volume of suspending liquid. Therefore, the liquid of mass W_l leaving the cell per unit time is

$$\frac{W_l}{t} = v \cdot A \cdot C \left(\frac{\rho_l}{\rho_p} \right) \quad (\text{A1.2})$$

where

ρ_l = density of the liquid at given temperature;

ρ_p = density of the particles in the slurry.

The net change of mass ΔW in the cell is the difference between the mass entering and leaving the cell, thus

$$\frac{\Delta W}{t} = v \cdot A \cdot C \frac{\rho_p - \rho_l}{\rho_p} \quad (\text{A1.3})$$

or,

$$v = \frac{\Delta W \cdot \rho_p}{t \cdot A \cdot C \cdot (\rho_p - \rho_l)} \quad (\text{A1.4})$$

Particle velocities are established by their electrophoretic velocity component into the chamber and the liquid velocity component coming from the chamber. Under steady flow conditions, this can be expressed by

$$v = E \cdot (v_e - v_l) \quad (\text{A1.5})$$

where

E = potential gradient

v_e = electrophoretic mobility

v_l = liquid velocity from the cell.

Rearranged, equation A1.5 becomes

$$v_e = \frac{v + E \cdot v_l}{E} \quad (\text{A1.6})$$

The liquid velocity is determined by the rate at which liquid is displaced divided by the cross-sectional area of the cell passageway available for liquid flow expressed by $A(1 - \phi)$, where the volume fraction of dispersed matter is ϕ . This gives

$$v_l = \frac{v \cdot \phi}{1 - \phi} \quad (\text{A1.7})$$

Substituting equation A1.7 and A1.4 into equation 6 and rearranging gives

$$v_e = \frac{\Delta W \cdot (1 - \phi + E \cdot \phi)}{t \cdot E \cdot A \cdot \phi \cdot (1 - \phi) \cdot (\rho_p - \rho_l)} \quad (\text{A1.8})$$

The potential gradient E cannot be determined reliably from the overall applied potential because of polarization effects and because of changes in cell resistance due to the deposition of solids on the electrode of opposite sign to that of the particles. However,

when a constant current flow (I) is maintained through the suspension chamber, the effective potential gradient across the cell entranceway is given by

$$E = \frac{I}{\lambda A} \quad (\text{A1.9})$$

where,

I = current

λ = specific conductance.

Hence, upon substituting equation A1.9 into equation A1.8, one obtains the expression

$$v_{\epsilon} = \frac{\Delta W \cdot [\lambda \cdot A \cdot (1 - \phi) + I \cdot \phi]}{t \cdot I \cdot A \cdot \phi \cdot (1 - \phi) \cdot (\rho_p - \rho_l)} \quad (\text{A1.10})$$

which relates the electrophoretic mobility to quantities readily determined with the Zeta Potential Analyzer. The electrophoretic mobility is expressed in units of centimeter / second per volt/centimeters, t in seconds, I in amperes, ϕ as volume fraction of dispersed matter, and both ρ_p and ρ_l in grams/cubic centimeter.

The zeta potential ζ of particles in dilute preparations is related approximately to their electrophoretic velocity v_{ϵ} by the expression

$$\zeta = \frac{4 \cdot \pi \cdot v_{\epsilon} \cdot \eta \cdot \lambda \cdot A}{D \cdot I} \quad (\text{A1.11})$$

where

η = liquid specific viscosity;

D = liquid dielectric constant,

hence, both are dimensionless. Substituting equation A1.7 and A1.10 into equation A1.5 to arrive at an expression for v and then substituting the result, with equation A1.9, into equation A1.11 gives

$$\zeta = \frac{4 \cdot \pi \cdot \Delta W \cdot \lambda \cdot \eta}{t \cdot I \cdot \phi \cdot (\rho_p - \rho_l) \cdot D} \quad (\text{A1.12})$$

which expresses the zeta potential in terms of readily measurable quantities. The zeta potential is obtained from equation A1.12 in electrostatic unit (e.s.u.) volts.

The e.s.u. volts are converted to absolute volts by a constant 300 volt/e.s.u., resulting in

$$\zeta = 3.77 \frac{\Delta V \lambda \eta}{t \cdot I \cdot \phi \cdot (\rho_p - \rho) \cdot D} \times 10^3 \quad (\text{A1.13})$$

where

η = poise = g cm⁻¹ sec⁻¹ ;

D = dielectric constant is dimensionless.

Note that all these measurements are to be made isothermally at a given temperature of interest. The values of ρ , and D of water as a function of temperature within the range of 15-35 °C are tabulated in the Table A1.

Table A1. Physical constants of water as a function of temperature

Temperature, °C	Absolute Density, g/cm ³	Viscosity, poise	Dielectric Constant,
18	0.998595	0.010559	81.1
19	0.998405	0.010299	80.74
20	0.998203	0.01005	80.36
21	0.997992	0.00981	80
22	0.99777	0.009579	79.63
23	0.997538	0.009358	79.27
24	0.997296	0.009142	78.89

APPENDIX 2

MATLAB™ PROGRAM ON SURFACE IONIZATION AND COMPLEXATION AT THE SPHALERITE/WATER INTERFACE

SINGLE SPHALERITE SYSTEM

MATLAB™ works with essentially one kind of object, a rectangular numerical matrix (in special cases, a matrix may be a scalar or a vector). The equations and parameters are formed into matrices, which are listed as followings.

- ◆ Concentration matrix

$$\text{CONC} = \left[\begin{array}{ccc} \text{A matrix from experiment data set 1 to 6} & & \\ \text{SH}_2 & \dots & \text{SH}_2 \\ \text{SZnOH}^- & \dots & \text{SZnOH}^- \\ \text{ZnSH}^+ & \dots & \text{ZnSH}^+ \\ \text{SZnOH}^- \text{--Zn}^{2+} & \dots & \text{SZnOH}^- \text{--Zn}^{2+} \\ \text{SZnOH}^- \text{--Na}^+ & \dots & \text{SZnOH}^- \text{--Na}^+ \\ \text{ZnSH}^+ \text{--Cl}^- & \dots & \text{ZnSH}^+ \text{--Cl}^- \end{array} \right]$$

- ◆ Physical constant matrix, and Equilibrium constant matrix

$$\text{CONS} = \begin{bmatrix} e \\ kT \\ N_s \\ B \\ \text{NaCl} \end{bmatrix} \quad \text{CSTK} = \begin{bmatrix} K_1 \\ K_2 \\ K_3 \\ K_4 \\ K_5 \\ K_6 \\ C_1 \end{bmatrix}$$

- ◆ a local charge variable matrix for calculating zeta potential

$$\text{VABS} = \begin{bmatrix} \zeta_1 & \dots & \zeta_6 \\ \sigma_{0,1} & \dots & \sigma_{0,6} \\ \text{SZn}_{(1)} & \dots & \text{SZn}_{(6)} \\ \text{Zn}_{(1)}^+ & \dots & \text{Zn}_{(6)}^+ \\ \text{ZnS}_{(1)} & \dots & \text{ZnS}_{(6)} \end{bmatrix}$$

MATLAB SCRIPT M-FILE*Zetacall.M*

```
cls
% This program fits the zeta potential with several parameters unknown to a set of data.
% we'll use a function called CONSTR that implements BFGS Quasi-Newton method
% with mixed quadratic and cubic line search algorithm for minimizing a nonlinear function
% of several variables with a matrix of constraints.
global Data CONS
% Experiment Data
Data = [2.43    0.00681
        4.46    -0.00586
        7.62    -0.00767
        9.94    -0.01262
        11.3    -0.02365
        12.5    -0.03923];
% Physical constants e, kT, Ns, B, NaCl
CONS=[1.60e-19;1.38e-23*298;6.87e18;9.65e4/(0.056*5);0.01];
% Initial independent parameter values K1, K2, K3, K4, K5, K6, C1
CSTKINI=[25;0.0000285;13.80384;1716.328;3081.101;1.09e3;0.6858];
options(1)=1;           % Set display parameter to on.
options(2)=1e-16;       % Termination tolerance on X.
options(3)=1e-16;       % Termination tolerance on F.
options(14)=10000;      % Maximum number of iterations.
VLB=zeros(7,1);        % Lower bounds X>0.
VUB=[];                 % No upper bounds.
[x,options]=constr('zetafun1',CSTKINI,options,VLB,VUB);
% The 6 Ks and C1 values have been obtained
x
% The total error of curve fitting is
options(8)
save zns x options(8)
quit
```

Zetafun1.M

```
function [f,g] = zetafun1(CSTK)
%   ZETAFUN1 is used by ZETACAL1. ZETAFUN1(CSTK) returns the error between the
%   zeta potential experimental data and those computed by the current functions with current
%   variables.
%   ZETAFUN1 uses a function called FMINU for calculating the zeta potential and
%   equilibrium concentrations of all species by satisfying mass balance, charge balance and
%   site balance simultaneously
%   Initial Experiment Fitting Data Zeta, Sigma_0, SZn, Zn, ZnS
VABSINI={ ...
    0.00068    -0.0048    -0.0088    -0.012    -0.025    -0.04
    0.000466   -0.001562   -0.00666   -0.00866   -0.04    -0.074
    0.001      0.0008      2e-6      2e-8      3e-8     1e-7
    0.0012     0.0007     3e-5     6e-6     8e-7     3e-8
    0.0006     1e-5      0.0006    1e-8     3e-10    2e-11
};

options(1)=1;          % Set display parameter on
options(2)=1e-16;      % Termination tolerance on X
options(3)=1e-16;      % Termination tolerance on F
[Z,options]=fminu('zetafun2',VABSINI,options,[],CSTK);
y=Data(:,2);
f=sum((y-Z(1,:)).^2);
g=[];
```

Zetafun2.M

```
function f = zetafun2(VABS,CSTK)
%   ZETAFUN2 is used by ZETAFUN1. ZETAFUN2(VABS,CSTK) returns the error
%   between the data and the values computed using mass balance, charge balance and site
%   balance by the current function with current variables. ZETAFUN2 uses following
%   equations
pH=Data(:,1);
Sigmad=-0.1174*sqrt(CONS(5))*sinh(19.46*VABS(1,:));
Capacity2=2.285*sqrt(CONS(5))*cosh(19.46*VABS(1,:));
Phi_B=VABS(1,)-Sigmad./Capacity2;
Phi_0=VABS(2,)/CSTK(7)+Phi_B;
```

```
a1=log10(CSTK(1))+log10(VABS(3,:))-2*pH-log10(VABS(4,:));
b1=log10(CSTK(2))+log10(VABS(3,:))+pH+CONS(1)*Phi_0/(2.303*CONS(2));
c1=log10(CSTK(3))+log10(VABS(5,:))-pH-CONS(1)*Phi_0/(2.303*CONS(2));
d1=log10(CSTK(4))+b1+log10(VABS(4,:))-2*CONS(1)*Phi_B/(2.303*CONS(2));
e1=log10(CSTK(5))+b1+log10(CONS(5))-CONS(1)*Phi_B/(2.303*CONS(2));
f1=log10(CSTK(6))+c1+log10(CONS(5))+CONS(1)*Phi_B/(2.303*CONS(2));
CONC(1,:)=10.^(a1);
CONC(2,:)=10.^(b1);
CONC(3,:)=10.^(c1);
CONCEST(1,:)=10.^(d1);
CONCEST(2,:)=10.^(e1);
CONCEST(3,:)=10.^(f1);
CONC(4,:)=CONC(2,:)-CONC(3,:)-Sigmad/CONS(4);
CONC(6,:)=0.5*((VABS(2,:)+CONS(3)*CONS(1)*oncs(pH))/CONS(4)-VABS(3,:)-...
    VABS(5,:)-CONC(1,:)-2*CONC(3,:));
CONC(5,:)=-(VABS(2,:)+Sigmad)/CONS(4)-2*CONC(4,:)+CONC(6,:);
f=sum((CONCEST(1,:)-CONC(4,:)).^2+(CONCEST(2,:)-CONC(5,:)).^2+(CONCEST(3,:)-...
    CONC(6,:)).^2);
```

Constr.M

```
function [x, OPTIONS, lambda,
HESS]=constr(FUN,x,OPTIONS,VLB,VUB,GRADFUN,P1,P2,P3,P4,P5,P6,P7,P8,P9,P10,P11,P12,
P13,P14,P15)
%CONSTR    Finds the constrained minimum of a function of several variables.
%    X=CONSTR('FUN',X0) starts at X0 and finds a constrained minimum to
%    the function which is described in FUN (usually an M-file: FUN.M).
%    The function 'FUN' should return two arguments: a scalar value of the
%    function to be minimized, F, and a matrix of constraints, G:
%    [F,G]=FUN(X). F is minimized such that G < zeros(G).
%    X=CONSTR('FUN',X,OPTIONS) allows a vector of optional parameters to
%    be defined. For more information type HELP FOPTIONS.
%    X=CONSTR('FUN',X,OPTIONS,VLB,VUB) defines a set of lower and upper
%    bounds on the design variables, X, so that the solution is always in
%    the range VLB < X < VUB.
```

```
% X=CONSTR('FUN',X,OPTIONS,VLB,VUB,'GRADFUN') allows a function
% 'GRADFUN' to be entered which returns the partial derivatives of the
% function and the constraints at X: [gf,GC] = GRADFUN(X).
% Copyright (c) 1990 by the MathWorks, Inc.
% Andy Grace 7-9-90.
% Modified by Qingsong Zhang, 1994
% X=CONSTR('FUN',X,OPTIONS,VLB,VUB,GRADFUN,P1,P2,..) allows
% coefficients, P1, P2, ... to be passed directly to FUN:
% [F,G]=FUN(X,P1,P2,...). Empty arguments ([]) are ignored.
global OPT_STOP OPT_STEP; OPT_STEP = 0; OPT_STOP = 0;
% Set up parameters. XOUT(:)=x;
if ~any(FUN<48) % Check alphanumeric
ctype = 1;
evalstr = [FUN,];
    evalstr=[evalstr, 'x'];
    for i=1:nargin - 6
        ctype = 2;
        evalstr = [evalstr, 'P',int2str(i)];
    end
    evalstr = [evalstr, ');
else
ctype = 3;
    evalstr=[FUN, 'g=g(:)'];
end
if nargin < 3, OPTIONS=[]; end
if nargin < 4, VLB=[]; end
if nargin < 5, VUB=[]; end
if nargin < 6, GRADFUN=[]; end
VLB=VLB(:); lenvlb=length(VLB);
VUB=VUB(:); lenvub=length(VUB);
bestf = Inf;
nvars = length(XOUT);
CHG = 1e-7*abs(XOUT)+1e-7*ones(nvars,1);
if lenvlb*lenvub>0
    if any(VLB(1:lenvub)>VUB), error('Bounds Infeasible'), end
end
```

```
for i=1:lenvlb
    if lenvlb>0,if XOUT(i)<VLB(i),XOUT(i)=VLB(i)+1e-4; end,end
end for i=1:lenvub
    if lenvub>0,if XOUT(i)>VUB(i),XOUT(i)=VUB(i);CHG(i)=-CHG(i);end,end
end
% Used for semi-infinite optimization:
s = nan; POINT = []; NEWLAMBDA = []; LAMBDA = []; NPOINT = []; FLAG = 2;
x(:) = XOUT;
if etype == 1,
    [f, g(:)] = feval(FUN,x);
elseif etype == 2
    [f, g(:)] = eval(evalstr);
else
    eval(evalstr);
end
ncstr = length(g);
if ncstr == 0
    g = -1;
    ncstr = 1;
    if etype ~= 3
        evalstr = ['[f,g] =', evalstr, ';'];
        etype = 3;
    end
    evalstr = [evalstr,'g=-1;'];
end
if length(GRADFUN)
    if ~any(GRADFUN<48) % Check alphanumeric
        gtype = 1;
        evalstr2 = [GRADFUN,'(x)'];
        for i=1:nargin - 6
            gtype = 2;
            evalstr2 = [evalstr2,'P',int2str(i)];
        end
        evalstr2 = [evalstr2, ')'];
    else
        gtype = 3;
```

```
        evalstr2=[GRADFUN,'];
    end
end
OLDX=XOUT;
OLDG=g;
OLDgf=zeros(nvars,1);
gf=zeros(nvars,1);
OLDAN=zeros(ncstr,nvars);
LAMBDA=zeros(ncstr,1);
sizep = length(OPTIONS);
OPTIONS = foptions(OPTIONS);
if lenvlb*lenvub>0
    if any(VLB(1:lenvub)>VUB), error('Bounds Infeasible'), end
end
for i=1:lenvlb
    if lenvub>0,if XOUT(i)<VLB(i),XOUT(i)=VLB(i)+eps; end,end
end
OPTIONS(18)=1;
if OPTIONS(1)>0
    disp('')
        disp('f-COUNT FUNCTION    MAX{g}    STEP Procedures');
end
HESS=eye(nvars,nvars);
if sizep<1 |OPTIONS(14)==0, OPTIONS(14)=nvars*100;end
OPTIONS(10)=1;
OPTIONS(11)=1;
GNEW=1e8*CHG;

%-----Main Loop-----
status = 0;
while status ~= 1
%-----GRADIENTS-----
    if ~length(GRADFUN) | OPTIONS(9)
% Finite Difference gradients
        POINT = NPOINT;
        oldf = f;
```

```
oldg = g;
ncstr = length(g);
FLAG = 0; % For semi-infinite
gg = zeros(nvars, ncstr); % For semi-infinite
% Try to make the finite differences equal to 1e-8.
CHG = -1e-8./(GNEW+eps);
CHG = sign(CHG+eps).*min(max(abs(CHG),OPTIONS(16)),OPTIONS(17));
OPT_STEP = 1;
for gcnt=1:nvars
    if gcnt == nvars, FLAG = -1; end
    temp = XOUT(gcnt);
    XOUT(gcnt)= temp + CHG(gcnt);
    x(:)=XOUT;
    if etype == 1,
        [f, g(:)] = feval(FUN,x);
    elseif etype == 2
        [f, g(:)] = eval(evalstr);
    else
        eval(evalstr);
    end
    OPT_STEP = 0;
% Next line used for problems with varying number of constraints
    if ncstr~=length(g), diff=length(g); g=v2sort(oldg,g); end
    gf(gcnt,1) = (f-oldf)/CHG(gcnt);
    gg(gcnt,:) = (g - oldg)/CHG(gcnt);
    XOUT(gcnt) = temp;
end
% Gradient check
    if OPTIONS(9) == 1
        gfFD = gf;
        ggFD = gg;
        x(:)=XOUT;
    if gtype == 1
        [gf(:), gg] = feval(GRADFUN, x);
    elseif gtype == 2
        [gf(:), gg] = eval(evalstr2);
```

```
        else
            eval(evalstr2);
        end
        disp('Function derivative')
            gradcrr(gfFD, gf, evalstr2);
        disp('Constraint derivative')
            gradcrr(ggFD, gg, evalstr2);
        OPTIONS(9) = 0;
    end
    FLAG = 1; % For semi-infinite
    OPTIONS(10) = OPTIONS(10) + nvars;
    f=oldf;
    g=oldg;
else
% User-supplied gradients
    if gtype == 1
        [gf(:), gg] = feval(GRADFUN, x);
    elseif gtype == 2
        [gf(:), gg] = eval(evalstr2);
    else
        eval(evalstr2);
    end
end
AN=gg';
how="";
%-----SEARCH DIRECTION-----
    for i=1:OPTIONS(13)
        schg=AN(i, :)*gf;
        if schg>0
            AN(i, :)= -AN(i, :);
            g(i)= -g(i);
        end
    end
end
    if OPTIONS(11)>1 % Check for first call
% For equality constraints make gradient face in
% opposite direction to function gradient.
```

```
if OPTIONS(7)~=5,
    NEWLAMBDA=LAMBDA;
end
[ma,na] = size(AN);
GNEW=gf+AN*NEWLAMBDA;
GOLD=OLDgf+OLDAN*LAMBDA;
YL=GNEW-GOLD;
sdiff=XOUT-OLDX;
% Make sure Hessian is positive definite in update.
if YL*sdiff<OPTIONS(18)^2*1e-3
    while YL*sdiff<-1e-5
        [YMAX,YIND]=min(YL.*sdiff);
        YL(YIND)=YL(YIND)/2;
    end
    if YL*sdiff < (eps*norm(HESS,'fro'));
        how=' mod Hess(2)';
        FACTOR=AN*g - OLDAN*OLDG;
        FACTOR=FACTOR.*(sdiff.*FACTOR>0).*(YL.*sdiff<=eps);
        WT=1e-2;
        if max(abs(FACTOR))==0; FACTOR=1e-5*sign(sdiff); end
        while YL*sdiff < (eps*norm(HESS,'fro')) & WT < 1/eps
            YL=YL+WT*FACTOR;
            WT=WT*2;
        end
    else
        how=' mod Hess';
    end
end
end
%-----Perform BFGS Update If YL'S Is Positive-----
if YL*sdiff>eps
    HESS=HESS+(YL*YL)/(YL*sdiff)-(HESS*sdiff*sdiff*HESS)/(sdiff*HESS*sdiff);
% BFGS Update using Cholesky factorization of Gill, Murray and Wright.
% In practice this was less robust than above method and slower.
% R=chol(HESS);
% s2=R*S; y=R\YL;
% W=eye(nvars,nvars)-(s2*s2)\(s2*s2') + (y*s2)\(y*y');
```

```
% HESS=R'*W*R;
    else
        how=[how,' (no update)'];
    end
else % First call
    OLDLAMBDA=(eps+gf*gf)*ones(ncstr,1)/(sum(AN'*AN')+eps);
end % if OPTIONS(11)>1
OPTIONS(11)=OPTIONS(11)+1;
    LOld=LAMBDA;
OLDAN=AN;
OLDgf=gf;
OLDG=g;
OLDF=f;
OLDX=XOUT;
XN=zeros(nvars,1);
if (OPTIONS(7)>0&OPTIONS(7)<5)
% Minimax and attgoal problems have special Hessian:
    HESS(nvars,1:nvars)=zeros(1,nvars);
    HESS(1:nvars,nvars)=zeros(nvars,1);
    HESS(nvars,nvars)=1e-8*norm(HESS,'inf');
    XN(nvars)=max(g); % Make a feasible solution for qp
end if lenvub>0,
    AN=[AN;-eye(lenvub,nvars)];
    GT=[g;-XOUT(1:lenvub)+VLB];
else
    GT=g;
end
if lenvub>0
    AN=[AN;eye(lenvub,nvars)];
    GT=[GT;XOUT(1:lenvub)-VUB];
end
[SD,lambda,howqp]=qp(HESS,gf,AN,-GT, [], [], XN,OPTIONS(13),-1);
lambda(1:OPTIONS(13)) = abs(lambda(1:OPTIONS(13)));
ga=[abs(g(1:OPTIONS(13)));g(OPTIONS(13)+1:ncstr)];
mg=max(ga);
if OPTIONS(1)>0
```

```
if howqp(1) == 'o'; howqp = ' '; end
disp([sprintf('%5.0f %12.6g %12.6g ',OPTIONS(10),f,mg), sprintf('%12.3g
',OPTIONS(18)),how, ' ',howqp]);
end
LAMBDA=lambda(1:ncstr);
OLDLAMBDA=max([LAMBDA';0.5*(LAMBDA+OLDLAMBDA)'])';
%-----LINESEARCH-----
MATX=XOUT;
MATL = f+sum(OLDLAMBDA.*(ga>0).*ga) + 1e-30;
infeas = (howqp(1) == 'i');
if OPTIONS(7)==0 | OPTIONS(7) == 5
% This merit function looks for improvement in either the constraint
% or the objective function unless the sub-problem is infeasible in which
% case only a reduction in the maximum constraint is tolerated.
% This less "stringent" merit function has produced faster convergence in
% a large number of problems.
    if mg > 0
        MATL2 = mg;
    elseif f >= 0
        MATL2 = -1/(f+1);
    else
        MATL2 = 0;
    end
    if ~infeas & f < 0
        MATL2 = MATL2 + f - 1;
    end
else
% Merit function used for MINIMAX or ATTGOAL problems.
    MATL2=mg+f;
end
if mg < eps & f < bestf
    bestf = f;
    bestx = XOUT;
end
MERIT = MATL + 1;
MERIT2 = MATL2 + 1;
```

```
OPTIONS(18)=2;
while (MERIT2 > MATL2) & (MERIT > MATL) & OPTIONS(10) < OPTIONS(14)
    OPTIONS(18)=OPTIONS(18)/2;
    if OPTIONS(18) < 1e-4,
        OPTIONS(18) = -OPTIONS(18);
        % Semi-infinite may have changing sampling interval
        % so avoid too stringent check for improvement
        if OPTIONS(7) == 5,
            OPTIONS(18) = -OPTIONS(18);
            MATL2 = MATL2 + 10;
        end
    end
    XOUT = MATX + OPTIONS(18)*SD;
    x(:)=XOUT;
    if etype == 1,
        [f, g(:)] = feval(FUN,x);
    elseif etype == 2
        [f, g(:)] = eval(evalstr);
    else
        eval(evalstr);
    end
    OPTIONS(10) = OPTIONS(10) + 1;
    ga=[abs(g(1:OPTIONS(13)));g(OPTIONS(13)+1:length(g))];
    mg=max(ga);
    MERIT = f+sum(OLDLAMBDA.*(ga>0).*ga);
    if OPTIONS(7)==0 | OPTIONS(7) == 5
        if mg > 0
            MERIT2 = mg;
        elseif f >= 0
            MERIT2 = -1/(f+1);
        else
            MERIT2 = 0;
        end
    end
    if ~infeas & f < 0
        MERIT2 = MERIT2 + f - 1;
    end
end
```

```

        else
            MERIT2=mg+f;
        end
    end
%-----Finished Line Search-----
    if OPTIONS(7)~=5
        mf=abs(OPTIONS(18));
        LAMBDA=mf*LAMBDA+(1-mf)*LOLD;
    end
    if max(abs(SD))<2*OPTIONS(2) & abs(gf*SD)<2*OPTIONS(3) & (mg<OPTIONS(4) | (howqp(1)
    == 'i' & mg > 0))
        if OPTIONS(1)>0
            disp([sprintf('%5.0f %12.6g %12.6g ',OPTIONS(10),f,mg),sprintf('%12.3g
            ',OPTIONS(18)),how, ', ',howqp]);
            if howqp(1) ~= 'i'
                disp('Optimization Terminated Successfully')
                disp('Active Constraints:'),
                find(LAMBDA>0)
            end
        end
        if (howqp(1) == 'i' & mg > 0)
            disp('Warning: No feasible solution found.')
        end
        status=1;
    else
        % NEED=[LAMBDA>0]|G>0
        if OPTIONS(10) >= OPTIONS(14) | OPT_STOP
            XOUT = MATX;
            f = OLDF;
            if ~OPT_STOP
                disp('Maximum number of iterations exceeded')
                disp('increase OPTIONS(14)')
            else
                disp('Optimization terminated prematurely by user')
            end
        end
        status=1;
    end
end

```

```
end
end end
% If a better unconstrained solution was found earlier, use it: if f > bestf
XOUT = bestx;
f = bestf;
end
OPTIONS(8)=f;
x(:) = XOUT;
```

Fminu.M

```
function [x,OPTIONS] = fminu(FUN,x,OPTIONS,GRADFUN,P1,P2,P3,P4,P5,P6,P7,P8,P9,P10)
%FMINU      Finds the minimum of a function of several variables.
%          X=FMINU('FUN',X0) starts at the matrix X0 and finds a minimum to the
%          function which is described in FUN (usually an M-file: FUN.M).
%          The function 'FUN' should return a scalar function value: F=FUN(X).
%          X=FMINU('FUN',X0,OPTIONS) allows a vector of optional parameters to
%          be defined. OPTIONS(1) controls how much display output is given; set
%          to 1 for a tabular display of results, (default is no display: 0).
%          OPTIONS(2) is a measure of the precision required for the values of
%          X at the solution. OPTIONS(3) is a measure of the precision
%          required of the objective function at the solution.
%          For more information type HELP FOPTIONS.
%          X=FMINU('FUN',X0,OPTIONS,'GRADFUN') enables a function'GRADFUN'
%          to be entered which returns the partial derivatives of the function,
%          df/dX, at the point X: gf = GRADFUN(X).
%          The default algorithm is the BFGS Quasi-Newton method with a
%          mixed quadratic and cubic line search procedure.
%          Copyright (c) 1990 by the MathWorks, Inc.
%          Andy Grace 7-9-90.
%          Modified by Qingsong Zhang, 1994
% -----Initialization-----
XOUT=x(:);
nvars=length(XOUT);
evalstr = [FUN];
```

```
if ~any(FUN<48)
    evalstr=[evalstr,'(x)'];
    for i=1:nargin - 4
        evalstr = [evalstr,'P',int2str(i)];
    end
    evalstr = [evalstr,')'];
end
if nargin < 3, OPTIONS=[]; end
if nargin < 4, GRADFUN=[]; end
if length(GRADFUN)
    evalstr2 = [GRADFUN];
    if ~any(GRADFUN<48)
        evalstr2 = [evalstr2,'(x)'];
        for i=1:nargin - 4
            evalstr2 = [evalstr2,'P',int2str(i)];
        end
        evalstr2 = [evalstr2,')'];
    end
end
end
f = eval(evalstr);
n = length(XOUT);
GRAD=zeros(nvars,1);
OLDX=XOUT;
MATX=zeros(3,1);
MATL=[f;0;0];
OLDF=f;
FIRSTF=f;
[OLDX,OLDF,HESS,OPTIONS]=optint(XOUT,f,OPTIONS);
CHG = 1e-7*abs(XOUT)+1e-7*ones(nvars,1);
SD = zeros(nvars,1);
diff = zeros(nvars,1);
PCNT = 0;
OPTIONS(10)=2; % Iteration count (add 1 for last evaluation)
status =-1;
while status ~= 1
    % Work Out Gradients
```

```
if ~length(GRADFUN) | OPTIONS(9)
    OLDF=f;
% Finite difference perturbation levels
% First check perturbation level is not less than search direction.
    f = find(10*abs(CHG)>abs(SD));
    CHG(f) = -0.1*SD(f);
% Ensure within user-defined limits
    CHG = sign(CHG+eps) * min(max(abs(CHG),OPTIONS(16)),OPTIONS(17));
    for gcnt=1:nvars
        XOUT(gcnt,1)=XOUT(gcnt)+CHG(gcnt);
        x(:) = XOUT; f = eval(evalstr);
        GRAD(gcnt)=(f-OLDF)/(CHG(gcnt));
        if f < OLDF
            OLDF=f;
        else
            XOUT(gcnt)=XOUT(gcnt)-CHG(gcnt);
        end
    end
% Try to set difference to 1e-8 for next iteration
% Add eps for machines that can't handle divide by zero.
    CHG = 1e-8./(GRAD + eps);
    f = OLDF;
    OPTIONS(10)=OPTIONS(10)+nvars;
% Gradient check
    if OPTIONS(9) == 1
        GRADFD = GRAD;
        x(:)=XOUT; GRAD(:) = eval(evalstr2);
        graderr(GRADFD, GRAD, evalstr2);
        OPTIONS(9) = 0;
    end
else
    OPTIONS(11)=OPTIONS(11)+1;
    x(:)=XOUT; GRAD(:) = eval(evalstr2);
end
%-----Initialization of Search Direction-----
if status == -1
    SD=-GRAD;
```

```
FIRSTF=f;
OLDG=GRAD;
GDOLD=GRAD*SD;
% For initial step-size guess assume the minimum is at zero.
OPTIONS(18) = max(0.001, min([1,2*abs(f/GDOLD)]));
if OPTIONS(1)>0
    disp([sprintf('%5.0f %12.6g %12.6g
',OPTIONS(10),f,OPTIONS(18)),sprintf('%12.3g ',GDOLD)]);
end
XOUT=XOUT+OPTIONS(18)*SD;
status=4;
if OPTIONS(7)==0; PCNT=1; end
else
%-----Direction Update-----
    gdnew=GRAD*SD;
    if OPTIONS(1)>0,
        num=[sprintf('%5.0f %12.6g %12.6g
',OPTIONS(10),f,OPTIONS(18)),sprintf('%12.3g ',gdnew)];
    end
    if (gdnew>0 & f>FIRSTF)~finite(f) % Case 1: New function is bigger than last and
gradient w.r.t. SD -ve
%    ...interpolate.
        how='inter';
        [stepsize]=cubic1(f,FIRSTF,gdnew,GDOLD,OPTIONS(18));
        if stepsize<0|isnan(stepsize), stepsize=OPTIONS(18)/2; how='C1f'; end
        if OPTIONS(18)<0.1&OPTIONS(6)==0
            if stepsize*norm(SD)<eps
                stepsize=exp(rand(1,1)-1)-0.1;
                how='RANDOM STEPLENGTH';
                status=0;
            else
                stepsize=stepsize/2;
            end
        end
    end
    OPTIONS(18)=stepsize;
    XOUT=OLDX;
```

```
elseif f<FIRSTF
    [newstep,fbest] =cubici3(f,FIRSTF,gdnew,GDOLD,OPTIONS(18));
    sk=(XOUT-OLDX)*(GRAD-OLDG);
    if sk>1e-20
% Case 2: New function less than old fun. and OK for updating HESS
% .... update and calculate new direction.
        how="";
        if gdnew<0
            how='incstep';
            if newstep<OPTIONS(18), newstep=2*OPTIONS(18)+1e-5;
how=[how,' IF']; end
        OPTIONS(18)=min([max([2,1.5*OPTIONS(18)]),1+sk+abs(gdnew)+max([0,OPTIONS(18)-1]),
(1.2+0.3*(~OPTIONS(7)))*abs(newstep)]);
        else % gdnew>0
            if OPTIONS(18)>0.9
                how='int_st';
                OPTIONS(18)=min([1,abs(newstep)]);
            end
        end %if gdnew
        [HESS,SD]=updhess(XOUT,OLDX,GRAD,OLDG,HESS,OPTIONS);
        gdnew=GRAD*SD;
        OLDX=XOUT;
        status=4;
% Save Variables for next update
        FIRSTF=f;
        OLDG=GRAD;
        GDOLD=gdnew;
% If mixed interpolation set PCNT
        if OPTIONS(7)==0, PCNT=1; MATX=zeros(3,1);
MATL(1)=f; end
        elseif gdnew>0 %sk<=0
% Case 3: No good for updating HESSIAN .. interpolate or halve step length.
            how='inter_st';
            if OPTIONS(18)>0.01
                OPTIONS(18)=0.9*newstep;
                XOUT=OLDX;
```

```
        end
        if OPTIONS(18)>1, OPTIONS(18)=1; end
    else
        % Increase step, replace starting point
        OPTIONS(18)=max([min([newstep-OPTIONS(18),3]),0.5*OPTIONS(18)]);
        how='incst2';
        OLDX=XOUT;
        FIRSTF=f;
        OLDG=GRAD;
        GDOLD=GRAD'*SD;
        OLDX=XOUT;
        end % if sk>
        % Case 4: New function bigger than old but gradient in on
        % ...reduce step length.
        else %gdnew<0 & F>FIRSTF
            if gdnew<0&f>FIRSTF
                how='red_step';
                if norm(GRAD-OLDG)<1e-10; HESS=cyc(nvars);
            end
            if abs(OPTIONS(18))<eps
                SD=norm(nvars,1)*(rand(nvars,1)-0.5)
                OPTIONS(18)=abs(rand(1,1)-0.5)*1e-6;
                how='RANDOM SD';
            else
                OPTIONS(18)=-OPTIONS(18)/2;
            end
            XOUT=OLDX;
        end %gdnew>0
        end % if (gdnew>0 & F>FIRSTF)~finite(F)
        XOUT=XOUT+OPTIONS(18)*SD;
        if OPTIONS(1)>0, disp([num,how]),end
        end %-----End of Direction Update-----
        % Check Termination
        if max(abs(SD))<2*OPTIONS(2) & (-GRAD'*SD) < 2*OPTIONS(3)
            if OPTIONS(1) > 0
                disp('Optimization Terminated Successfully')
```

```
        disp('Gradient less than options(2)')
        disp([' NO OF ITERATIONS=', int2str(OPTIONS(10))]);
    end
    status=1;
elseif OPTIONS(10)>OPTIONS(14)
    if OPTIONS(1)>=0
        disp('Warning: Maximum number of iterations has been exceeded');
        disp('    - increase options(14) for more iterations.')
    end
    status=1;
else
% Line search using mixed polynomial interpolation and extrapolation.
    if PCNT~=0
        while PCNT > 0
            x(:) = XOUT; f = eval(evalstr); OPTIONS(10)=OPTIONS(10)+1;
            [PCNT,MATL,MATX,steplen,f,
how]=searchq(PCNT,f,OLDX,MATL,MATX,SD,GDOLD,OPTIONS(18), how);
            OPTIONS(18)=steplen;
            XOUT=OLDX+steplen*SD;
        end
    else
        x(:)=XOUT; f = eval(evalstr); OPTIONS(10)=OPTIONS(10)+1;
    end
end
end
end
x(:)=XOUT;
f = eval(evalstr);
if f > FIRSTF
    OPTIONS(8) = FIRSTF;
x(:)=OLDX;
else
    OPTIONS(8) = f;
end
end
```